NASA CR-132687

ANALYTICAL EVALUATION OF ILM SENSORS

By Raymond J. Kirk

SEPTEMBER 1975

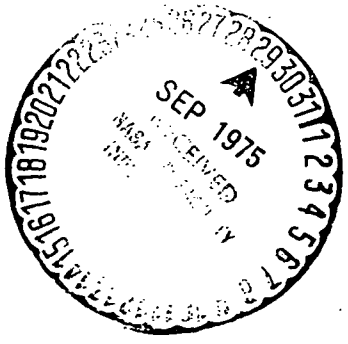

VOLUME II

APPENDICES

Prepared under Contract No. NAS1-13489 by
HONEYWELL INC.
Systems and Research Center
Minneapolis, Minnesota

for

NATIONAL AERONAUTICS AND SPACE ADMINISTRATION

Analytical Evaluation of ILM Sensors

Volume II

Appendices

Contract No. NAS1-13489

Systems and Research Center
Honeywell Inc.

PAGE INTENTIONALLY BLANK

SECTION IX

APPENDICES

PAGE INTENTIONALLY BLANK

APPENDIX A. TENTATIVE MLS ACCURACY REQUIREMENTS

GENERAL

Safe flights and landings generally require the following aircraft performance:

- o The aircraft path deviations should be within safe limits.
- o The aircraft path rates (such as sink rate) should be within safe limits.
- o The aircraft attitude changes should be comfortable to pilot and passengers.
- o The aircraft control surface movements should be within reasonable mechanical limits and should allow adequate margins for response to air turbulence and other factors.
- o The aircraft control column activity should be comfortable to the pilot.
- o For manual flight the display activity should be acceptable to the pilot.

The MLS shall not compromise the ability of the aircraft to maintain these criteria.

The factors of error magnitude, duration, spectral content and zone of occurrence are important as well as the factors of aircraft type, AFCS configuration, gain, and transient response.

Error specifications should be directed toward guidance signal errors which are related to these factors, and should register the influence of data rate variations and not be unduly affected by irrelevant, higher frequency variations. Bias and noise as used by RTCA SC-117 do not account for these factors. A method which does is described in this Chapter.

Path following errors and control motion noise are the concepts used to delineate accuracy.*

DEFINITIONS

Error and Noise Definitions

Angular Error -- The angular error is the difference between the processed sampled data output and the true position angle at the sampling time. The angular error budget is partitioned into two categories, bias and noise.

Angle Bias (Includes Receiver Bias) -- Bias is the long-term misalignment between a specific MLS course and a selected course, and includes the MLS ground system as well as the MLS airborne receiver mean errors which cannot be reduced to zero by real-time calibration techniques.

* Since the path following error and control motion concepts for specifying accuracy are new, this document also presents the RTCA SC-117 accuracy specifications.

Angle Noise (Includes Receiver Noise) -- Angle noise is defined as spatial and temporal perturbations in the guidance signal. It originates from both ground and airborne equipment and the environment.

Path Following Noise -- Path following noise is defined as that portion of angle noise which can cause aircraft motion; it exhibits relatively slow variations.

Control Motion Noise -- Control motion noise is that portion of angle noise which affects control surface, wheel, column motion, and aircraft attitude; it exhibits moderately fast variations.

Extraneous Noise -- Extraneous noise is that angle noise which exhibits variations too rapid to affect aircraft control and guidance.

Path Following Error -- Path following error is defined as the angular deviation from a predetermined course of an aircraft perfectly following MLS guidance commands. The error is thus due to angle bias and path following noise in the guidance signal.

Range Error -- The range error is the difference between the suitably processed DME range and the true distance at any given point in time. DME bias and noise errors have the same general definition as for angle guidance.

Course Linearity Error -- Course linearity error is the deviation of the angle coding scale factor from the nominal, about a selected course. Linearity errors affect effective AFCS gain and display sensitivity, and con-

tribute to aircraft instability.

Accuracy Zones

The following zones are defined within the MLS coverage in order to facilitate definition of system accuracies. These zones are based on the functional use of the MLS data and the operational significance of the MLS errors. The zones are as follows:

- o Initiation Zone
- o Maneuvering Zone
- o Landing Zone
- o Roll-Out Zone
- o Missed Approach Zone

ERROR DETERMINATION

Path following noise and errors and control motion noise are determined by passing the time records through standardized filters. The filter characteristics are based on a wide range of existing aircraft response properties, and are believed to be adequate for any foreseeable aircraft as well. The frequency response of the aircraft lateral or vertical/longitudinal channel is divided into three major spectral regions--a low, middle, and high frequency region, as follows:

- o Low - Aircraft path following components
  (0 to 1.5 radian/second-longitudinal channel)
  (0 to .5 radian/second-lateral channel)

- o Middle - Control surface motions, wheel and column motion, aircraft attitude.
  (.5 to 10 radians/second-longitudinal channel)
  (.3 to 10 radians/second-lateral channel)

o High - Does not affect aircraft control and guidance.

In terms of spectral density, the bias would be lower frequency limit of noise (approximately 0 to .05 radians/second for a 60-second record).

While the term "path following error" suggests the difference between a desired flight path and the actual flight path taken by an aircraft following the guidance, in practice this error is estimated by instructing the test pilot to fly a desired course, and measuring the difference between the filtered guidance indication and the corresponding position measurement determined by a high-accuracy instrument such as a theodolite. The errors and spectral distribution thus obtained give an accurate estimate of the path following parameters. A similar technique is used to determine the control motion noise.

Treatment of Sudden, Large Errors

Interference or multipath can occasionally cause large, sudden changes in angular indication. Provision shall be made to handle such transients while maintaining validation and coast requirements. Capability of "coasting" through periods of transients shall be provided, which rejects loss of data for a period of time up to 2 seconds, except that those functions, actively in use to determine flare altitude, shall be limited to 0.5 seconds coasting time.

Bias

The angular bias is determined by averaging the time error record of a test flight (the difference between the MLS-derived angle and the tracker-derived angle) over a period of 60 seconds.

Path Following Error

Path following error must not exceed the path following error specification more than 5% of the time over any 60-second portion of a flight record. The flight record here is obtained at the output of the standard path following filter. The procedure is described in Figure A-1.

Control Motion Noise

Control motion noise must not exceed control motion noise specification more than 5% of the time over any 60-second portion of a flight record. The procedure is shown in Figure A-1. The flight record here is obtained at the output of the standard control motion filter.

ACCURACY SPECIFICATIONS

The accuracy requirements for the MLS are presented in Tables A-1 and A-2. The method of measuring the errors is specified in Figure A-2 and Table A-3. The values contained in Tables A-1 and A-2 include the effects of multipath and EMI.

The exceptional path following error or control motion noise existing less than 5% of any 60-second period which exceed the stated limits shall be of such a magnitude and length that they present no hazard to flight or excessive strain on the aircraft, its pilot or passengers.

The azimuth error tolerances are listed in feet at the error window of the minimum guidance altitude (MGA); the angular error figures are premised on the given distances to the error windows. For shorter runways, the same equipment would yield superior guidance (in feet) at the MGA.

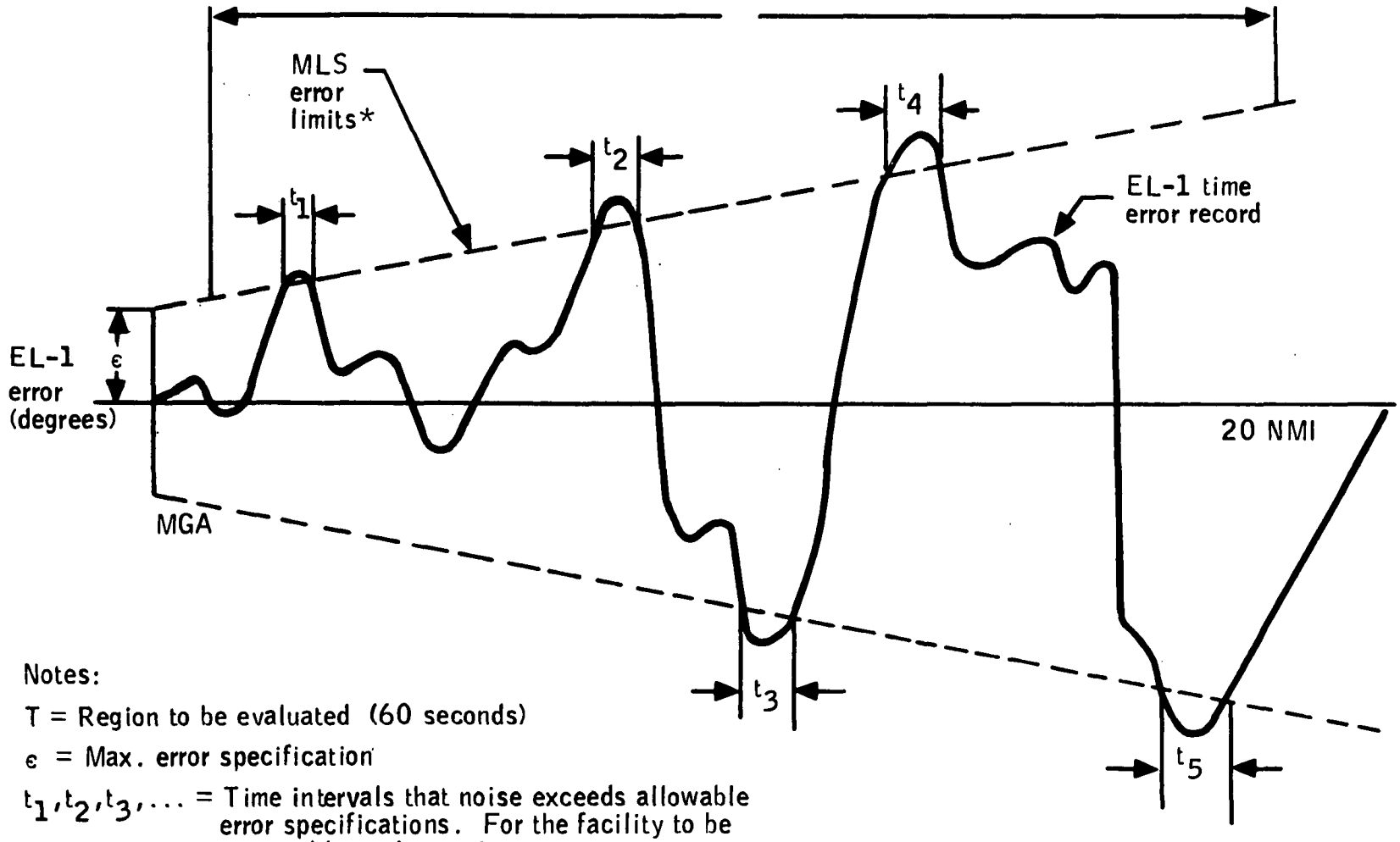

Notes:

T = Region to be evaluated (60 seconds)

ε = Max. error specification

$t_1, t_2, t_3, \ldots$ = Time intervals that noise exceeds allowable error specifications. For the facility to be acceptable in this region:

$$\frac{100\left[T - (t_1 + t_2 + t_3 \ldots)\right]}{T} \geq 95\%$$

Figure A-1 -- Time Error Record Analysis of Path Following Filter Output and Control Motion Filter Output

Table A-1 -- Path Following Error Specification,
Type 3 Equipment

	Bias		Path following Noise		Path following Error (2σ)		Distance To error Window	Path following error allowable degradation (1)		
	Ft (3)	Degree	Ft (3)	Degree	Ft (3)	Degree		W/distance (2)	With Az angle	With El angle
Azimuth	10	.038	9	.034	14	.092	15,000′	Linearly to 0.16° at 20 NM	2:1 in angle from ℄ error at ±60° Az	2:1 in angle from 9° to 20°
Elevation	1.2	.06	1.4	.07	1.8	.092	1,145′	1.5:1 in angle at 20 NM	None	Proportional to angle above 2°
DME	-	-	-	-	40	-	16,000′	10:1 at 20 NM	None	None
Flare	1.2	.03	1.4	.032	1.8	.04	2,500′ (4)	2.5:1 in angle at 5 NM	None	4:1 angle from 2° to 8° elevation
Rate limits to be determined										

(1) Degradation varies linearly between the limits indicated (see figure A-2.) Proportionality between bias and path following noise shall be maintained.
(2) R = slant range. Range is measured from elevation reference datum.
(3) Measured at error window; azimuth figures hold throughout the rollout zone.
(4) The linear errors hold throughout the touchdown zone.

Table A-2 -- Control Noise Specification

Antenna signal	Noise (2σ)	Allowable degradation		
		With distance	With azimuth angle	With elevation angle
Azimuth	0.04°	1.4:1 at 20 nmi	None	None
Elevation	0.05°	1.4:1 at 20 nmi	None	None
DME	40 feet	10:1 at 20 nmi	None	None
Flare	.02	1.5:1 at 5 nmi	None	None

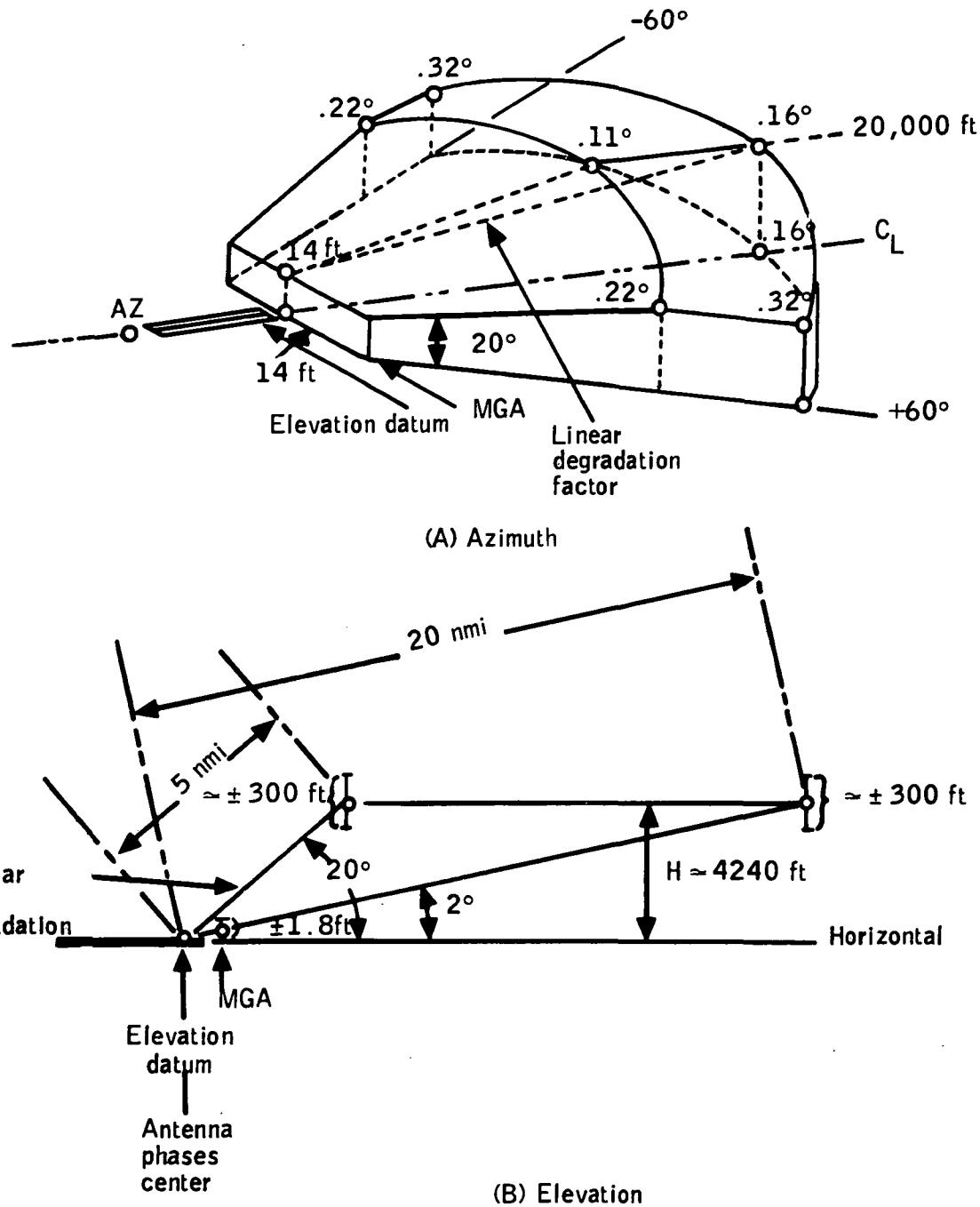

Figure A-2 -- Allowable Degradation Characteristics for Type 3 Subsystem

ERROR INTERPRETATION

Procedures are outlined below which relate the measured parameters to the specification for accuracy. Refer to Figure A-3 for definition of points outlined below and to Table A-4 for the filter configurations.

Point A: MLS Raw Error Data.

Point B: Time Average over any 60-second Portion of Flight Course. Course Bias - See Table A-1 for limits.

Point C: Path Following Error; see Table A-1 for limits; use technique described in Figure A-1 for calculation.

Point D: Use Table A-2 for limits.

Data Rate: The MLS signal format shall accommodate different data rates in different configurations. The format shall be capable of providing the minimum information update rates for the functions in each configuration as shown in Table A-3.

TABLE A-3. MLS MINIMUM INFORMATION UPDATE RATES

FUNCTION	UPDATES PER SECOND
All angle functions except Flare	5
Flare	10
Aircraft Carrier Landing -	
Azimuth	10
Elevation	10
DME Interrogation Rate -	
Normal	40
On-Ground	5
NOTE: All numbers update per second	

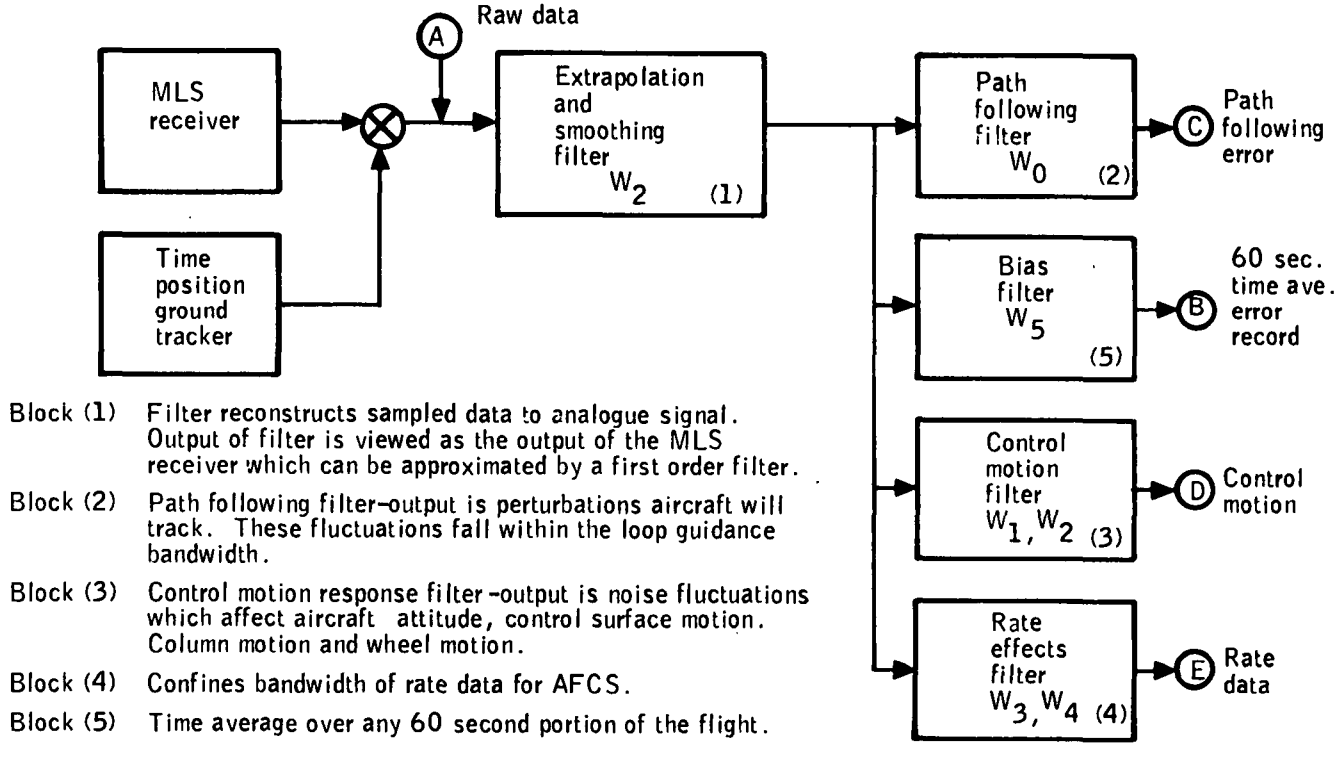

Block (1) Filter reconstructs sampled data to analogue signal. Output of filter is viewed as the output of the MLS receiver which can be approximated by a first order filter.

Block (2) Path following filter-output is perturbations aircraft will track. These fluctuations fall within the loop guidance bandwidth.

Block (3) Control motion response filter-output is noise fluctuations which affect aircraft attitude, control surface motion. Column motion and wheel motion.

Block (4) Confines bandwidth of rate data for AFCS.

Block (5) Time average over any 60 second portion of the flight.

Figure A-3 -- MLS Measurement Methodology

Table A-4 -- Filter Configurations and Corner Frequencies

Guidance function	Corner frequencies (radians/sec)					
	ω_0	ω_1	ω_2	ω_3	ω_4	ω_5
AZ	.05	0.3	10	2	4	.05
El	1.5	0.5	10	2	4	.05
Flare	2.0	0.5	10	2	4	.05
DME	10	0.5	10	TBD	TBD	.05

Filter configurations

Smoothing filter $\dfrac{\omega_2}{S+\omega_2}$

Path following filter $\dfrac{\omega_n^2}{S^2+2\xi\omega_n S+\omega_n^2}$; $\xi = 1$; $\omega_0 = .64\omega_n$

$$\omega_0=\omega_n \sqrt{1 - 2\xi^2 + (4\xi^4 - 4\xi^2 + 2)}^{1/2}$$

Control Motion filter: $\dfrac{S}{S+\omega_1}$

Rate filter: $\left(\dfrac{S}{S+\omega_3}\right)\left(\dfrac{\omega_4}{S+\omega_4}\right)$

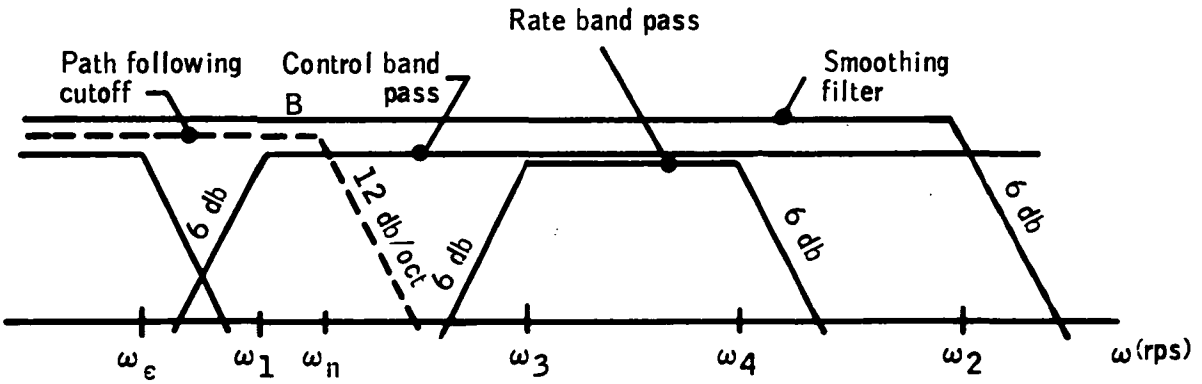

ANGULAR ERROR TOLERANCE RATIONALE

The MLS error budget uses lineal feet at the MGA as the primary error standard. The allowable angular error at the MGA depends on the distance of equipment from the MGA.

Azimuth

The azimuth angular error figures cited are for the longest runway for which that equipment is intended to be used. It should be noted that both A2 and A3 equipment meet the most stringent requirements in the MGA. The degradation factors are structured so as to give highly accurate centerline guidance for parallel runway operation (100 feet at 10 NM for type A3 equipment), and quite accurate guidance throughout the coverage (600 feet at 20 NM at ±60° azimuth) for ATC interface and curved path approaches.

Elevation

The elevation errors are specified lineally at the MGA. Since the steeper slopes intersect the MGA closer to the equipment, the angular error can degrade and still maintain the same altitude error (at steeper slopes the DME error will predominate anyway). For higher elevation angles at longer range, the degradation factors are structured to maintain constant vertical error at a given altitude.

APPENDIX B. MARSAM II COMPUTER PROGRAM SUMMARY

INTRODUCTION

The overall purpose of the MARSAM II program was to develop and implement a mathematical computer model for use in the performance assessment of reconnaissance sensor systems of varied types operating on prescribed aerial flight profiles against ground targets in specified background and weather environments. MARSAM II (the mathematical model acronym) addresses those aspects of sensor performance as are related to the capability of such systems to provide target identification detail. Specifically, the types of aerial sensor systems considered in the MARSAM II model are: frame and panoramic cameras, television, the visual observer, vertical and forward-looking infrared, side-looking and forward-looking radar, and ELINT. As applicable to the different sensor types, film record and/or display modes of operation are considered. In addition, there is provided as an integral part of the MARSAM II computer model a stored library of characteristic data for numerous target-elements, backgrounds, and weather conditions (such data is readily expanded or modified by the user analyst). Where the provided library data base is considered applicable to a given problem, the task of preparing model inputs is significantly eased for the user. Available outputs from MARSAM II range from detailed sensor system performance parameters and associated probability measures of detection, recognition and identification to mission success measures. The MARSAM II computer model was developed as a tool for use by sensor systems design analysts in their

preliminary sensor performance sensitivity studies and for use by systems operations analysts in establishing total reconnaissance or reconnaissance-strike system requirements. The usefulness of MARSAM II as an analytical tool may be measured in terms of the degree to which the user analyst becomes familiar with the extent of analytical detail and assumptions in the model and utilizes the model output not necessarily as only an end result for his particular problem, but also as meaningful input to additional assessment measures he has developed to evaluate system performance. References 3 and 11 describe the model and its use in detail. Part 1 summarizes the objectives, scope, and structure of the MARSAM II mathematical model. Part II presents the detailed systems analysis of the reconnaissance sensors addressed in the model.

MARSAM II SUMMARY DESCRIPTION

Figure B-1 illustrates the capabilities implemented in the MARSAM II model for the performance assessment of sensor systems of varied types operating on prescribed aerial flight profiles against ground targets in specified background and weather environments. Specifically, MARSAM II addresses those aspects of reconnaissance sensor performance as relate to capability to provide target identification detail. In summary, the MARSAM II model has been structured for efficient use by sensor system design analysts in their preliminary sensor performance sensitivity studies and by systems operation

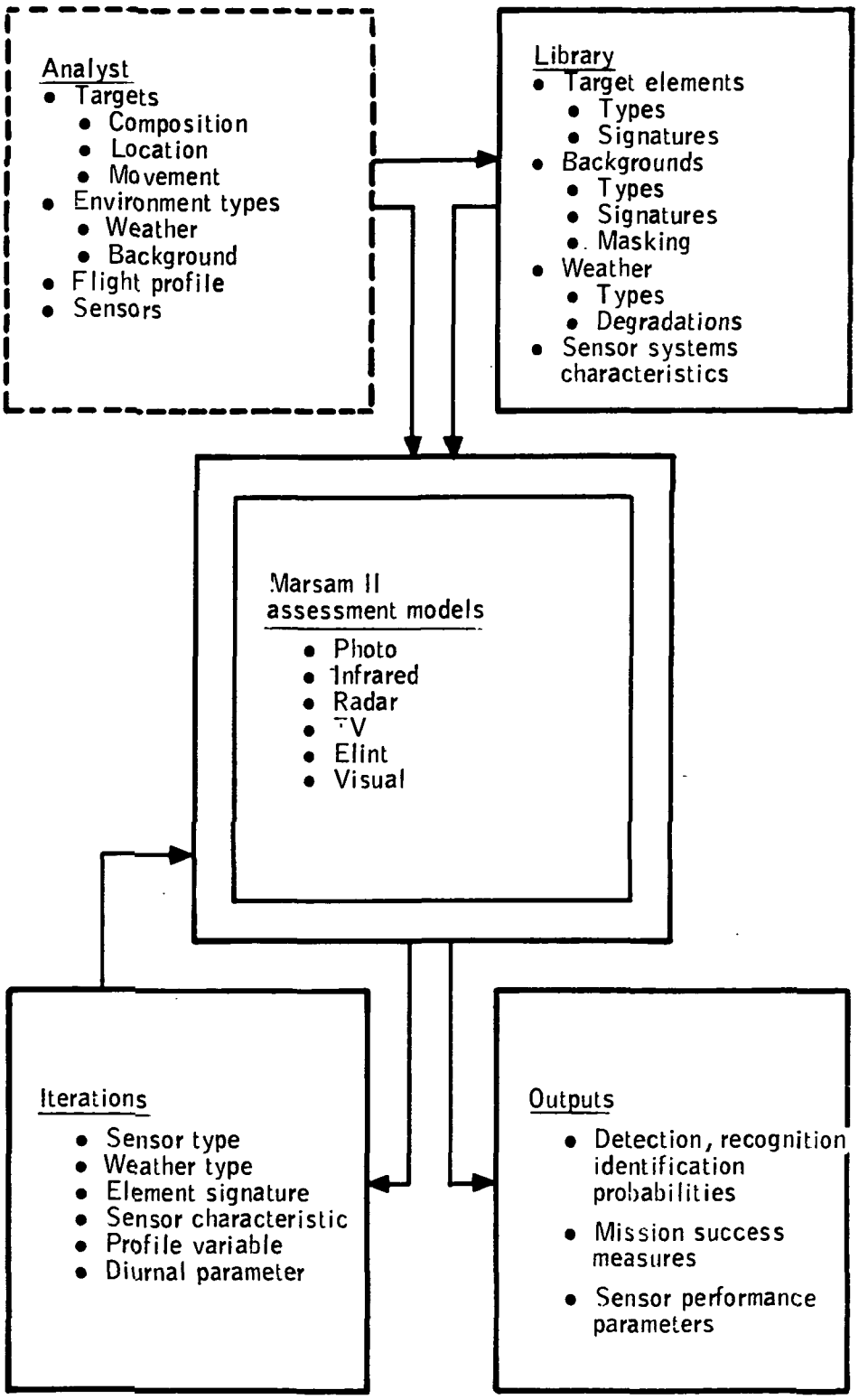

Figure B-1 -- MARSAM II Capabilities Summary

analysts in establishing or evaluating total reconnaissance or reconnaissance-strike system requirements. The particular analytical approaches followed and the level of detail considered in the various MARSAM II sensor models were dictated to a great extent by the nature and current general availability of input characteristic data, particularly that relating to sensor performance specifications and to target and background signatures. Thus, for example, while (a) the modulation transfer function approach to evaluation of reconnaissance sensor system performance and (b) the capability to examine in great detail the spectral and spatial variation in signatures may be desirable and mathematically tenable, there is a lack of sufficient data to exercise such considerations productively.

Simplification of model use results from availability of a library of target-element*/environment/sensor-system characteristic data, such library data base being an integral part of MARSAM. To input a problem to the model, the analyst describes target composition by a code number for each of the target elements within the target. Similarly, atmospheric and background environment characteristics may be input, in the main, by specification of code numbers. Thus, such code number inputs are used as the means to obtain from the library and input to the model a majority of the required target-element, enviroment, and sensor-system characteristic data (library data is readily expanded or modified as desired by the analyst).

Further simplification and efficiency of model use results from the automatic manner of sensor-to-target offset consideration. That is, for a specified sensor and specified flight speed and altitude, the model automatically determines and assesses sensor performance at only those aircraft-to-target offset distances for which at least one target element falls within the sensor field of view.

* In the vernacular of MARSAM, a target is defined as a group of one or more target elements where, for example, a target element may be a man, a truck, a boat, a hangar, a surface opening, etc.

MARSAM PROGRAM STRUCTURE

As indicated in the summary information flow diagram of Figure B-2, the MARSAM program consists of computer models which address the performance of sensors generically classed as to operation in the visual, the infrared, or the radio-frequency portion of the electromagnetic spectrum.

The four basic sections of the MARSAM Program are the computer program itself, the fixed data deck, the library data deck, and the executive deck. Included in the program section are all the required sensor system and subsystem option routines. The fixed data section contains data which is constant for all sensor models in the MARSAM Program. The library section consists of stored characteristic data for target elements, background and weather environments, and sensor subsystems. Such library data is available for use and modification through code-number call in the execution list. The execution list section, generated by the user, selects the data, defines a particular type of problem run, and specifies the desired output.

TV and FLIR Sensor Model Summary

This section presents a brief description and data flow diagram for the TV and FLIR sensor models in the MARSAM II computer programs. The basis for development and the detailed analytical treatment for each sensor model is contained in Reference 11. Also described here is the Human Factors Display Model which is utilized by both the TV and FLIR models.

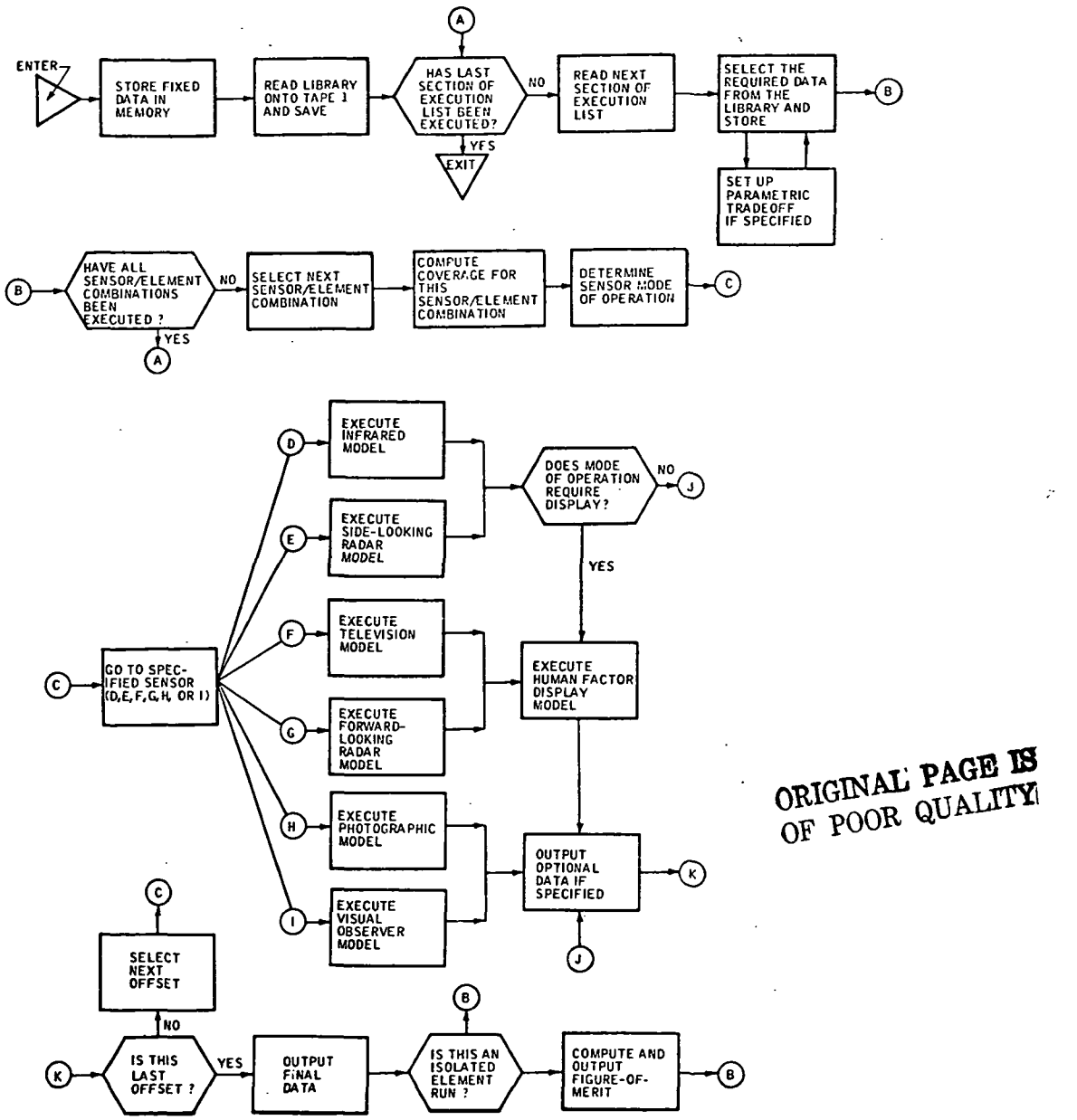

Figure B-2 --MARSAM Program Information Flow

Television (TV) Sensor Model (see Figure B-3)

The television sensor model addresses near real-time forward-viewing airborne television sensors. Alternate modes of system operation addressed within the model include (a) moving display, (b) stationary display, or (c) tracking. The moving display mode refers to a continuous and real-time presentation of data to an observer. The stationary display mode refers to the selection of a single frame of data and display of that frame for a period of time which equals or exceeds the normal frame time. While the two previously described modes generally apply to fixed sensor depression angles, the third mode refers to target-element tracking by continuously changing the sensor viewing angle so that the element is maintained in the field-of-view center until overflown. The model attempts only to predict the observer's target-element recognition performance under conditions of tracking; i.e., tracking accuracy is not evaluated. Outputs include probabilities of target-element detection and recognition.

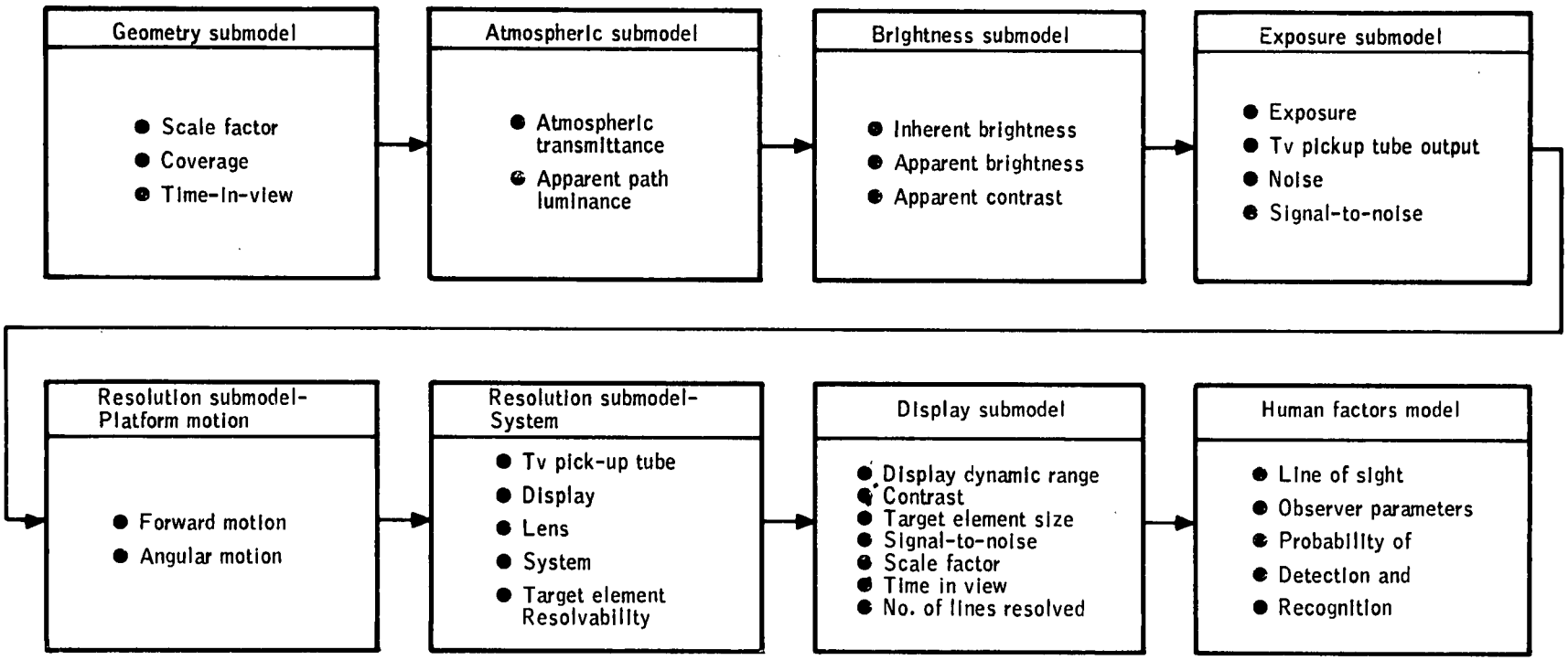

Figure B-3 -- Television Sensor Model Data Flow

Forward-Looking Infrared (FLIR) Model (see Figure B-4)

The forward-looking infrared model is addressed to forward-looking scanning systems in which imagery from successive scans is presented in near-real time to an operator-observed display. Alternate modes of operation considered in the model include (a) moving display, (b) stationary display, or (c) tracking. System operation within the 0.3- to 15-micron spectral region is considered. Model outputs include predictions of acquired target-element detection and recognition probabilities.

Human Factors Display Model (see Figure B-5)

The human factors display viewing model is drawn from model developments performed by Defense Research Corporation (DRC) under the sponsorship of the Advanced Research Projects Agency (ARPA). Depending on the sensor system considered, up to five probability submodels are used to determine target-element detection and recognition probabilities, i.e., an element size and contrast submodel, a search mode submodel, a confusing objects submodel, a signal-to-noise submodel, and a recognition submodel.

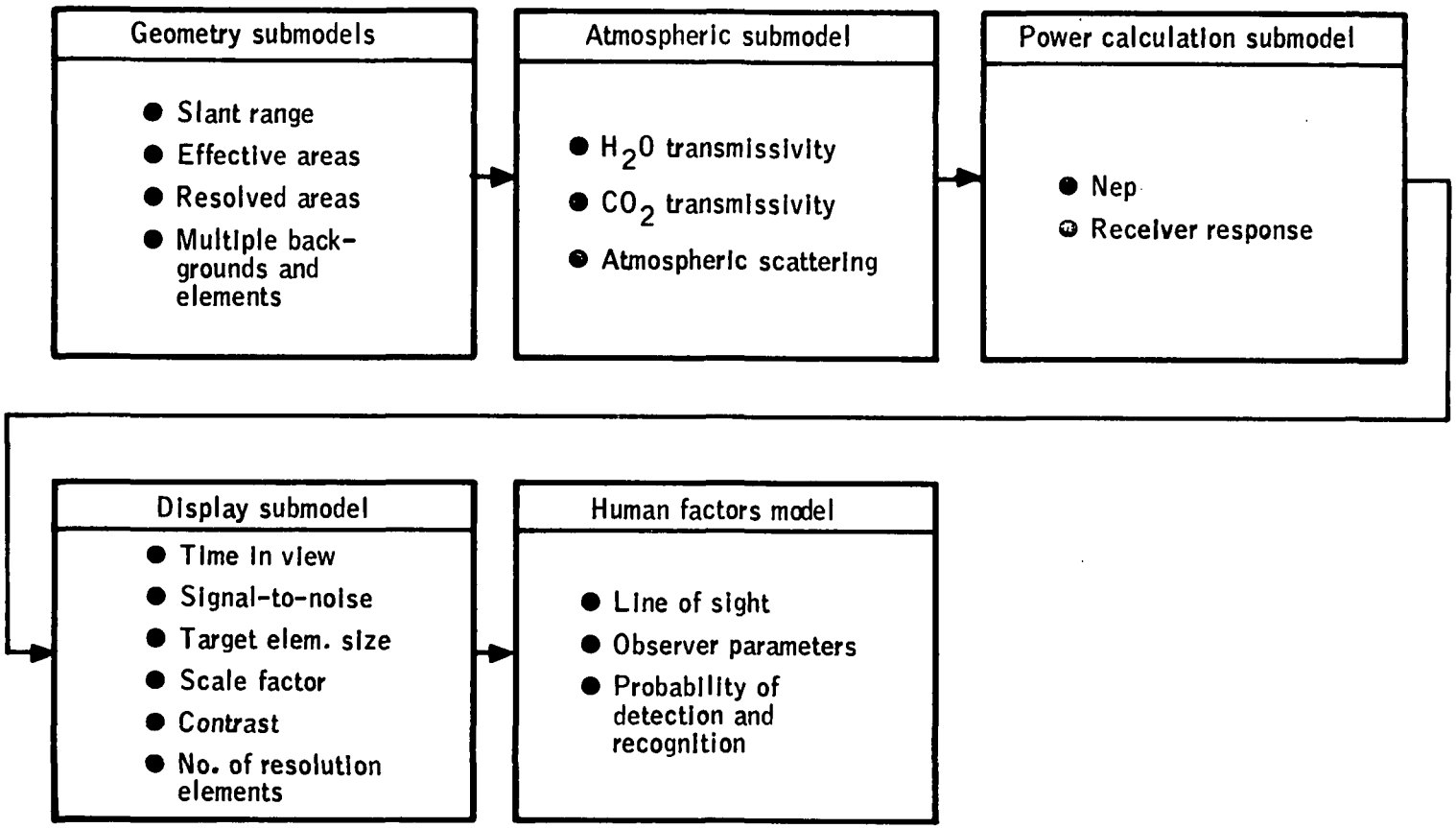

Figure B-4 -- Forward Looking Infrared Model Data Flow

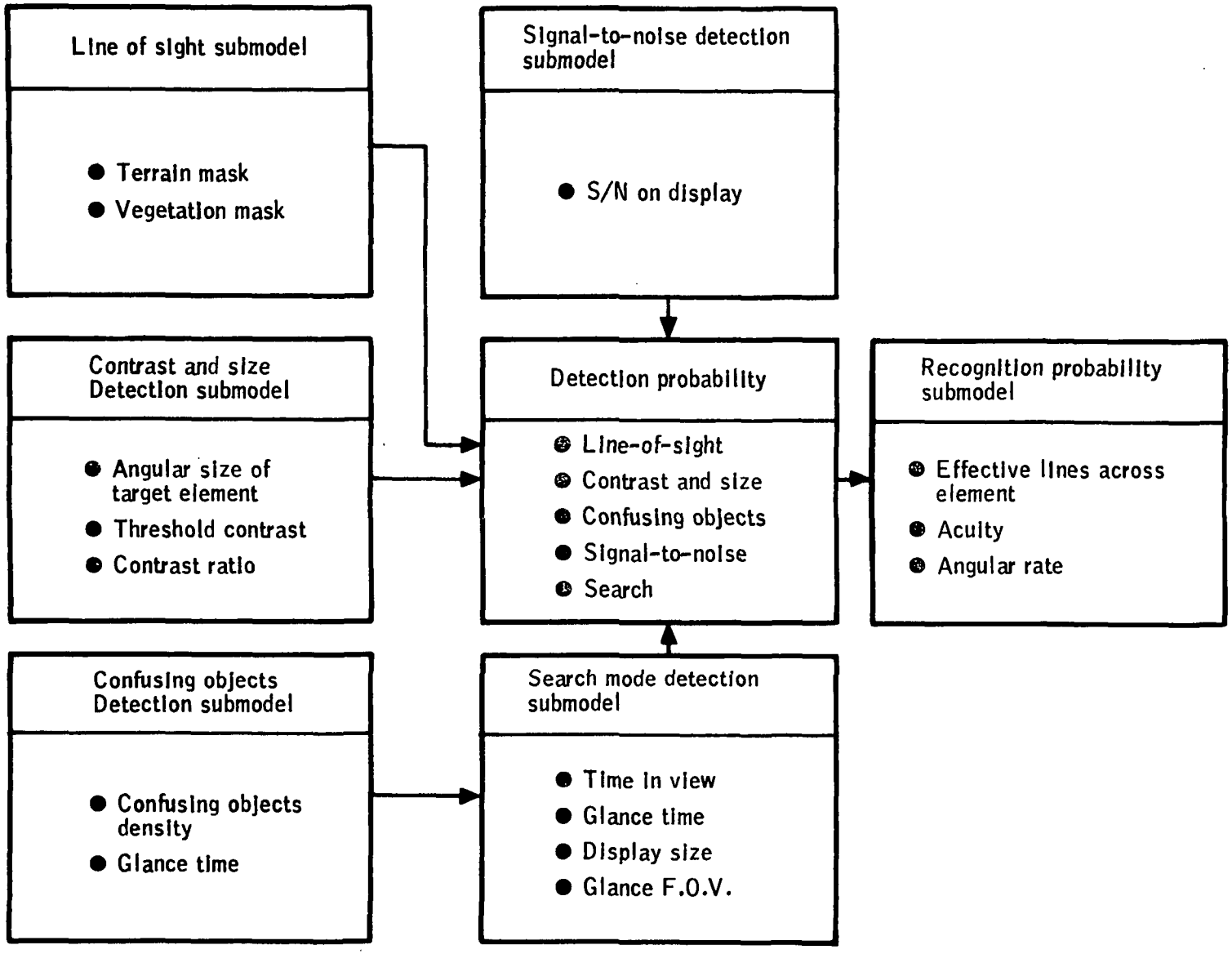

Figure B-5 -- Human Factors Display Model Data Flow

LIBRARY DATA

This section contains and references the characteristic environment, target-element, and sensor subsystem data stored in the MARSAM library. The ten major categories of stored data, accompanied by a brief description of the types of data contained, are listed below:

- o Terrain Characteristics
  - Line-of-sight probability data for six terrain types
- o Weather Characteristics
  - Data applicable to the photographic, television, visual observer, and infrared sensor models for five weather conditions
  - Data applicable to the radar sensor models for ten weather conditions
- o Turbulence Characteristics
  - Data applicable to the photographic sensor models for three turbulence types
- o Target-Element Signatures
  - Dimensions, photo/visual reflectivity, emissivity, and radar cross-section for 81 target elements
- o Background Signatures
  - Photo/visual reflectivity, emissivity, and normalized radar cross-section for 15 backgrounds.
- o Sensor Subsystem Characteristics
  - Performance characteristics for:

    A forward-looking infrared subsystem

    A TV image orthicon subsystem

    A TV vidicon subsystem

A forward-looking radar subsystem

A side-looking radar subsystem

A panoramic camera subsystem

- o Lens Subsystem Characteristics
  - Performance characteristics for two lenses, one applicable to the photographic sensor model and one applicable to the television sensor model.
- o Film Subsystem Characteristics
  - Data applicable to photographic systems for three film types and three developer/development-time combinations for each film
  - Data applicable to vertical infrared systems for one film type with seven developer/development-time combinations
- o Filter Subsystem Characteristics
  - Filter factor and filter function data for four filter types
- o Display Subsystem Characteristics
  - Performance characteristics for one cathode ray tube

Computer listings of all library data are given in Reference 3.

APPENDIX C

SCATTERING OF ELECTROMAGNETIC WAVES

INTRODUCTION

Various sensors which could be used for an ILM depend on their operation on the reflective properties of the terrain in the microwave region. Many measurements of these properties have been made, however, the preponderance of the data is at incidence angles between 10 and 80 degrees. Since ILM sensors must operate with incidence angles from about 84 to 89 degrees, these data are not directly usable.

In an attempt to obtain usable data, a theoretical formulation of electromagnetic scattering was developed and programmed on a computer under the assumption that if the theoretical model corresponded to the measured data at those points where data was available, the model could be used to generate the needed data at higher incidence angles. The model used was a statistically rough surface using the Kirchoff approximation and at first appeared to give good correspondence. It was later noted that the formulation was missing a cosine of the incidence angle. After correcting the model, no set of parameters in the theoretical model could give correspondence with the measured data. Several explanations are possible for this. It has been pointed out that the source from which the model was obtained has an error in the dominant term of the equation at high incidence angles. Another problem is that only diffuse reflections are considered in the model with specular components

handled independently. When the incidence angle is very high, the diffusely backscattered radiation may be less than the specularly backscattered radiation. Specular backscatter at high incidence angles seems a contradiction in terms but for a finite illumination it is meaningful. Since the illuminated surface is determined by the antenna pattern, this component depends primarily on the antenna used to measure it.

Because of the lack of success in obtaining a good theoretical model for scattering, the model, with the cosine removed, was used as an empirical fit in some sensor analyses. The total exercise demonstrate the need for subsequent measurement of typical terrain scattering at these angles.

SCATTERING PRINCIPLES

When an electromagnetic wave strikes an object, it is partially reflected in all directions. This reflection is the basis of radar, and extensive measurements have been made of the reflection from natural and man-made surfaces for use in radar-performance calculation. However, most of these measurements have been made in the backscattered direction, at incidence angles between 10 and 80 degrees. Therefore even for radar sensor analysis at high incidence angles the data is not directly usable.

The scattering in other directions is also important for sensor analysis. It is the source of multipath distortion, and a major contributor to mutual interference between sensors operating from different platforms. To properly evaluate sensor performance, it is therefore necessary to establish

the scattering properties of the surfaces involved.

The technique selected to establish the scattering properties is to obtain a theoretical model of scattering which can be justified from physical principles. Any such model will have various parameters which can be adjusted to modify the scattering properties, so that it can represent various surfaces. The model will be applied to the measured backscattered data to establish the values of the parameters for the surface, and these parameters will then be used to generate angular relationships.

Definitions for Scattering Parameters

The most physical scattering parameter is the reflection coefficient. It is defined in terms of the field strengths at the reflecting interface as

$$R = \frac{E_R}{E_I} \qquad \text{(C-1)}$$

where R is the reflection coefficient
E_R is the reflected field
E_I is the incident field

While this is an adequate parameter for perfectly conducting, finite size, smooth targets, it is difficult to use.

A more tractable scattering parameter is the differential radar cross section, derived from the radar range equation. The radar range equation is

$$P_r = \frac{P_t G_t}{4\pi r^2} \times \frac{\sigma}{4\pi r^2} \times \frac{\lambda^2 G_R}{4\pi} \qquad \text{(C-2)}$$

where P_r is the received power

G_t is the gain of the transmitting antenna

σ is the radar cross section

λ is the wavelength

G_R is the receiver antenna gain

r is the range from the radar to the target

The first term expresses the power density at the target. The second term is an expression which relates scattering to an equivalent area which captures all the incident power and isotropically reradiates all the power. The third term represents the capture of all the energy impinging on the receiver aperture.

Since the scattering of an isolated target is neither perfect nor isotropic, the radar cross section is a complicated function of incident and reflected angles, frequency, polarization, target geometry, etc., and contains all the deviations from perfect isotropic scattering.

For an area target, the concept of cross section is generalized to a dimensionless cross section per unit area, such that the radar range equation becomes:

$$P_r = \frac{P_t \lambda^2}{(4\pi)^3 r^4} \int_s \gamma G_t G_R \, dS \qquad \text{(C-3)}$$

where s is the reflecting surface

γ is the differential cross section per unit surface area.

G_t, G_R are the antenna gains in the direction of the differential area dS

This equation is often used in the form:

$$P_r = \frac{P_t G_t G_R \lambda^2}{(4\pi)^3 r^4} \int_s \gamma \, dS \qquad \text{(C-4)}$$

which assumes that the gain across the antenna beamwidth is constant and zero outside the beam. By examining this equation, it can be seen that for finite targets

$$\gamma = \frac{4 \pi A}{\lambda^2} R^2 \qquad \text{(C-5)}$$

where A is the target area

R is the reflection coefficient

λ is the wavelength.

The scattering geometry which will be used throughout is shown in Figure C-1. Horizontal polarization is defined as having the E vector in the XY plane, vertical polarization has the E vector in the XZ plane.

SMOOTH SURFACE REFLECTION

Scattering from an infinite smooth surface is the familiar mirror reflection obeying Snell's law. That is, any energy that is not absorbed or transmitted is reflected such that the angle of incidence is equal to the angle of reflection. Furthermore, the amplitude of the reflected field strength and the change in phase at reflection depends

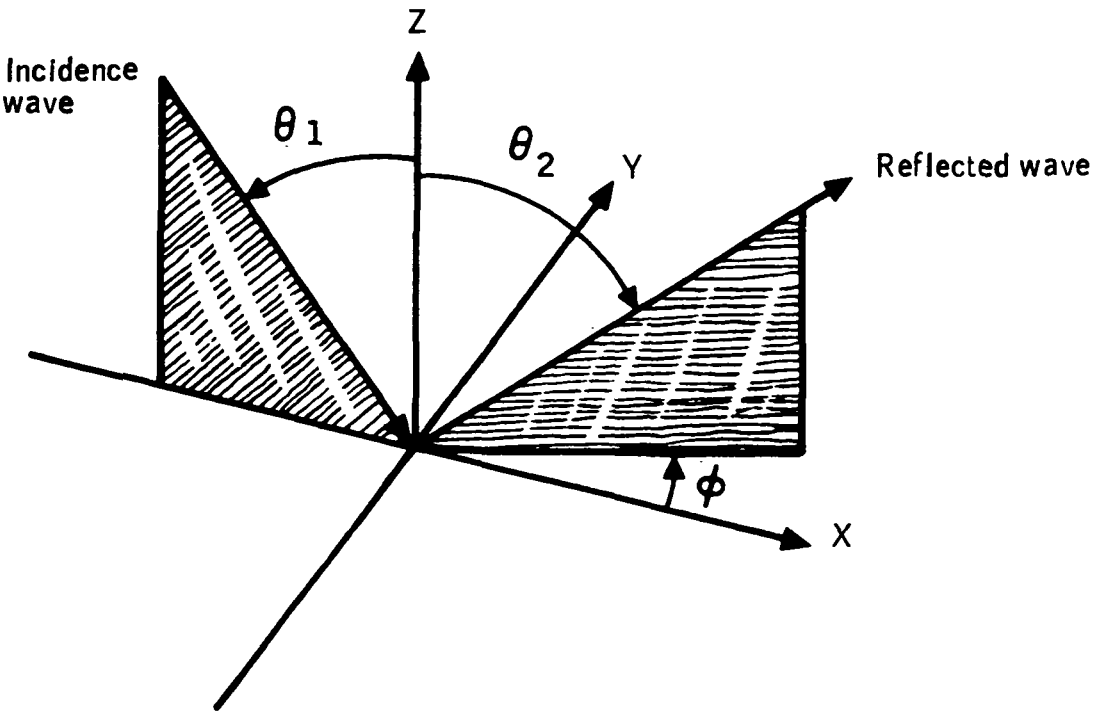

Figure C-1 -- Scattering Geometry

on the Fresnel reflection coefficient, which is a function of the polarization of the incident wave and the properties of the surface. For non-magnetic surfaces, the coefficients are:

$$R_V = \frac{\varepsilon_r \cos\theta_i - \sqrt{\varepsilon_r - \sin^2\theta_i}}{\varepsilon_r \cos\theta_i + \sqrt{\varepsilon_r - \sin^2\theta_i}} \qquad \text{(C-6)}$$

$$R_H = \frac{\cos\theta_i - \sqrt{\varepsilon_r - \sin^2\theta_i}}{\cos\theta_i + \sqrt{\varepsilon_r - \sin^2\theta_i}} \qquad \text{(C-7)}$$

where θ_i is the angle of incidence

ε_r is the complex permittivity

R_V is the reflection coefficient for vertical polarization

R_H is the reflection coefficient for horizontal polarization

For a perfectly conducting surface, ε_r becomes infinite and $R_V=1=-R_H$. Thus, all the energy is reflected, the vertically polarized portion with no phase change and the horizontally polarized component with a 180° phase change. However, if the surface is not perfectly conducting the reflection coefficient at low grazing (high incidence) angles becomes $R_V=R_H=-1$. Some values of the reflection coefficients are shown in Figure C-2 for typical earth and sea permittivities.

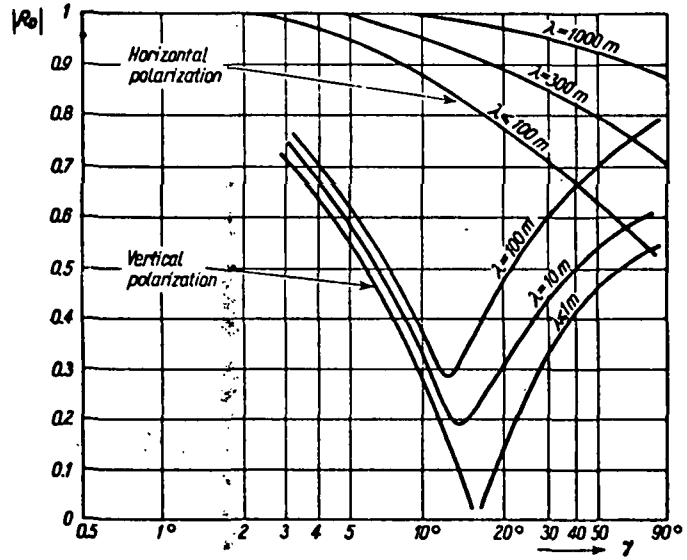

Reflection coefficient of a perfectly plane earth with $\varepsilon/\varepsilon_0 = 10$, $\sigma = 10^{-3}$ mho/m.

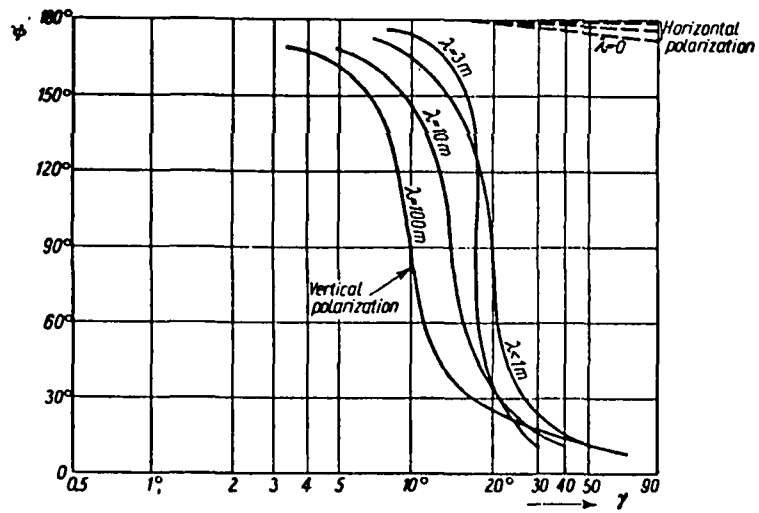

Phase Φ of the reflection coefficient of a perfectly plane earth. $\varepsilon/\varepsilon_0 = 10$, $\sigma = 10^{-3}$ mho/m.

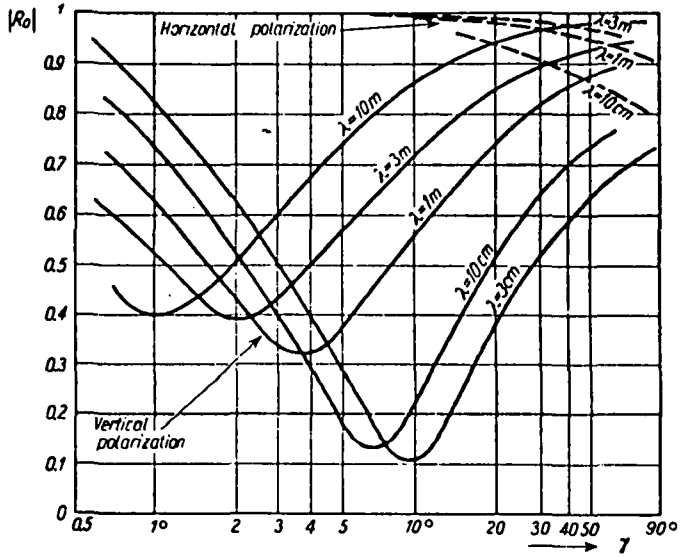

Reflection coefficient of a very smooth sea. $\varepsilon/\varepsilon_0 = 80$, $\sigma = 4$ mho/m.

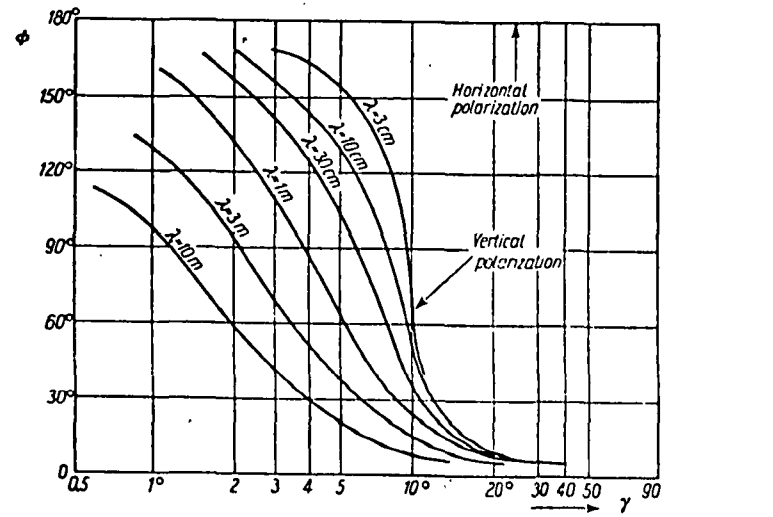

Phase Φ of the reflection coefficient of a very smooth sea. $\varepsilon/\varepsilon_0 = 80$, $\sigma = 4$ mho/m.

Figure C-2 -- Fresnel Reflection Coefficients

If the size of the surface is less than infinite, the energy will not be redirected perfectly due to the effect of fields on the edges of the surface. As the surface becomes smaller, the spread of the reflected beam increases. This aperture phenomenon is the szme as the diffraction in optics, or the gain functions for reflecting or aperture antennas. Figure C-3 illustrates this phenomenon.

The differential cross section of the target is:

$$\gamma_{pg} = \frac{4\pi}{\lambda^2} XY \ \text{sinc}^2 \frac{\pi \xi_x X}{\lambda} \ \text{sinc}^2 \frac{\pi \xi_y Y}{\lambda} \ |\alpha_{pg}|^2 \qquad \text{(C-8)}$$

where X is the dimension in the x direction

Y is the dimension in the Y direction

$$\text{sincx} = \frac{\sin x}{x}$$

$\xi_x = \sin \theta_1 - \sin \theta_2 \cos \phi$

$\xi_y = -\sin \theta_2 \sin \phi$

α is the polarization dependent reflection coefficient

g is the transmitting polarization

p is the receiving polarization

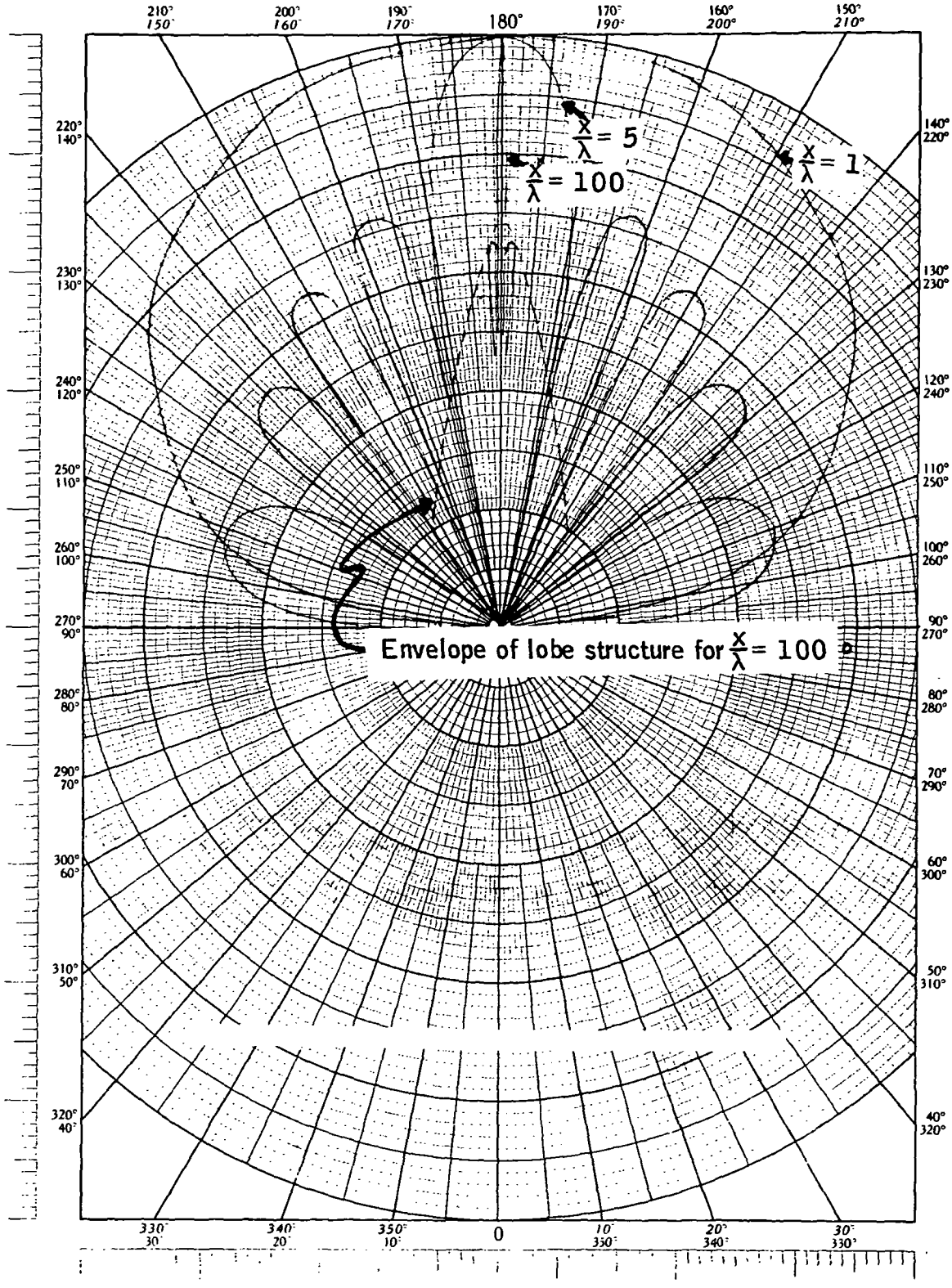

Figure C-3 -- Specular Scattering from a Smooth Finite Surface

For linear polarizations,

$$\alpha_{VV} = -\cos\Theta_2 \cos\emptyset R_V \qquad \text{(C-9)}$$

$$\alpha_{HV} = \sin\emptyset R_V \qquad \text{(C-10)}$$

$$\alpha_{VH} = \cos\Theta_1 \cos\Theta_2 \sin\emptyset R_H \qquad \text{(C-11)}$$

$$\alpha_{HH} = \cos\Theta_1 \cos\emptyset R_H \qquad \text{(C-12)}$$

STATISTICAL SURFACE MODELS

Most scattering of interest does not involve smooth flat surfaces, but rather rough surfaces. Grass, concrete, weeds, lake or ocean water are all examples of rough surfaces. A high sea state is considerably rougher than a concrete slab, but they are both rough.

Equations

The equations for scattering can be derived by assuming that the electric field at any point on the surface is the field that would be present on a tangent plane to that point. Then, either the Helmholtz integral can be evaluated in the far field (Ref. C-1) or the total area of "specular points" which have parallel tangent planes can be evaluated from the statistics of the surface roughness (Ref. C-3). Either technique leads to the same formula for scattering.

The Helmholtz integral at a point in the far field distance r from the surface is (Ref. C-1)

$$E = \frac{j \exp(jKr)}{4\pi r} \int_S (Fv\text{-}p) \cdot n \, e^{iv.r} \, dS \qquad \text{(C-13)}$$

where E is the electric field strength at the point per unit incident field

F is the Fresnel reflection coefficient

$V = K_1 - K_2$

K_1 is the propagation vector of the incident wave

K_2 is the propagation vector of the reflected wave

n is the unit normal to the surface

$p = K_1 + K_2$

For a finite surface area in cartesian coordinates,

$$E = \frac{jk \exp(jkr)}{4 \pi r} \int_S (a\rho'_x + c\rho'_y - b) \; e^{j\vec{v}\cdot\vec{r}} \; dS \qquad \text{(C-14)}$$

where $a = (1-F)\sin\theta_1 + (1+F) \sin \theta_2 \cos\phi$

$b = (1-F) \cos \theta_2 - (1-F) \cos \theta_1$

$c = (1+F) \sin \theta_2 \cos\phi$

$\rho(x,y)$ is the height of the surface at (x,y)

$$\rho'_x = \frac{d\rho}{dx}$$

Since the field due to a perfectly conducting area of the same size is

$$E = \frac{jkA \cos \theta_1 \exp (jkr)}{2 \pi r} \qquad \text{(C-15)}$$

A reflection coefficient for the rough surface can be defined as

$$\rho = \frac{1}{2A\cos\theta_1} \int_S (a\rho'_x + C \; \rho'_y - b) \; e^{i\vec{v}\cdot\vec{r}} dS \qquad \text{(C-16)}$$

where $\vec{v} = \frac{2\pi}{\lambda} \left[(\sin \theta_1 - \sin\theta_2 \cos \phi)\, \vec{i} - \sin\theta_2 \sin\phi \vec{j} - (\cos\theta_1 + \cos\theta_2)\, \vec{k}\right]$

$\vec{i}, \vec{j}, \vec{k}$ is the unit vector triad

F is the local reflection coefficient. Neglecting the effects of fields at the edges of the surface and assuming the surface to be isotropically rough, the mean value for a perfectly conducting surface is (ref. C-1)

$$\langle\rho\rangle = \chi(V_Z)\ \mathrm{sinc}\ \frac{V_x X}{2}\ \mathrm{sinc}\ \frac{V_y Y}{2} \qquad \text{(C-17)}$$

where V_x is the x component of v

$\chi(V_x)$ is the characteristic function of the random variable ρ

The mean value of ρ is thus the reflection reduction factor to account for the finite size of the reflecting surface. Its value is of significance only near the specular direction (incidence equal to reflection), where the definition of near depends on the size of the surface.

The variance of ρ has values of significance at angles other than specular. Since the received power is proportional to ρ^2, power will be scattered over other angles. This power is referred to as the diffuse reflection. The mean square value of the reflection coefficient, obtained by multiplying ρ by its conjugate, taking the expectation, changing to cylindrical coordinates and integrating overall angles is (Ref. C-1).

$$\langle\rho\bar{\rho}\rangle = \frac{2\pi|F|^2}{A^2} \int_0^\infty J_o(V_{xy}T) \langle e^{tV_Z(\rho-\bar{\rho})}\rangle T\,dT \qquad \text{(C-18)}$$

where F is the local Fresnel reflection coefficient defined on pp. C-20 and C-21

$V_{xy} = \sqrt{V_x^2 + V_y^2}$

J_o is the Bessel function of order zero

T is a dummy radial distance variable

The integral in the expression for $\langle \rho\rho^* \rangle$ depends on $\langle e^{iv_t(\zeta - \zeta)} \rangle$, which is the characteristic function of the probability distribution of ζ. Therefore, to proceed further it is necessary to define this distribution. By the central limit theorem, it can be expected that the surface is Guassianaly distributed in height. Two correlation functions, corresponding to "peaky" and more smoothly bumpy surfaces will be investigated. The characteristic function for a gaussian surface is:

$$\langle e^{iv_z(\zeta - \zeta)} \rangle = \exp\left(-V_z^2 \sigma^2 (1 - C(\tau))\right) \qquad \text{(C-19)}$$

where σ^2 is the variance of surface height

$C(\tau)$ is the correlation coefficient

Slightly Rough Surfaces

If the surface is slightly rough in the sense that $V_z^2 \sigma^2 << 1$, then the power series for the exponential will converge rapidly enough that only the first term has significant contribution to reflection. In this case, the integral is readily evaluated yielding (Ref. C-1, C-4)

$$\langle \rho\rho^* \rangle = \frac{\pi |F|^2 V_z^2 \sigma^2 T^2}{A} \exp\left(-V_z^2 \sigma^2 - \frac{V_{xy}^2 T^2}{4}\right) \qquad \text{(C-20)}$$

if $C(\tau) = e^{-\tau^2/T^2}$

and

$$\langle \rho\rho^* \rangle = \frac{2\pi |F|^2 V_z^2 \sigma^2 T^2}{A \cos^2\theta (1 + V_{xy}^2 T^2)^{3/2}} \exp\left(-V_z^2 \sigma^2\right) \qquad \text{(C-21)}$$

if $C(\tau) = e^{-|\lambda|/T}$

The first form corresponds to smooth bumps, the second form to peaks, In both cases the specular component is ignored.

The differential cross section, obtained by multiplying by the target aperture gain and rearranging terms is

$$\gamma = (2\pi)^4 \left(\frac{\sigma}{\lambda}\right)^2 \left(\frac{T}{\lambda}\right)^2 |F|^2 \left(\frac{V_z}{K}\right)^2 \text{Exp}\left[-(2\pi)^2 \left(\frac{\sigma}{\lambda}\right)^2 \left(\frac{V_z}{K}\right)^2 + \left(\frac{T}{\lambda}\right)^2 \left(\frac{V_{xy}}{2K}\right)^2\right] \qquad \text{(C-22)}$$

$$\text{for } C(\tau) = e^{-\tau^2/T^2}$$

$$\gamma = \frac{2(2\pi)^4 |F|^2 \left(\frac{V_z}{K}\right)^2 \left(\frac{\sigma}{\lambda}\right)^2 \left(\frac{T}{\lambda}\right)^2 \exp -2\pi \left(\frac{\sigma}{\lambda}\right)^2 \left(\frac{V_z}{K}\right)^2}{\left(1 + (2\pi)^2 \left(\frac{T}{\lambda}\right)^2 \left(\frac{V_{xy}}{K}\right)^2\right)^{3/2}} \qquad \text{(C-23)}$$

$$\text{for } C(\tau) = e^{-|\tau|/T}$$

In this form the independence of the basic equations from frequency is evident. Except for defining roughness and correlation length in terms of wavelengths, these equations are independent of frequency.

Very Rough Surfaces

The other case which can be easily evaluated is the very rough surface, in the sense that $V_z \sigma^2 >> 1$. Since $V_z \sigma^2$ is very large, the characteristic function will have significant values only near $\tau=0$. Further, since the correlation function is by definition an even function, it's McLaurin series will contain only even powers. Since $C_j(0)=1$, this term contributes nothing to the expansion of the characteristic function about zero. Thus the only term of interest is the second derivative. Taking this expansion and performing the integration (ref C-4).

$$\langle \rho\rho^* \rangle = \frac{2\pi |F|^2}{A\, V_t^2 \sigma^2 C''(0)} \exp - V_{xy}^2 / 2V_z^2 \sigma^2 |C_j''(0)| \qquad \text{(C-24)}$$

for $C = e^{-t^2/T}$

$$\langle \rho\rho^* \rangle = \frac{2\pi F^2 V_z^2 \sigma^2}{T^2 A (V_z^2 \sigma^2 / T^2 + V_{xy}^2)^{3/2}} \qquad \text{(C-25)}$$

for $C = e^{-|\tau|/T}$

Converting to differential cross section,

$$\gamma = \frac{2 |F|^2 \left(\frac{V_z}{R}\right) \left(\frac{T}{\lambda}\right)^2}{\left(\frac{V_z}{R}\right)^4 \left(\frac{\sigma}{\lambda}\right)^2} \exp\left[- \frac{\left(\frac{T}{\lambda}\right)^2 \left(\frac{V_{xy}}{R}\right)^2}{4 \left(\frac{\sigma}{\lambda}\right)^2 \left(\frac{V_z}{R}\right)^2} \right] \qquad \text{(C-26)}$$

for $C(z) = e^{-\tau^2/T^2}$

$$\gamma = \frac{4\pi |F|^2 \left(\frac{V_z}{R}\right)^2 \left(\frac{\sigma}{\lambda}\right)^2}{\frac{T}{\lambda}\left[(2\pi)^2 \left(\frac{V_z}{R}\right)^4 \left(\frac{\left(\frac{\sigma}{\lambda}\right)^2}{\frac{T}{\lambda}} \right)^2 + \left(\frac{V_{xy}}{R} \right)^2 \right]^{3/2}} \qquad \text{(C-27)}$$

for $C(\tau) = e^{-|\tau|/T}$

where the equations are again written to emphasize the frequency independence of the basic equations.

Shadowing

At very low grazing angles, significant portions of the surface may be shadowed by the surface roughness, as the back sides of hills are shadowed from the sun. Obviously, these areas which are in the shadow cannot contribute to the reflected power.

To a first approximation, the effect of shadowing can be considered by multiplying the differential cross section by a shadowing function which represents the probability that a ray path is blocked from hitting an area of the reflecting surface. For backscattering from a normally distributed surface, regardless of surface correlation properties, this shadowing function is given by (ref C-5).

$$S_I = \exp.\ (-1/4 \tan \theta_1 \operatorname{erfc}(R\cot \theta_1)) \qquad \text{(C-28)}$$

where θ_1 is the incidence angle

$R = \frac{T}{2\sigma}$ for gaussian correlation

$\frac{T}{\sqrt{2}\sigma}$ for exponential correlation.

The function S is shown for various values of k in Figure C-4. If $k\cot \theta_1 >> 1$, the complementary error function can be approximated by its asymptotic expansion yielding:

$$S_I = \exp\left(- \frac{1}{2\sqrt{\pi}\ K} \tan^2\theta_1\ e^{-R^2 \cot^2 \theta_1}\right) \qquad \text{(C-29)}$$

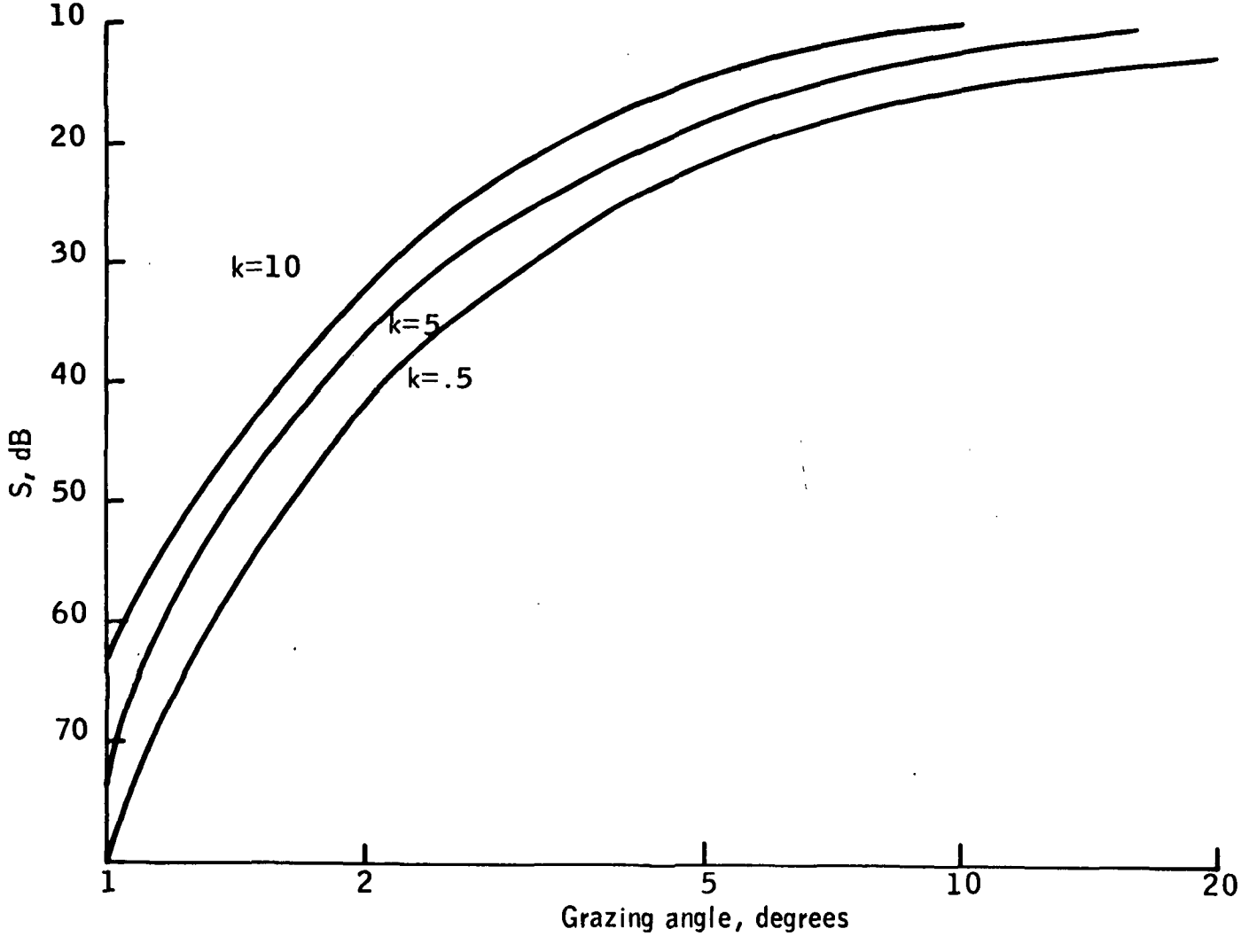

Figure C-4 -- The Shadowing Function

For bistatic scattering, the only change necessary is to allow for the probability that an area which is illuminated cannot be seen by the receiver. If the reflected angle is less than the incident angle, i.e., nearer the zenith, this probability is zero. Otherwise, the shadowing function is of the same form as the incidence shadowing function, replacing the incidence angle with the reflected angle. Thus

$$S_R = \begin{cases} \exp\left(-1/4 \tan\theta_2 \operatorname{erfc}(R\cot\theta_2)\right) & |\theta_2| > |\theta_1| \\ 1 & |\theta_2| < |\theta_1| \end{cases} \qquad \text{(C-30)}$$

The overall shadowing function is the product of the incidence and reflected shadowing functions or

$$S = S_I S_R \qquad \text{(C-31)}$$

Polarization Dependency

The local Fresnel reflection coefficient used in the scattering equations is a function of the angles of incidence and reflection, the local slope of the surface, the complex permittivity of the surface, and the polarization of the incidence and received waves.

Assuming that all reflected energy comes from specular points, the local Fresnel coefficient for arbitrary scattering angles and linear polarization can be derived by geometry (Reference C-7):

$$F_{VV} = \frac{a_2 a_3 R_v(i) + \sin\theta_2 \sin^2\phi R_H(i)}{a_1 a_4} \qquad \text{(C-32)}$$

$$F_{HV} = \sin\phi \frac{\sin\theta_2 a_2 R_H(i) - \sin\theta_1 a_3 R_V(i)}{a_1 a_4} \quad \text{(C-33)}$$

$$F_{VH} = \sin\phi \frac{\sin\theta_2 a_2 R_V(i) - \sin\theta_1 a_3 R_H(i)}{a_1 a_4} \quad \text{(C-34)}$$

$$F_{HH} = \frac{-\sin\theta_1 \sin\theta_2 \sin^2\phi R_V(i) - a_2 a_3 R_H(i)}{a_1 a_4} \quad \text{(C-35)}$$

where $a_1 = 1+a_5$

$a_2 = \cos\theta_1 \sin\theta_2 + \sin\theta_1 \cos\theta_2 \cos\phi$

$a_3 = \sin\theta_1 \cos\theta_2 + \cos\theta_1 \sin\theta_2 \cos\phi$

$a_4 = \cos\theta_1 + \cos\theta_2$

$a_5 = \sin\theta_1 \sin\theta_2 \cos\phi - \cos\theta_1 \cos\theta_2$

$i = \arctan\sqrt{\frac{1+a_5}{1-a_5}}$

F_{JK} is the local Fresnel coefficient for J polarized transmission and K polarized reception.

Since this set of equations defines a scattering matrix, the reflection for arbitrary polarizations can be derived from it. In particular, for the circular polarizations.

$$F_{LR} = \frac{F_{HH} + F_{VV} + j\,(F_{HV} - F_{VH})}{2} \quad \text{(C-36)}$$

$$F_{RR} = \frac{F_{HH} - F_{VV} + j(F_{HV} + F_{VH})}{2} \quad \text{(C-37)}$$

$$F_{RL} = \frac{F_{HH} + F_{VV} - j\,(F_{HV} - F_{VH})}{2} \quad \text{(C-38)}$$

$$F_{LL} = \frac{F_{HH} - F_{VV} - j\,(F_{HV} + F_{VH})}{2} \quad \text{(C-39)}$$

For linearly polarized backscattering, the expression for F_{VV} and F_{HH} become the same since i goes to zero. Thus, for backscatter,

$$F_{VV} = F_{HH} = \frac{a_2 a_3}{a_1 a_4} R_V(0) = \frac{R_v(\sigma)}{\cos\theta_i} \qquad \text{(C-40)}$$

Since measurements have shown differences between horizontally and vertically polarized backscatter, some other factor must cause the difference. A plausable explanation lies in the assumption of isotropic roughness. Consider the bump of Figure C-5. If radiation is incident on this bump and specular point backscatter occurs, the field at the surface appears to be locally horizontally polarized, regardless of its polarization relative to the mean surface plane. However, the slope or correlation distance seen by a horizontally or vertically polarized wave can be considerably different. In the figure, a horizontally polarized wave sees a steeper slope than a vertically polarized wave. Therefore, it is possible that different surface parameters should be used for different polarizations.

Computer Program

Since the scattering equations of the previous sections are extremely complex, a FORTRAN subroutine has been written to compute the differential cross section. All of the models given in the previous sections are included in this program, as are all combinations of vertical, horizontal, and circular polarization.

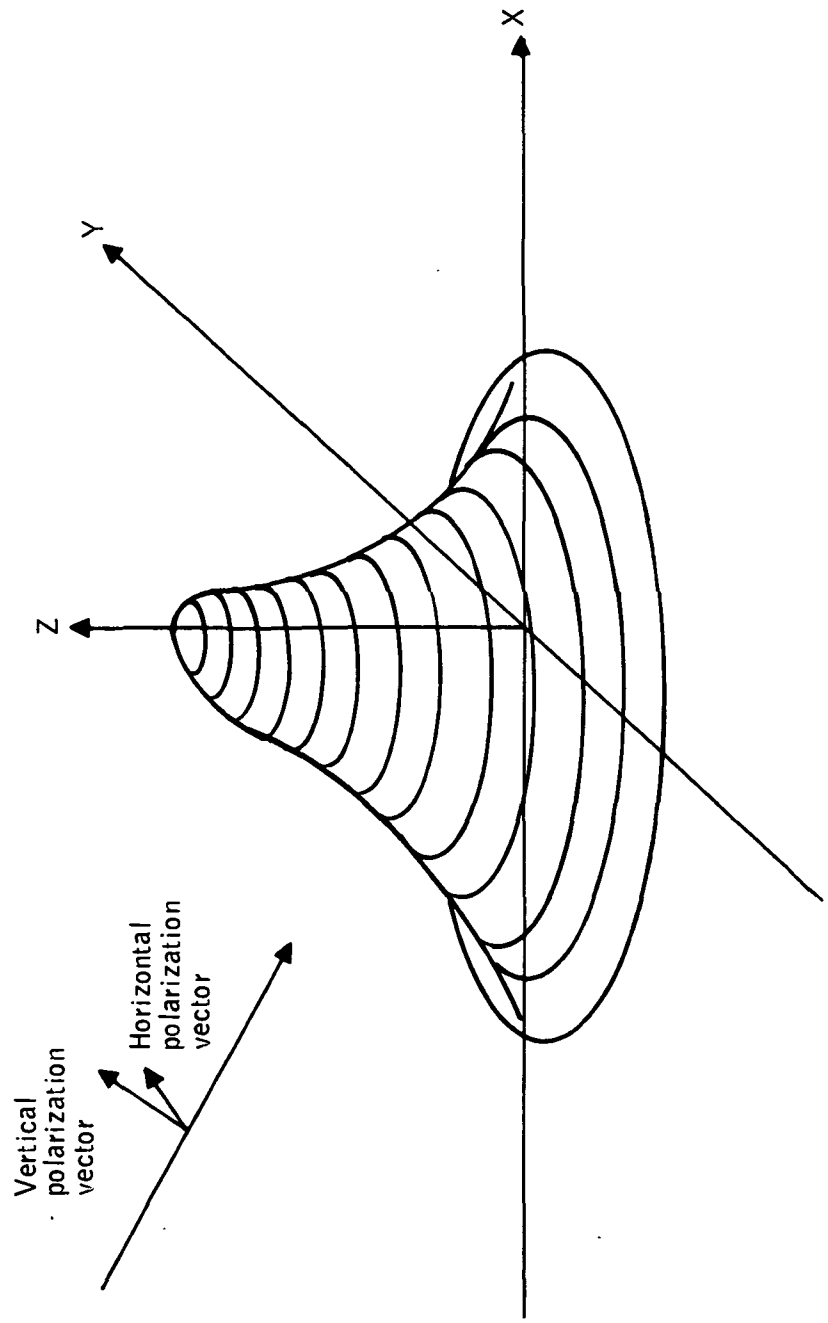

Figure C-5 -- Isotrophic Roughness

Being a subroutine, the scattering equations can be included in other analysis programs. The subroutine is called by the statement

CALL STSCAT (AINC, AREFL, AOAZ, PRMTIV, IPOL, ICOR, ROUGH, SLOPE, GAMDB)

where AINC is the incidence angle θ_1, in degrees

AREFL is the reflection angle, θ_2, in degrees

AOAZ is the angle off azimuth, ϕ, in degrees

PRMTIV is the surface permittivity, a complex number

IPOL is an indicator of polarization,

IPOL = 1 vertically transmission and reception

IPOL = 2 vertical transmission, horizontal reception

IPOL = 3 horizontal transmission, vertical reception

IPOL = 4 horizontal transmission and reception

IPOL = 5 left circular transmission and reception

IPOL = 6 right circular transmission and reception

IPOL = 7 right circular transmission,
left circular reception

IPOL = 8 left circular transmission,
right circular reception

ICOR is an indicator of surface correlation type

ICOR = 0 gaussianly correlated surface

ICOR = 1 exponentially correlated surface

ROUGH is the scale surface roughness $\sigma/_\lambda$

SLOPE is the scale surface slope $T/_\lambda$

GAMDB is the differential cross section γ, in decibels.

A main program, used to test the subroutine and establish surface parameter values has also been written. The test program obtains back-scattering cross sections from 10 to 80 degrees, and plots these cross sections along with a set of values which are input. By examining the resultant plot, it can be immediately determined how well the theoretical results match the measured data.

The name of the test program is TSTSCAT. The program reads in from the teletype values for the constant (measured) plot, scale roughness, scale slope, and permittivity. Polarization and correlation are changed by modifying the program. The call to STSCAT is made with continuation lines to enable modifying IPOL and ICOR with literals. Line 180 is IPOL, line 190 is ICOR. Thus, to enter a value of IPOL, the following program modification would be made

180 &[IPOL] ,

where [IPOL] is the value of IPOL, to change correlation, the equivalent modification is

190 & [ICOR] ,

A listing of the entire program, including the test drive program and the subroutine STSCAT follows:

```
1**RUN *;LIBRARY/PLOT,R
010     DIMENSION RESULT(10),ANGLE(10),INGAM(10),YPLT(2)
011     REAL INGAM
12     REAL KPLT
020     CHARACTER REP*3,YES*3
021     COMPLEX PRMTIV
23     YES="YES"
24     REP="NOP"
030     PRINT 60
031 31 PRINT 34
032     READ 33,(INGAM(I),I=1,10)
033 33 FORMAT(10F6.1)
034 34 FORMAT("INPUT ARRAY TO MATCH.")
040 40 PRINT 70
050     READ 80,RGH
060 60 FORMAT("INPUT PARAMETERS.")
070 70 FORMAT("SURFACE ROUGHNESS")
080 80 FORMAT(F6.4)
090 90 FORMAT("SURFACE SLOPE")
100     PRINT 90
110     READ 80,SLP
111     PRINT 112
112 112FORMAT("PERMITTIVITY",)
113     READ 114,PRMTIV
114 114FORMAT(2F6.1)
115     PRINT 115,PGH
116 115FORMAT(//"ROUGHNESS=",F6.4)
117     PRINT118,PRMTIV
118 118FORMAT("PERMITIVITY=",F6.2,"+J",F6.2)
120     DO 10 I=1,8
130     THETA1=I/5.729
140     THETA2=-THETA1
150      PHI=0
160     CALL STSCAT(THETA1,THETA2,PHI,
1706 PRMTIV,
1806 4,
1906 1,
2006 RGH,
2106 SLP,
2206     SIG)
```

```
230      RESULT(I)=SIG
240  10 ANGLE(I)=10*I
250     PRINT 260,SLP
260  260FORMAT("SLOPE=",F6.2)
270     PRINT 20,(ANGLE(I),I=1,10)
280     PRINT 30,(RESULT(I),I=1,10)
281     PRINT 282
282  282FORMAT(//)
290  15 CONTINUE
300  50 CONTINUE
305     PRINT 306
306  306FORMAT("PLOT ")
307     READ 380,REP
308     IF(REP.NE.YES) GO TO 338
310  20 FORMAT(10HINCIDENCE ,10F6.2)
320  30 FORMAT(10HCROSS SECT,10F6.2)
321     NMPT=2
322     YMAX=-10
323     YMIN=-50
324     CALL PLOT(XPLT,YPLT,YMAX,YMIN,NMPT,1,36)
325     KPLT=0
326     LPLT=1
327     DO 337 JPLT=1,36
328     XPLT=8+2*JPLT
329     LPLT1=LPLT+1
330     YPLT(1)=KPLT/5.0*(RESULT(LPLT1)-RESULT(LPLT))+RESULT(LPLT)
331     YPLT(2)=KPLT/5.0*(INGAM(LPLT1)-INGAM(LPLT))+INGAM(LPLT)
332     CALL PLOT(XPLT,YPLT,YMAX,YMIN,NMPT,0,36)
333     KPLT=KPLT+1
334     IF(KPLT.LT.5)GO TO 337
335     KPLT=KPLT-5
336     LPLT=LPLT+1
337  337CONTINUE
338  338PRINT 370
340     READ 380,REP
350     IF(REP.EQ.YES)GO TO 40
361     PRINT 364
362     READ 380,REP
363     IF(REP.EQ.YES)GO TO 31
364  364FORMAT("ANOTHER ARRAY",)
365  370 FORMAT("ANOTHER CASE")
370  380FORMAT(A3)
380                                     STOP
390                                     END
1010 SUBROUTINE STSCAT(AINC,AREFL,AOAZ,PRMTIV,IPOL,ICOR,ROUGH,SLOPE,GAMDB)
1020     COMPLEX PRMTIV,BVV,BVH,BHV,BHH,RVERT,RHORZ,BETA,BCONJ,CTEMP
1030     SNINC=SIN(AINC)
1040     SNREF=SIN(AREFL)
1050     SNOAZ=SIN(AOAZ)
1060     CSINC=COS(AINC)
1070     CSREF=COS(AREFL)
1080     CSOAZ=COS(AOAZ)
1082   TEMP1=AINC+AREFL
1083     IF(TEMP1.LT..00001)GO TO 430
1090     A5=CSINC*CSREF-SNINC*SNREF*CSOAZ
```

```
1100      TEMP1=(1-A5)/(1+A5)
1110      TEMP1=SQRT(TEMP1)
1120      LINC=ATAN(TEMP1)
1130      SLINC=SIN(LINC)
1140      CLINC=COS(LINC)
1150      CTEMP=PRMTIV-SLINC**2
1160      CTEMP=CSQRT(CTEMP)
1170      RVERT=(PRMTIV*CLINC-CTEMP)/(PRMTIV*CLINC+CTEMP)
1180      RHORZ=(CLINC-CTEMP)/(CLINC+CTEMP)
1190      A2=CSINC*SNREF+SNINC*CSREF*CSOAZ
1200      A3=SNINC*CSREF+CSINC*SNREF*CSOAZ
1210      IF(IPOL.GT.4)GO TO 230
1220      GO TO(230,270,310,350),IPOL
1230  230 BVV=A2*A3*RHORZ+SNINC*SNREF*SNOAZ**2*RVERT
1240      IF(IPOL.GT.4)GO TO 270
1250       BETA=BVV/(1-A5)
1260       GO TO 440
1270  270 BVH=SNOAZ*(SNREF*A2*RVERT-SNINC*A3*RHORZ)
1280      IF(IPOL.GT.4)GO TO 310
1290       BETA=BVH/(1-A5)
1300       GO TO 440
1310  310 BHV=SNOAZ*(SNREF*A2*RHORZ-SNINC*A3*RVERT)
1320      IF(IPOL.GT.4)GO TO 350
1330       BETA=BHV/(1-A5)
1340       GO TO 440
1350  350 BHH=-(SNINC*SNREF*SNOAZ**2*RHORZ+A2*A3*RVERT)
1360      IF(IPOL.GT.4)GO TO 390
1370       BETA=BHH/(1-A5)
1380       GO TO 440
1390  390 IF(IPOL.LE.6)GO TO 420
1400       BETA=((REAL(BHH)+REAL(BVV)-AIMAG(BHV)+AIMAG(BVH))**2+(AIMAG(BHH)
1410     &          -REAL(BVH)+AIMAG(BVV)+REAL(BHV))**2)/4
1420       GO TO 450
1430  420 BETA=((REAL(BHH)-REAL(BVV)-AIMAG(BVH)-AIMAG(BHV))**2+(AIMAG(BHH)
14406           +REAL(BVH)-AIMAG(BVV)+REAL(BHV))**2)/4
1450       GO TO 450
1458  430 BETA=(PRMTIV+1-2*CSQRT(PRMTIV))/(PRMTIV-1)
1460  440 BETA=BETA*CONJG(BETA)
1470  450 EXYSQ=SNINC**2+SNREF**2-SNINC*SNREF*CSOAZ
1480       IF(ICOR.GT.0)GO TO 580
1490       IF((ROUGH*(CSINC+CSREF))**2.LT.1)GO TO 540
1500       GAMMA=2*BETA*(SLOPE/(ROUGH*(CSINC+CSREF)**2))**2*EXP(-.25*(SLOPE
1510     &          /(ROUGH*(CSINC+CSREF)))**2*EXYSQ)
1520       K=SLOPE/(2*ROUGH)
1530       GO TO 670
1540  540 GAMMA=1.5585455E3*BETA*(SLOPE*ROUGH)**2*EXP(-39.478417*((ROUGH*
1550     &          (CSINC+CSREF))**2+.25*SLOPE**2*EXYSQ))
1560  560 K=SLOPE/(2*ROUGH)
1570       GO TO 670
1580  580 IF((ROUGH*(CSINC+CSREF))**2.LT.1)GO TO 630
1590       TEMP1=39.478417*((CSINC+CSREF)*ROUGH)**4/SLOPE**2+EXYSQ
1600       GAMMA=12.56637*BETA*ROUGH**2/(SLOPE*TEMP1*SQRT(TEMP1))
1610       K=SLOPE/(1.414*ROUGH)
1620        GO TO 670
1630  630 TEMP1=1+39.474817*EXYSQ*SLOPE**2
```

```
      GAMMA=3.1170909E3*BETA*(ROUGH*SLOPE)**2*EXP(-39.478417*(ROUGH*(
     &          CSINC+CSREF))**2)/(TEMP1*SQRT(TEMP1))
       K=SLOPE/(1.414*ROUGH)
  670 IF(CSINC.GT.CSREF)GO TO 750
      TEMP1=ABS(SNREF/CSREF)
      IF(K/TEMP1.LT.1)GO TO 730
      TEMP2=EXP(-(K/TEMP1)**2)
      SHADR=EXP(-TEMP1**2*TEMP2/(3.5549*K))
      GO TO 760
  730 SHADR=EXP(-(TEMP1-K)/3.5549)
      GO TO 760
  750 SHADR=1
  760 TEMP1=ABS(SNINC/CSINC)
      IF(K/TEMP1.LT.1)GO TO 810
      TEMP2=EXP(-(K/TEMP1)**2)
      SHADI=EXP(-TEMP1**2*TEMP2/(3.55490707*K))
      GO TO 820
  810 SHADI=EXP(-(TEMP1-K)/3.5449077)
  820 GAMMA=GAMMA*SHADR*SHADI
  830 IF(GAMMA.GT.0)GO TO 870
      PRINT 880,GAMMA
  850 GAMDB=99.99
      GO TO 890
  870 GAMDB=10*ALOG10(GAMMA)
  880 FORMAT(11HGAMMA ERROR,F6.2)
  890 RETURN
      END
```

Correspondence with Measured Data

Ohio State University has, over the past two decades, conducted an extensive program of differential cross section measurement for various surfaces. In order to verify the theoretical solution, data from this study was compared to theoretical predictions.

The complex permittivity of concrete and asphalt were measured by Peake (Ref.62) by sawing a section of paving material and measuring the permittivity in a waveguide bridge. The values he found were:

Concrete,	X-band	$\varepsilon = 6.5 + j1.5$
	K-band	$\varepsilon = 5.5 + j\ .5$
Asphalt,	X-band	$\varepsilon = 4.3 + j\ .1$
	K-band	$\varepsilon = 2.5 + j\ .6$

Using these values of permittivity, several comparison runs were made. Figures C-6 and C-7 show the best matches found for concrete at X-band. Both vertical and horizontal polarization show significant deviations only at near vertical incidence. This is not an error in the theory, but is merely a result of ignoring the specular component of the reflection. At near vertical incidence, concrete at X-band appears quite smooth, and thus has a significant specular return. Since Peakes equipment only measured over a 1 foot square, the specular component can easily be significant at angles relatively far from vertical incidence. In both horizontal and vertical polarization, the best match was obtain for the same roughness, .024, but with slightly different slopes.

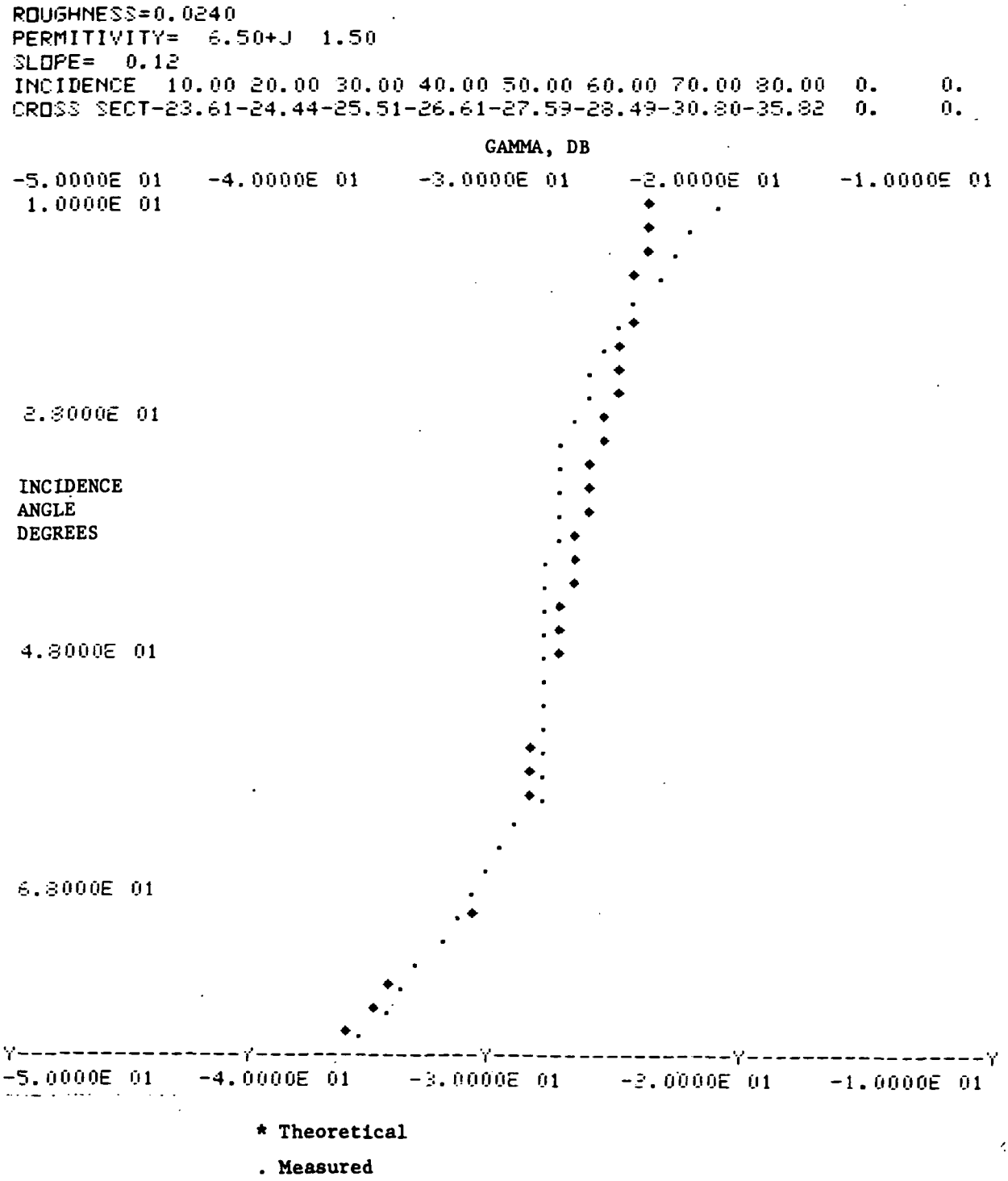

Figure C-6--Best Match for Backscatter from Concrete at X-band, vertical polarization

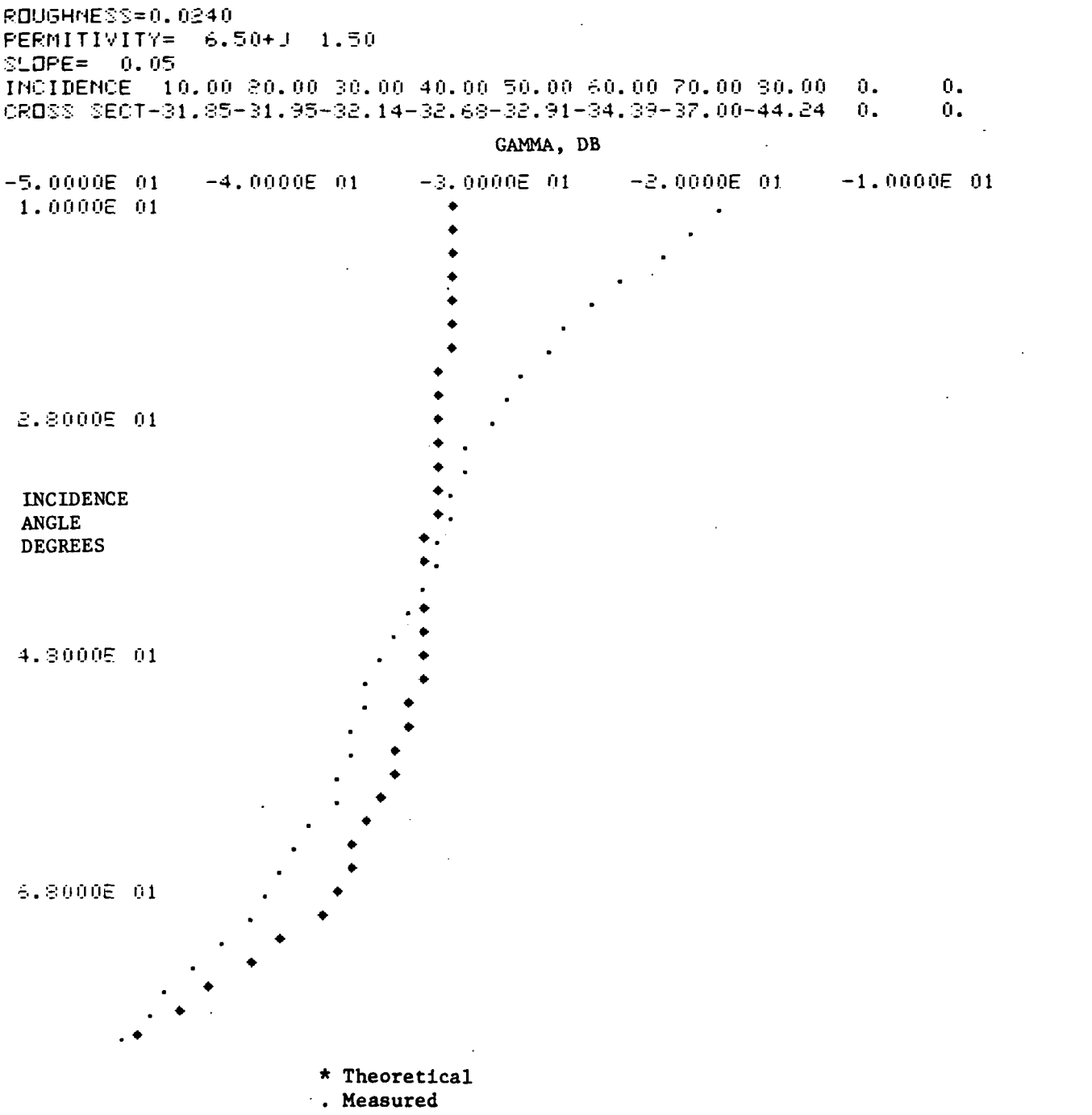

Figure C-7-- BEST MATCH FOR BACKSCATTER FROM CONCRETE AT X-BAND, HORIZONTAL POLARIZATION

Taking the surface parameters which yield the best data at X-band and directly scaling them to K-band yield figures C-8 and C-9. These figures show a relatively good match between the theoretical prediction and the measured data. A few other values for the slope and roughness parameters have been attempted, with poorer results.

Figure C-10 shows the result of a computation for vertical polarized X-band backscatter off an asphalt surface. Again, the only significant deviation between theory and measurement is at angles which could have significant specular contributions.

APPLICATION OF SCATTERING MODELS TO ILM

Information on the scattering properties of natural surface is required in several areas of the ILM sensor analysis. Scattering data provides a means for

- o Differential cross section estimation
- o Multipath environment definition
- o Mutual interference analysis

Extension of Cross Section Data

The most obvious usage of scattering models is to extrapolate available radar cross section data. Nearly all of the measured cross section data available is for incidence angles between 10 and 80 degrees. For the ILM program, 84 to 88 degrees are typical incidence angles. Thus at incidence angles of interest, very little data is available. Further, the beamwidth

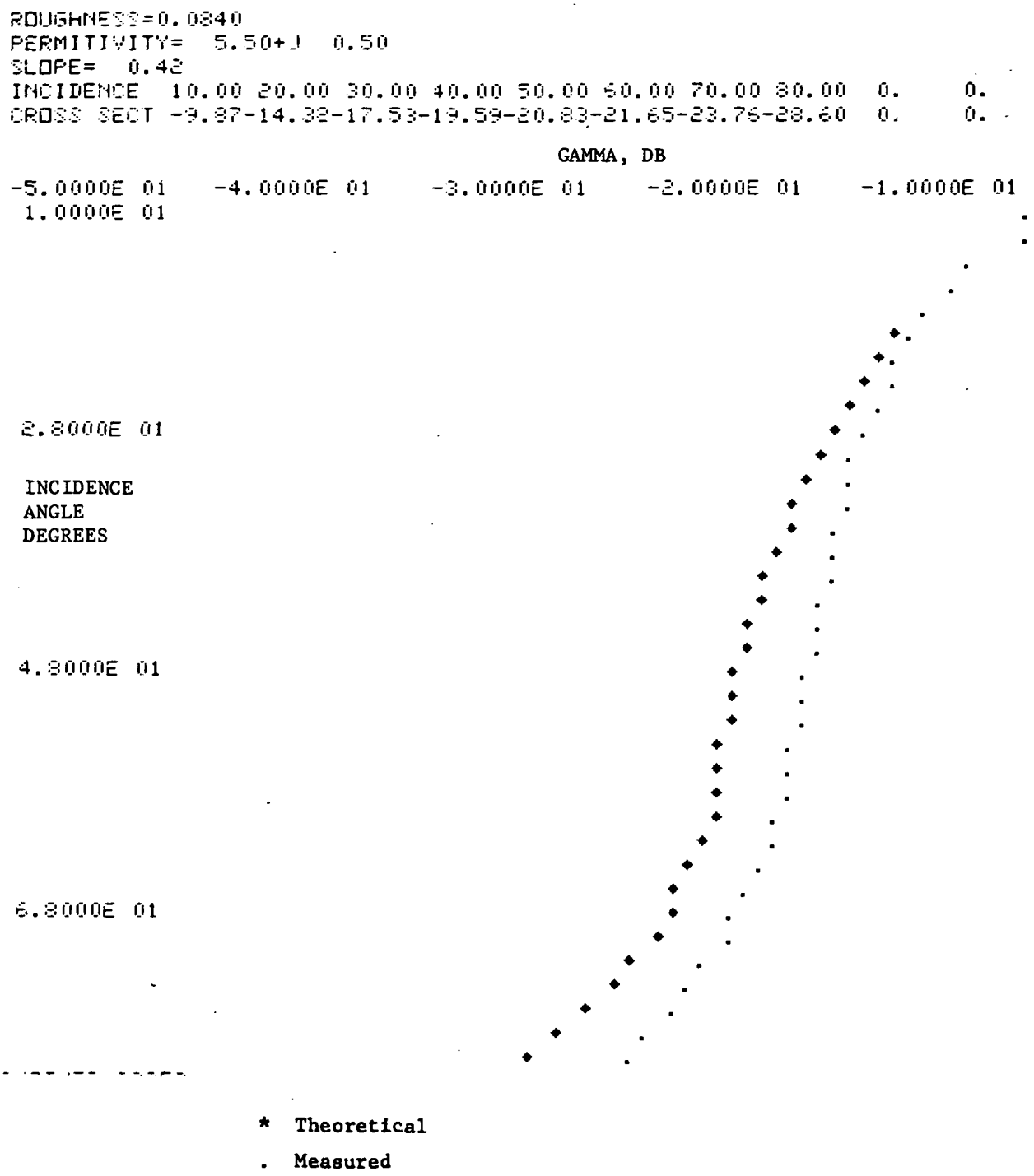

Figure C-8-- Backscatter from concrete at K_a band, vertical polarization

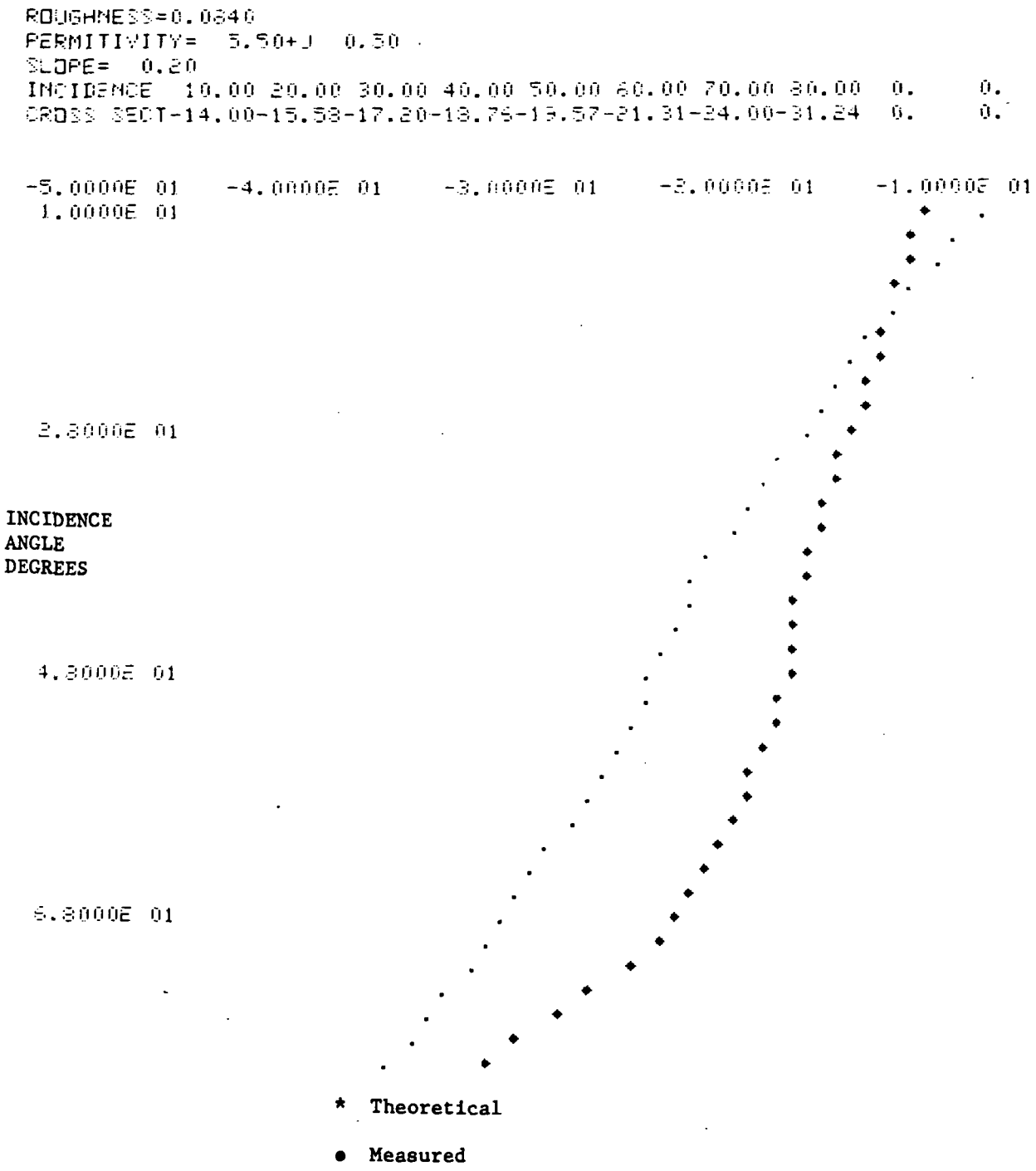

Figure C-9--Backscatter from concrete at K_a band, horizontal polarization

ROUGHNESS=0.1500
PERMITIVITY= 4.30+J 0.10
SLOPE= 0.10
INCIDENCE 10.00 20.00 30.00 40.00 50.00 60.00 70.00 80.00 0. 0.
CROSS SECT-26.30-26.04-25.35-24.38-23.40-22.91-23.37-30.01 0. 0.

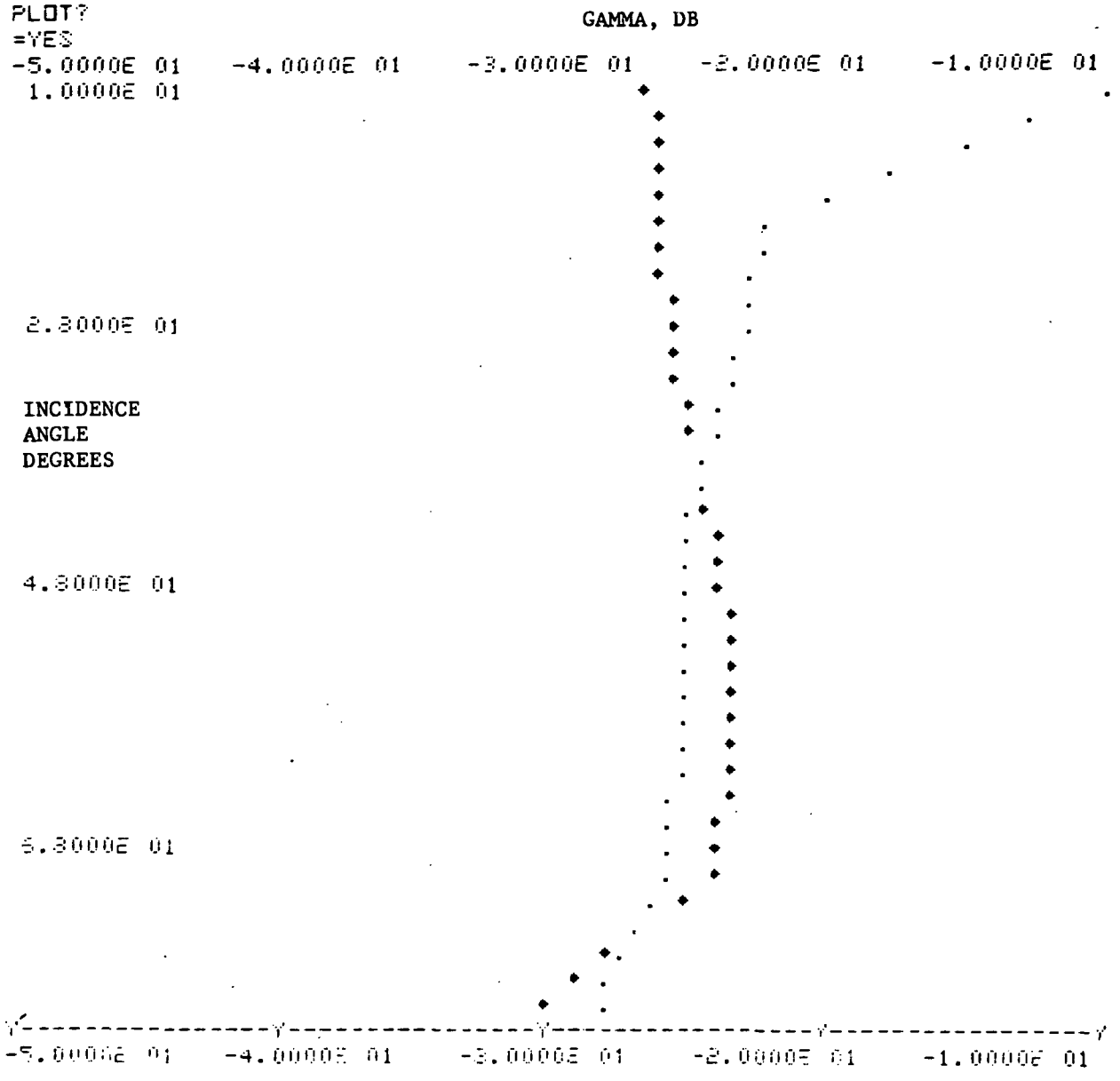

Figure C-10-- Backscatter from Asphalt at X-band, vertical polarization

and sidelobe levels of the measuring antenna are not normally known. At high incidence angles where the differential cross section is relatively high and changing slowly with angle these items are fairly unimportant. However, at low grazing angles, the cross section is low and varies rapidly with angle. Therefore, antennas of different beamwidth (or systems with diffeerent pulse width for a pulse measuring system) can have large discrepancies when measuring the same surface, since the major power contribution may come from slightly different angles. Also, when the cross section is very low and the measuring system uses a CW technique, significant error contributions can be made by energy entering the sidelobes. Thus, even that data which is available at these low grazing angles is of questionable validity. Since a computer program is available which provides cross section data in good agreement with the high angle measured data, which is in some sense mathematically reasonable, and which is intuitively correct, the outputs from this program can be used with some confidence.

The same caveat applies to using the theoretical results as was mentioned in criticizing the measurements. The cross section is changing rapidly with incidence angle, and thus some gain function must be included in the integration of the radar range equation

$$P_r = \frac{P_t \lambda^2}{(4\pi)^3} \int_S \frac{G_t G_R \gamma}{R^4} \, dS \qquad \text{(C-41)}$$

Multipath Analysis

Traditional multipath analyses have assumed a microscopically smooth, perfectly conducting surface. Under this conditions, the energy incident on the surface is completely reflected in the specular direction, with a phase reversal for horizontal polarization and phase modification for vertical polarization. The reflected wave is perfectly coherent, and hence the signal at the receiving antenna is purely a function of geometry.

From the foregoing analysis, it can be seem that although specular multipath exists, it is only one component of the multipath. Diffuse multipath or that energy received from reflections at angles other than the specular is another important contributor. The data on scattering at arbitrary angles allows calculation of this effect.

Since scattering from natural surfaces covers the entire hemisphere, it is feasible that some contribution to the diffuse multipath comes from the entire area contained by the horizon. In order to simplify the analysis, it is necessary to limit the area of multipath contribution. If the very rough gaussianly correlated model is used, the mean square value of the reflection coefficient for an differential area dS can be represented by:

$$\langle \rho^2 \rangle = \frac{dS}{4\pi r^2} \quad \frac{\cot^2 \beta_o}{\cos^4 \xi_{xy}} \quad \exp\left(-\frac{\tan^2 \xi_{xy}}{\tan^2 \beta_o}\right) \qquad \text{(C-42)}$$

where r is the distance from the area to the receiver

$\beta_o = \tan^{-1} \frac{2\sigma}{T}$ is the mean square value of the slope of the irregularities

and ξ_{XY} is the angle between the bisector of the incident and reflected rays and the Z-axis.

In this model, all significant contributions to the received energy come from areas where $\xi_{xy} < \beta_o$. By extending this approximation to all models the glistening surface, i.e., that area having significant contribution to the diffuse multipath signal, may be defined.

It can be derived geometrically that if the area is not limited by the antenna patterns of the transmitting and receiving antennas, the glistening surface is approximately a trapazoid with sides defined by (ref. C-1).

$$\beta = \beta_o$$

and ends defined by

$$d_i = h_i \cot 2\beta_o \quad i=r,t$$

where d_i is the distance to the start of the glistening surface from the ith antenna

as shown in Figure C-11.

Limiting the area of integration to this surface, the mean value of received diffuse multipath power is given by the bistatic radar range equation:

$$P_r = \frac{P_t \lambda^2}{(4\pi)^3} \int_S \gamma \frac{(\theta_1, \theta_2, \phi)\, G_t(\theta_1 - \theta_t, \frac{\phi}{2})\, G_R(\theta_2 - \theta_R, \frac{\phi}{2})}{R_1^2 R_2^2} dS \qquad (C\text{-}43)$$

where θ_t is the transmitting depression angle

θ_r is the receiving elevation angle

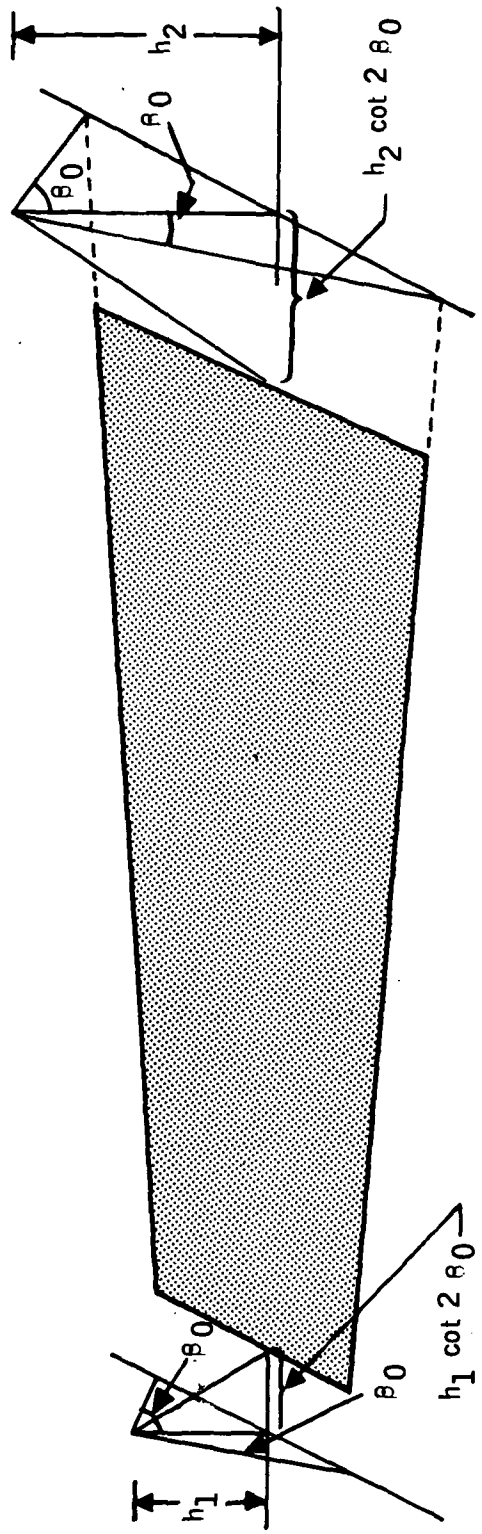

Figure C-11 -- The Glistening Surface

Many analyses (ref C-1 chapter 7 for example) have shown that the distribution of this power is approximately uniform in phase and Rayleigh in power. Since any other assumption yields an extremely complex expression depending on surface parameters, polarization, etc., the Rayleigh distribution will be assumed here. Thus the diffuse multipath appears at the receiver as an additive noise term, which provides an upper limit on the signal to noise ratio.

Since the width of the glistening surface is very narrow, the azimuth antenna gain variation and change in cross section can be approximated as a constant. The width of the glistening surface is:

$$\omega = \left[h_2 + {}_{\ell} h_2 \tan\theta_2 (h_1 - h_2) \right] \tan \beta_o$$

where h_1 is the height of the transmitting antenna

h_2 is the height of the receiving antenna

ℓ is the ground range from the transmitter to the receiver

The total diffuse multipath power is then:

$$P_r = \frac{P_t \lambda^2}{(4\pi)^3} \int_{h_2 \cot\beta_o}^{h_1 \cot\beta_o} \frac{\gamma \left(\tan^{-1}\left(\frac{\ell - r}{h_1}\right), \tan^{-1}\left(\frac{r}{h_2}\right), 0\right) G_t \left(\tan^{-1}\left(\frac{h_1}{\ell - r}\right) - \theta_t, 0\right)}{(\ell - r)^2 r^2}$$

$$\frac{G_r \left(\tan^{-1}\left(\frac{h_2}{r}\right) - \theta_r, 0\right) \left(r h_1 + (\ell - r) h_2\right)^2 \tan \beta_o}{} \, dr$$

This expression is directly usable for a CW system or a pulse system with wide pulses, however, since the path length is varying throughout the range of the dummy variable r , this power is spread over time. For a ground radar at nearly zero antenna height, the maximum range difference occurs at the end of the glistening surface nearest the aircraft. Assuming the glistening surface to extend all the way to the aircraft, the maximum range difference is from .02 to .1 times the slant range. Thus the maximum time difference is from .06 l_s to .3 l_s microseconds, with l_s in Km. In a high resolution pulse radar, the integral must be broken up into differential ranges, and the diffuse multipath from a given resolution cell applied to the appropriate cell. The total multipath is then the sum of all the multipath elements at that time difference.

Mutual Interference Analysis

One source of mutual interference between imaging radars is the probability that the backscattering of a pulse from one aircraft illuminates the antenna of another aircraft, giving a phantom image.

If only the mainlobes of the antennas are considered, this problem is very similar to the simple radar problem. However, the general scattering equations show that high angle diffuse scattering or specular scattering entering the back or side lobes may be of a higher level than direct backscatter. Thus, the general scattering equations should be used in any mutual interference analysis.

REFERENCES

1. Beckmann and Spizzichino, The Scattering of Electro Magnetic Waves from Rough Surfaces, MacMillan, 1963.

2. Semenov, Scattering of Electromagnetic Waves from Restricted Portions of Rough Surfaces with Finite Conductivity, Radiotekhnika i Electronica V, 110, 1965, p. 1952.

3. Barrick, D. E., Rough Surface Scattering Based on the Specular Point Theory, AP16 1968, P449.

4. Beckmann, Scattering by Composite Rough Surfaces, Proc. IEEE, Vol. 53 No. 8, August 1965, p. 1012.

5. Beckmann, Shadowing by Random Rough Surfaces, AP13, May 1965, p. 384.

6. Ruck, Barrick, Stuart, and Krichbaum, Radar Cross Section Handbook, Vol. 2, Plenum Press, 1970.

7. Mitzner, K.: Change in Polarization on Reflection from a Tilted Plane, Radio Science, Vol. 1, 1966, pg. 27.

PAGE INTENTIONALLY BLANK

APPENDIX D

ATMOSPHERIC ATTENUATION OF MICROWAVES

GASEOUS ABSORPTION

The absorption of microwave energy by atmospheric gases is due to cyclotron resonance of the molecules of the constituent gases. In the frequency range of microwave sensors, the absorption is due to the 1.35 cm resonance of water vapor and a series of resonances of oxygen centered about .5 cm.

The general theory of gaseous absorption of microwaves has been formulated by VanVleck (Reference D-1) and the constants in the formula measured by Birnbaum and Maryott (Reference D-2), Artman and Gordon (Reference D-3), and Becker and Autler (Reference D-4).

The absorption by oxygen is given by:

$$\alpha_o = \frac{34}{\lambda^2} P \left(\frac{293}{T}\right)^2 \left[\frac{\Delta V_1}{1/\lambda^2 + \Delta V_1^2} + \frac{\Delta V_2}{(2+1/\lambda)^2 + \Delta V_2^2} + \frac{\Delta V_2}{(2-1/\lambda)^2 + \Delta V_2^2}\right] \quad \text{(D-1)}$$

where

α_o is the attenuation in dB/Km

λ is the wavelength in cm

P is the pressure in atmospheres

T is the temperature in degrees Kelvin

$\Delta V_1 = .018\ P\ \left(\frac{293}{T}\right)^{3/4}$

$\Delta V_2 = .049\ P\ \left(\frac{300}{T}\right)^{3/4}$

The absorption by water vapor is

$$\alpha_\omega = \frac{.0318P}{\lambda^2}\left(\frac{293}{T}\right)^{5/2} e^{-644/T}\left[\frac{\Delta V_3}{\left(1/\lambda - \frac{1}{1.35}\right)^2 + \Delta V_3^2} + \frac{V_3}{\left(1/\lambda + \frac{1}{1.35}\right)^2 + \Delta V_3^2}\right] + \frac{.05\ V_3}{\lambda^2}\left(\frac{293}{T}\right) \qquad \text{(D-2)}$$

where

α_ω is the water vapor absorption in dB/Km

$\Delta V_3 = .087\ P\left(\frac{318}{T}\right)^{1/2}(1+.0046\rho)$

ρ is the absolute humidity in gms/m^3

Many experiments have shown these equations to accurately represent the gaseous absorption of the atmosphere. By integrating these functions over the transmission path, the total path gaseous absorption may be found.

A simple model for gaseous absorption in the atmosphere which corresponds fairly accurately to observations is the bi-exponential model. In this model, the attenuation coefficient due to gaseous absorption at 35 GHz is:

$$\alpha_g = \alpha_d\ e^{-\frac{h(68.6 - 2.75k)}{T_o}} + \alpha_\omega\ e^{-\frac{100h}{2090 - T_o}} \qquad \text{(D-3)}$$

where

$\alpha_d \approx \frac{15.8P}{T_o^2}$ is the ground level dry absorption coefficient

h is the altitude (Km)

k is the temperature/lapse rate

T_o is the ground level temperature (°K)

$\alpha_\omega \approx (24 - \frac{T_o}{20}) \frac{Pw \times 10^{-3}}{101.3}$ is the ground level wet absorption coefficient

P is the atmospheric pressure (KPa)

W is the absolute humidity (g/m^3)

This model is useful because of its analytical tractability. Since the maximum gaseous attenuation of interest is less than 5 dB, any errors caused by the use of this formula will be insignificant.

ATTENUATION BY CLOUDS OR FOG

Attenuation of microwave by clouds or fog is of a considerably different nature than that due to either rain or water vapor. This is due to the scattering characteristics of the very small ($<$.01 cm) diameter drops. Fog attenuation was derived by Gunn and East (Reference D-5) with the results shown in Table D-1. Attenuation at frequencies below X band are not significant over the path lengths considered, for example at 3 GHz with a 30 m visibility, it requires a 50 Km path to obtain 1 dB of path attenuation.

The data in Table D-1 is presented in terms of $dB/Km/g/m^3$ which requires knowledge of the amount of condensed water. Based on attenuation measure-

ments at several frequencies, an empirical relationship between RVR and water content accurate to about ±10% is

$$3.04 - 1.37 \log V = \log W \qquad \text{(D-4)}$$

where

V is the RVR in feet

W is the water content in gm/m^3

In this relationship, zero visibility would require infinite water content. However, the highest reported water content of clouds is about 4.0 gm/m^3 in isolated cases of cumulus congestus clouds. Thus, zero visibility fog will be considered to have a water content of 4.0 gm/m^3. Under these assumptions, the fog water content of Table D-2 will be used for the analysis.

Table D-1. Specific Attenuation dB/Km per g/m^3 Condensed Water in Cloud or Fog

Temperature, °C	C Band	X Band	Ku Band	Ka Band
	6 GHz	9 GHz	15 GHz	35 GHz
20°	.018	.055	.111	.523
10°	.024	.073	.155	.586
0°	.035	.101	.228	.827
-8°	.045	.131	.291	1.043

Table D-2. Assumed Water Content of Fog

RVR, ft	g/m^3 of Water
1,200	.065
700	.14
150	1.1
0	4.0

ATTENUATION BY RAIN

The attenuation of microwaves by rain is the most significant and simultaneously the least predictable of all atmospheric degradations. The theoretical foundation for predicting rain attenuation is the paper of Ryde and Ryde (Reference D-6), which assumed a particular distribution of water drop sizes and derived expression for attenuation based on Mie scattering. The resultant attenuation values can be quite closely approximated by a function of the form

$$A = kaR^b \qquad \text{(D-5)}$$

where

A is the specific attenuation (dB/Km)

a is a function of frequency

k is a function of temperature and frequency

R is the rainfall rate (mm/hr)

b is a function of frequency

Values of the parameters k,a, and b are given in Table D-3.

Table D-3. Factors in the Specific Attenuation Equation for Rain

Band	Coefficient a	Exponent b	Temperature Factor k 0°	10°	18°	30°
C 6 GHz	.0027	1.25	.85	.93	1.0	.86
X 9 GHz	.0079	1.28	.76	.90	1.0	.90
Ku 15 GHz	.033	1.16	.81	.92	1.0	.93
Ka 35 GHz	.17	1.05	.86	.96	1.0	.95

Several measurement programs, summarized by Medhurst (Reference D-7) seemed to show a wide variance from this theory. Medhurst rederived the theoretical attenuations based on drop size distributions which would yield minimum and maximum attenuation limits, and shows that measured attenuations lie outside even these bounds. However, the assumption of uniform rain over the propagation path is maintained throughout Medhurst's work. In certain types of rain, particularly cumuliform rain, there exist large gradients of rain fall rate in both space and time. Recent experiments (Reference D-8 and D-9) designed to account for these variations have shown extremely good agreement with Ryde's theory. In Reference D-8, attenuation of signals transmitted from an aircraft to a ground station was correlated with radar reflectivity of the rain, using the approximation

$$Z = 200\ R^{1.6} \qquad \text{(D-6)}$$

where

Z is the radar reflectivity factor.

The only attenuation measurements which differed from Rydes theory via the reflectivity approximation were measurement where there was evidence of hail or snow mixed in the rain. In these cases, the attenuation was significantly less than it would be for pure rain, as theory predicts.

Therefore, it appears that inconsistancies in measured data are due more to inaccuracies in measuring the spatial and temporal variations of the rain than to any basic fault in Rydes theory. Medhurst's minimum and maximum limits are not reasonable for radar performance calculation, since it is highly improbably that any rain shower would consist of uniformly sized drops, pathologically sized to provide the highest or lowest possible attenuation. Any arbitrary variance in attenuation would be as mathematically viable as Medhurst's minimum and maximum.

ATTENUATION BY ICE AND SNOW

Solid water can be present in the atmosphere in several forms: ice fog or cloud, hail, or snow. Because of the different dielectric constants of solid water, its attenuation is generally insignificant. However, if the solid water is coated with a layer of liquid water, it's attenuation can be as great or even greater than the attenuation of the equivalent liquid water particle.

Therefore, the specific attenuation of ice fog or ice clouds will be considered to be zero, as will the attenuation of hail or snow if the air temperature surrounding the hail or snow is below 0°C. If the

surrounding air is above 0°C, the specific attenuation will be considered to be anywhere between zero and the value for the equivalent amount of rain.

ILM WEATHER DATA

There are four basic climatological conditions to be investigated for ILM. They are:

- o CASE 1: Summer Rain, Maritime Tropical Climate
- o CASE 2: Radiation or Advection Fog, Temperate Climate
- o CASE 3: Inland Evaporation - Fog, Temperate Climate
- o CASE 4: Winter Snow, Temperate Climate

Variations in RVR for cases 2 and 3 will be accounted for by using subcases, where

- o Subcase 2 (or 3).1 is 1200 ft RVR
- o Subcase 2.2 is 700 ft RVR
- o Subcase 2.3 is 150 ft RVR
- o Subcase 2.4 is 0 ft RVR

Case 1 is representative of a summer thunderstorm on the gulf coast, with cloud tops to 50,000 ft and 16 mm/hr rainfall. Case 2 is representative of coastal fog, or fog associated with high pressure cells in the Midwest. Case 3 is frontal fog, usually experienced in the East and South during the spring. Case 4 is a typical winter snow storm caused by maritime polar air over-running modified continental polar air.

The vertical profiles for the various cases is shown in Figure D-1.

Based on the weather cases defined above, specific attenuation profiles for C, X, Ku and Ka bands have been computed as shown in Tables D-4 through D-10. Gaseous absorption was computed using the VanVleck equations. Rain, cloud, and fog attenuations were computed by interpolating values from Tables D-1 through D-3.

Since the fog for weather case 2 is only 60m thick, it can be assumed to be at constant temperature. Therefore, Table D-5 is only the gaseous attenuation. The specific attenuation of fog must be added in the first 60m to compute the total specific attenuation. Values of fog attenuation for weather case 2 are given in Table D-11 on page D-15.

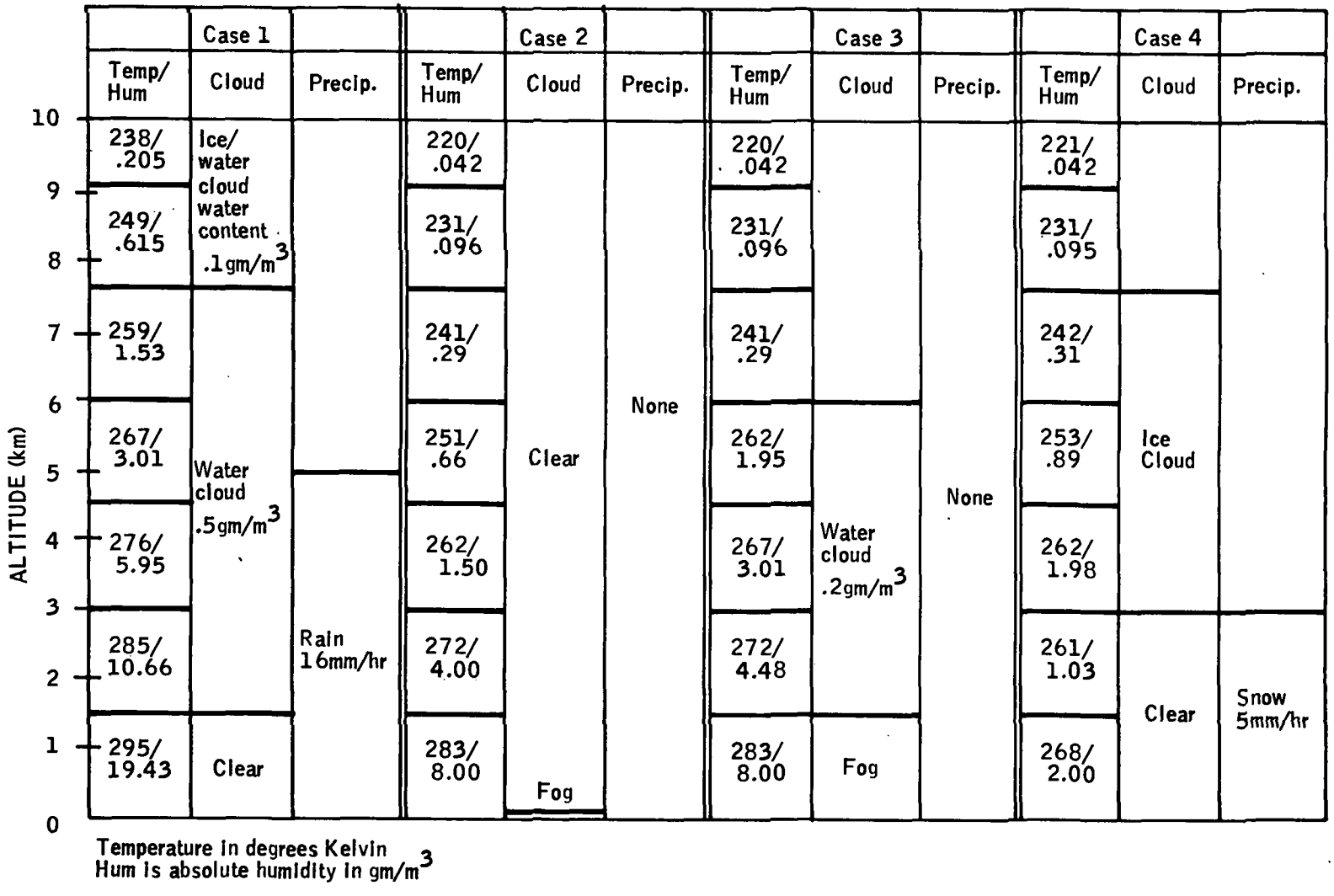

Figure D-1 -- Vertical Weather Profiles

Table D-4-- SPECIFIC ATTENUATION DB/KM, ILM WEATHER CASE 1

ALTITUDE KILOMETERS	C BAND 6 GHZ	X-BAND 9 GHZ	KU BAND 15 GHZ	KA BAND 35 GHZ	TEMP °K
0.00	0.9000E-01	0.2775E 00	0.8412E 00	0.3196E 01	295.0000
0.10	0.9043E-01	0.2785E 00	0.8430E 00	0.3199E 01	294.3500
0.20	0.9087E-01	0.2796E 00	0.8449E 00	0.3201E 01	293.7000
0.30	0.9131E-01	0.2807E 00	0.8469E 00	0.3204E 01	293.0500
0.40	0.9176E-01	0.2817E 00	0.8488E 00	0.3207E 01	292.4000
0.50	0.1016E 00	0.3115E 00	0.9091E 00	0.3475E 01	291.7500
0.60	0.1022E 00	0.3132E 00	0.9136E 00	0.3481E 01	291.0908
0.70	0.1019E 00	0.3117E 00	0.9086E 00	0.3468E 01	290.4316
0.80	0.1015E 00	0.3097E 00	0.9035E 00	0.3453E 01	289.7725
0.90	0.1010E 00	0.3078E 00	0.8984E 00	0.3438E 01	289.1133
1.00	0.1005E 00	0.3058E 00	0.8933E 00	0.3424E 01	288.4541
1.10	0.1001E 00	0.3039E 00	0.8882E 00	0.3409E 01	287.7949
1.20	0.9963E-01	0.3019E 00	0.8832E 00	0.3394E 01	287.1357
1.30	0.9918E-01	0.3000E 00	0.8782E 00	0.3380E 01	286.4766
1.40	0.9874E-01	0.2981E 00	0.8732E 00	0.3365E 01	285.8174
1.50	0.9830E-01	0.2962E 00	0.8682E 00	0.3351E 01	285.1582
1.60	0.9789E-01	0.2944E 00	0.8638E 00	0.3338E 01	284.5512
1.70	0.9750E-01	0.2928E 00	0.8596E 00	0.3326E 01	283.9606
1.80	0.9711E-01	0.2911E 00	0.8554E 00	0.3314E 01	283.3701
1.90	0.9680E-01	0.2894E 00	0.8513E 00	0.3302E 01	282.7795
2.00	0.9659E-01	0.2876E 00	0.8475E 00	0.3290E 01	282.1890
3.00	0.9470E-01	0.2699E 00	0.8100E 00	0.3172E 01	276.2835
4.00	0.9492E-01	0.2626E 00	0.7938E 00	0.3119E 01	270.9718
5.00	0.9827E-01	0.2693E 00	0.8045E 00	0.3147E 01	265.5238
6.00	0.2038E-01	0.5701E-01	0.1258E 00	0.4496E 00	259.5714
7.00	0.1654E-01	0.4633E-01	0.1021E 00	0.3651E 00	253.0682
8.00	0.3352E-02	0.8336E-02	0.1778E-01	0.6311E-01	246.2572
9.00	0.2663E-02	0.6629E-02	0.1410E-01	0.5007E-01	239.0394

Table D-5 -- SPECIFIC ATTENUATION DB/KM, ILM WEATHER CASE 2

ALTITUDE KILOMETERS	C BAND 6 GHZ	X-BAND 9 GHZ	KU BAND 15 GHZ	KA BAND 35 GHZ	TEMP °K
0.00	0.7765E-02	0.1041E-01	0.2143E-01	0.6914E-01	282.7000
0.10	0.7563E-02	0.1011E-01	0.2070E-01	0.6675E-01	282.0000
0.20	0.7366E-02	0.9821E-02	0.1999E-01	0.6440E-01	281.3000
0.30	0.7174E-02	0.9538E-02	0.1929E-01	0.6210E-01	280.6000
0.40	0.6987E-02	0.9261E-02	0.1861E-01	0.5985E-01	279.9000
0.50	0.6804E-02	0.8991E-02	0.1794E-01	0.5765E-01	279.2000
0.60	0.6625E-02	0.8729E-02	0.1729E-01	0.5551E-01	278.5164
0.70	0.6451E-02	0.8472E-02	0.1665E-01	0.5341E-01	277.8328
0.80	0.6281E-02	0.8222E-02	0.1603E-01	0.5137E-01	277.1492
0.90	0.6116E-02	0.7978E-02	0.1542E-01	0.4936E-01	276.4656
1.00	0.5955E-02	0.7741E-02	0.1483E-01	0.4740E-01	275.7820
1.10	0.5798E-02	0.7509E-02	0.1424E-01	0.4549E-01	275.0984
1.20	0.5644E-02	0.7283E-02	0.1367E-01	0.4361E-01	274.4148
1.30	0.5495E-02	0.7063E-02	0.1311E-01	0.4178E-01	273.7313
1.40	0.5349E-02	0.6848E-02	0.1257E-01	0.4000E-01	273.0477
1.50	0.5208E-02	0.6639E-02	0.1204E-01	0.3825E-01	272.3641
1.60	0.5072E-02	0.6449E-02	0.1160E-01	0.3682E-01	271.6913
1.70	0.4942E-02	0.6269E-02	0.1120E-01	0.3552E-01	271.0220
1.80	0.4814E-02	0.6093E-02	0.1080E-01	0.3424E-01	270.3528
1.90	0.4690E-02	0.5922E-02	0.1042E-01	0.3299E-01	269.6835
2.00	0.4569E-02	0.5755E-02	0.1004E-01	0.3177E-01	269.0142
3.00	0.3514E-02	0.4298E-02	0.6729E-02	0.2106E-01	262.3213
4.00	0.2737E-02	0.3330E-02	0.5026E-02	0.1571E-01	255.5751
5.00	0.2140E-02	0.2592E-02	0.3769E-02	0.1178E-01	248.7470
6.00	0.1683E-02	0.2039E-02	0.2892E-02	0.9060E-02	241.6786
7.00	0.1328E-02	0.1616E-02	0.2270E-02	0.7149E-02	234.7717
8.00	0.1051E-02	0.1288E-02	0.1803E-02	0.5715E-02	227.8819
9.00	0.8357E-03	0.1034E-02	0.1457E-02	0.4654E-02	220.9921

Table D-6 -- SPECIFIC ATTENUATION DB/KM, ILM WEATHER CASE 3.1

ALTITUDE KILOMETERS	C BAND 6 GHZ	X-BAND 9 GHZ	KU BAND 15 GHZ	KA BAND 35 GHZ	TEMP °K
0.00	0.9346E-02	0.1521E-01	0.3165E-01	0.1077E 00	282.7000
0.10	0.9185E-02	0.1503E-01	0.3126E-01	0.1064E 00	282.0800
0.20	0.9030E-02	0.1485E-01	0.3088E-01	0.1052E 00	281.4600
0.30	0.8879E-02	0.1468E-01	0.3051E-01	0.1040E 00	280.8400
0.40	0.8733E-02	0.1452E-01	0.3016E-01	0.1028E 00	280.2200
0.50	0.1234E-01	0.2551E-01	0.5410E-01	0.1919E 00	279.6000
0.60	0.1233E-01	0.2567E-01	0.5457E-01	0.1935E 00	278.8578
0.70	0.1232E-01	0.2584E-01	0.5506E-01	0.1951E 00	278.1156
0.80	0.1232E-01	0.2602E-01	0.5556E-01	0.1968E 00	277.3734
0.90	0.1232E-01	0.2620E-01	0.5607E-01	0.1985E 00	276.6312
1.00	0.1233E-01	0.2639E-01	0.5659E-01	0.2002E 00	275.8891
1.10	0.1234E-01	0.2658E-01	0.5713E-01	0.2020E 00	275.1469
1.20	0.1236E-01	0.2678E-01	0.5768E-01	0.2038E 00	274.4047
1.30	0.1237E-01	0.2698E-01	0.5823E-01	0.2057E 00	273.6625
1.40	0.1240E-01	0.2721E-01	0.5881E-01	0.2076E 00	272.9203
1.50	0.1245E-01	0.2756E-01	0.5948E-01	0.2100E 00	272.1781
1.60	0.1241E-01	0.2769E-01	0.5975E-01	0.2110E 00	271.7507
1.70	0.1235E-01	0.2775E-01	0.5991E-01	0.2116E 00	271.4226
1.80	0.1229E-01	0.2781E-01	0.6007E-01	0.2122E 00	271.0945
1.90	0.1223E-01	0.2788E-01	0.6024E-01	0.2129E 00	270.7664
2.00	0.1218E-01	0.2796E-01	0.6042E-01	0.2136E 00	270.4383
3.00	0.1187E-01	0.2893E-01	0.6263E-01	0.2219E 00	267.1575
4.00	0.1133E-01	0.2881E-01	0.6253E-01	0.2218E 00	264.2066
5.00	0.1969E-02	0.2485E-02	0.4184E-02	0.1332E-01	258.1250
6.00	0.1671E-02	0.2031E-02	0.2924E-02	0.9179E-02	242.5000
7.00	0.1328E-02	0.1616E-02	0.2270E-02	0.7149E-02	234.7717
8.00	0.1051E-02	0.1288E-02	0.1803E-02	0.5715E-02	227.8819
9.00	0.8357E-03	0.1034E-02	0.1457E-02	0.4654E-02	220.9921

Table D-7 -- SPECIFIC ATTENUATION DB/KM, ILM WEATHER CASE 3.2

ALTITUDE KILOMETERS	C BAND 6 GHZ	X-BAND 9 GHZ	KU BAND 15 GHZ	KA BAND 35 GHZ	TEMP °K
0.00	0.1117E-01	0.2075E-01	0.4344E-01	0.1522E 00	282.7000
0.10	0.1106E-01	0.2069E-01	0.4338E-01	0.1520E 00	282.0800
0.20	0.1096E-01	0.2065E-01	0.4334E-01	0.1519E 00	281.4600
0.30	0.1086E-01	0.2061E-01	0.4332E-01	0.1518E 00	280.8400
0.40	0.1076E-01	0.2058E-01	0.4331E-01	0.1518E 00	280.2200
0.50	0.1234E-01	0.2551E-01	0.5410E-01	0.1919E 00	279.6000
0.60	0.1233E-01	0.2567E-01	0.5457E-01	0.1935E 00	278.8578
0.70	0.1232E-01	0.2584E-01	0.5506E-01	0.1951E 00	278.1156

Table D-8 -- SPECIFIC ATTENUATION DB/KM, ILM WEATHER CASE 3.3

ALTITUDE KILOMETERS	C BAND 6 GHZ	X-BAND 9 GHZ	KU BAND 15 GHZ	KA BAND 35 GHZ	TEMP °K
0.00	0.3453E-01	0.9163E-01	0.1943E 00	0.7217E 00	282.7000
0.10	0.3507E-01	0.9325E-01	0.1986E 00	0.7359E 00	282.0800
0.20	0.3562E-01	0.9487E-01	0.2029E 00	0.7501E 00	281.4600
0.30	0.3618E-01	0.9650E-01	0.2073E 00	0.7644E 00	280.8400
0.40	0.3674E-01	0.9813E-01	0.2116E 00	0.7787E 00	280.2200
0.50	0.1234E-01	0.2551E-01	0.5410E-01	0.1919E 00	279.6000
0.60	0.1233E-01	0.2567E-01	0.5457E-01	0.1935E 00	278.8578
0.70	0.1232E-01	0.2584E-01	0.5506E-01	0.1951E 00	278.1156

Table D-9 -- SPECIFIC ATTENUATION DB/KM, ILM WEATHER CASE 3.4

ALTITUDE KILOMETERS	C BAND 6 GHZ	X-BAND 9 GHZ	KU BAND 15 GHZ	KA BAND 35 GHZ	TEMP °K
0.00	0.1051E 00	0.3058E 00	0.6502E 00	0.2442E 01	282.7000
0.10	0.1076E 00	0.3124E 00	0.6676E 00	0.2500E 01	282.0800
0.20	0.1101E 00	0.3191E 00	0.6850E 00	0.2557E 01	281.4600
0.30	0.1127E 00	0.3257E 00	0.7025E 00	0.2615E 01	280.8400
0.40	0.1152E 00	0.3324E 00	0.7199E 00	0.2672E 01	280.2200
0.50	0.1234E-01	0.2551E-01	0.5410E-01	0.1919E 00	279.6000
0.60	0.1233E-01	0.2567E-01	0.5457E-01	0.1935E 00	278.8578
0.70	0.1232E-01	0.2584E-01	0.5506E-01	0.1951E 00	278.1156

Table D-10 -- SPECIFIC ATTENUATION DB/KM, ILM WEATHER CASE 4

ALTITUDE KILOMETERS	C BAND 6 GHZ	X-BAND 9 GHZ	KU BAND 15 GHZ	KA BAND 35 GHZ	TEMP °K
0.00	0.8527E-02	0.1019E-01	0.1506E-01	0.4630E-01	268.0000
0.10	0.8314E-02	0.9928E-02	0.1465E-01	0.4504E-01	267.3400
0.20	0.8107E-02	0.9677E-02	0.1425E-01	0.4380E-01	266.6800
0.30	0.7905E-02	0.9431E-02	0.1386E-01	0.4260E-01	266.0200
0.40	0.7709E-02	0.9192E-02	0.1348E-01	0.4142E-01	265.3600
0.50	0.7517E-02	0.8958E-02	0.1311E-01	0.4027E-01	264.7000
0.60	0.7308E-02	0.8705E-02	0.1271E-01	0.3905E-01	264.3387
0.70	0.7104E-02	0.8459E-02	0.1233E-01	0.3786E-01	263.9773
0.80	0.6906E-02	0.8220E-02	0.1195E-01	0.3670E-01	263.6160
0.90	0.6714E-02	0.7988E-02	0.1158E-01	0.3556E-01	263.2547
1.00	0.6527E-02	0.7761E-02	0.1123E-01	0.3446E-01	262.8934
1.10	0.6345E-02	0.7541E-02	0.1088E-01	0.3339E-01	262.5320
1.20	0.6168E-02	0.7327E-02	0.1054E-01	0.3234E-01	262.1707
1.30	0.5996E-02	0.7119E-02	0.1021E-01	0.3132E-01	261.8094
1.40	0.5829E-02	0.6917E-02	0.9885E-02	0.3032E-01	261.4480
1.50	0.5666E-02	0.6720E-02	0.9571E-02	0.2935E-01	261.0867
1.60	0.5495E-02	0.6527E-02	0.9344E-02	0.2869E-01	261.0499
1.70	0.5324E-02	0.6339E-02	0.9149E-02	0.2814E-01	261.1155
1.80	0.5159E-02	0.6157E-02	0.8960E-02	0.2761E-01	261.1811
1.90	0.4999E-02	0.5982E-02	0.8777E-02	0.2709E-01	261.2467
2.00	0.4844E-02	0.5811E-02	0.8599E-02	0.2659E-01	261.3123
3.00	0.3542E-02	0.4374E-02	0.7089E-02	0.2228E-01	261.9685
4.00	0.2709E-02	0.3332E-02	0.5237E-02	0.1646E-01	256.9718
5.00	0.2095E-02	0.2557E-02	0.3825E-02	0.1200E-01	250.9702
6.00	0.1664E-02	0.2019E-02	0.2882E-02	0.9039E-02	242.7857
7.00	0.1318E-02	0.1604E-02	0.2258E-02	0.7114E-02	235.4751
8.00	0.1044E-02	0.1279E-02	0.1791E-02	0.5678E-02	228.5066
9.00	0.8262E-03	0.1023E-02	0.1442E-02	0.4609E-02	221.9449

Table D-11. Specific Attenuation of Fog for Weather Case 2. (Db/km)

Subcase	RVR	C Band	X Band	Ku Band	Ka Band
2.1	1200 ft	.0015	.0047	.010	.038
2.2	700 ft	.0033	.010	.022	.082
2.3	150 ft	.026	.080	.171	.645
2.4	0 ft	.096	.292	.620	2.34

REFERENCES

D-1. VanVleck, J.H.: Theory of Absorption by Uncondensed Gases. Propagation of Short Radio Waves, MIT Radiation Lab Series, Vol. 13, 1951.

D-2. Birnbaum, G. and Maryott, A. A.: Microwave Absorption in Compressed Oxygen. Phys. Rev., Vol. 99, p. 1886, 1955.

D-3. Artman, J.O., and Gordon, J.P.: Absorption of Microwaves by Oxygen in the Millimeter Wavelength Region. Phys. Rev., Vol. 96, p. 1237, 1954.

D-4. Becker, G.B., and Autler, S.H.: Water Vapor Absorption of Electro-Magnetic Radiation in the Centimeter Wavelength Range. Phys. Rev., Vol. 70, p. 300, 1946.

D-5. Gunn, K.L.S., and East, T.W.R.: The Microwave Properties of Precipitation Particles. Quart. Jour. Roy. Meteorol. Sec. Vol. 80, p. 522, 1954.

D-6. Ryde, J.W., and Ryde, D.: Attenuation of Centimeter Wave by Rain, Hail, Fog, and Clouds. General Electric Co., Wembly England, 1945.

D-7. Medhurst, R. G.: Rainfall Attenuation of Centimeter Waves: Comparison of Theory and Measurement. AP 13, 1965, p. 55d.

D-8. McCormick, K.S.: A Comparison of Precipitation Attenuation and Radar Backscatter Along Earth-Space Paths. AP 20, 1972, p. 747.

D-9. Crane, R.K.: The Rain Range Experiment: Propagation through a Simulated Rain Environment. AP 22, 1974, p. 321.

APPENDIX E

RADIOMETRY COMPUTER PROGRAMS

A set of computer programs has been written for use in the analysis of microwave radiometry. The main programs are:

- o Skytemp
- o Pathtemp
- o Emis

The first program, Skytemp, performs the integration of specific attenuations to obtain the radiometric sky temperature at various incidence angles. It assumes a flat earth and a layered atmosphere, and assumes that all significant attenuation occurs in the first 10Km of atmosphere. Thermometric temperatures and specific attenuations are read from files pre-stored on the H-6080 disk file system, and sky temperatures are output to the disk on a file names FLTSKY in a format which is easy for the computer to use in further calculations.

Pathtemp is a very similar program, which integrates the specific attenuation to obtain the total one way attenuation on any glide path from any altitude to the ground. It also computes the path emission observed at any altitude (under 10Km) and at depression angles from .01745 rad to .157 rad (1° to 9°), for the ILM weather cases. Its output is to a disk file named FLTPATH for path temperature or FLATRANS for path attenuation.

EMIS uses as inputs a description of a statistical rough surface (roughness, slope, and permittivity), sky temperatures, and ground level thermometric temperatures. It computes the integrated sum of same sense and cross polarized reflected sky emission, and the diffuse percentage of power reflected from the hemisphere for both horizontal and vertical polarization based on exponentially correlated random rough surface scattering theory. The radiometric temperature contributions of diffuse sky, specular sky, and emissivity are computed and summed. The results are output to a temporary disk file for later printing.

Listings of the programs and results of interest are attached. Included are:

- o Total oneway path attenuations for 2,6, and 16 Km ranges on one to nine degree glide slopes
- o Perceived radiometric path temperature for the same conditions
- o Apparent surface radiometric temperatures for selected glide slopes and grass, concrete, and snow surfaces

Grass is described on the printout as a surface with roughness = .5, correlation length = 3.2, and permittivity 10+j10. Concrete has roughness = .084, correlation length .2, and permittivity 5.5+j.5. Snow is roughness .1, correlation length 1.0, and permittivity 3.2+j85.

Program Skytemp

```
      DIMENSION ALPHA(28,10),THIK(28),THED(18),TSKY(18,10),TEMP(28,10)
      DATA THIK/20*.1,8*1./
    CALL ATTACH(20,'D00048/FLALPHA;',3,0,IS,)
   CALL ATTACH(21,'D00048/FLTEMP;',3,0,ISTAT,)
      REWIND 20
      REWIND21
      READ(20,241,END=49)((ALPHA(I,J),I=1,28),J=1,10)
49    READ(21,242,END=50)((TEMP(I,J),I=1,28),J=1,10)
50    DO 200 K=1,18
       IF(K.GE.10) GO TO 100
      THED(K)=K
      THETA=K/57.29
      GO TO 120
100   THED(K)=K-9
      THETA=THED(K)/5.729
120   CONTINUE
      SINTH=SIN(THETA)
      DO 190 L=1,10
      IF(K.NE.1)GO TO 145
145   CONTINUE
      ATTENJ=1.
      TSKY(K,L)=0.0
      DO 190 I=1,28
      ATTENI=ATTENJ*EXP(-.23*ALPHA(I,L)*THIK(I)/SINTH)
      TSKY(K,L)=TSKY(K,L)+(200.+TEMP(I,L))*(ATTENJ-ATTENI)
      ATTENJ=ATTENI
190   CONTINUE
200   CONTINUE
      CALL ATTACH(22,'D00048/FLTSKY;',3,0,ISTAT,)
      REWIND22
       WRITE(22,240)((TSKY(I,J),I=1,18),J=1,10)
240   FORMAT(6E12.4)
241   FORMAT(2(10E12.4/),8E12.4)
242   FORMAT(14F4.2)
      CALL DETACH(20,IS,)
      CALL DETACH(21,IS,)
      CALL DETACH(22,IS,)
      STOP
      END
```

Program Pathtemp

```
0010      DIMENSION TAUA(28),PATHT(28),ALPHA(28),TEMP(28),THIK(28)
0020      DATA THIK/20*.1,8*1./
0030      CALL ATTACH(20,'D00048/FLALPHA;',3,0,IS,)
0040      CALL ATTACH(21,'D00048/FLTEMP;',3,0,IS,)
0050      CALL ATTACH(22,'D00048/FLTPATH;',3,0,IS,)
0060      CALL ATTACH(23,'D00048/FLATRANS;',3,0,IS,)
0070      REWIND20
0080      REWIND21
0090      REWIND 22
0100      REWIND 23
0110      DO 290 IWX=1,10
0120      READ(20,300)(ALPHA(I),I=1,28)
0130      READ(21,310)(TEMP(I),I=1,28)
0140      DO 280 IGS=1,9
0150      THETA=IGS/57.29
0160      CSTH=SIN(THETA)
0170      PTRAN=1.0
0180      PTMP=0.0
0190      DO 250 J=1,28
0200      EXPFAC=EXP(-.2301*ALPHA(J)*THIK(J)/CSTH)
0210      PTRAN=PTRAN*EXPFAC
0212      IF(PTRAN.GT.0.)GO TO 220
0214      TAUA(J)=99.99999
0216      GO TO 222
0220  220 TAUA(J)=10.*ALOG10(PTRAN)
0222  222 CONTINUE
0230      PTMP=(PTMP-200.-TEMP(J))*EXPFAC+200.+TEMP(J)
0240      PATHT(J)=PTMP
0250  250 CONTINUE
0260      WRITE(22,320)(PATHT(I),I=1,28)
0270      WRITE(23,330)(TAUA(I),I=1,28)
0280  280 CONTINUE
0290  290 CONTINUE
0300  300 FORMAT(2(10E12.4/),8E12.4)
0310  310 FORMAT(14F4.2)
0320  320 FORMAT(5E14.6)
0330  330 FORMAT(5E14.6)
0340      CALL DETACH(20,IS,)
0350      CALL DETACH(21,IS,)
0360      CALL DETACH(22,IS,)
0370      CALL DETACH(23,IS,)
0380      STOP
0390  END
```

```
010      DIMENSION GAMSUM(2,18),REFOUT(18),GLTMP(10),EMSV(2),SPEC(2),SPSKY(10)
011      DIMENSION SPCSKY(9,10)
012      DIMENSION TSKY(9,10),WXCS(10),TD(10,2)
014      DIMENSION TAPP(10,2),TSPEC(10,2),TEMIT(10,2),EMIT(2)
020      DATA RGH,SLP,PRMRE,PRMIM/.5,3.2,10.,10./
025       DATA GLTMP/295.,8*282.7,268./
26        CALL ATTACH(21,'D00048/OUTPUT;',3,0,IS,)
027       REWIND 21
030       DATA DINC/89./
31       CALL ATTACH(20,'D00048/FLTSKY;',3,0,ISTAT,)
32       REWIND 20
033       READ(20,34)((SPCSKY(I,J),I=1,9),(TSKY(K,J),K=1,9),J=1,10)
034   34 FORMAT(6F12.4)
035  040 PRINT 36
036  036 FORMAT("ROUGH SUFACE PARAMETERS,RGH,SLP,PRMRE,PRMIM")
037       READ 38,DAT1,DAT2,DAT3,DAT4
038  038 FORMAT(4F8.4)
039       KSPEC=90-DINC
040       AINC=DINC/57.29
041       IF(DAT1.EQ.0.)GO TO 43;RGH=DAT1;SLP=DAT2;PRMRE=DAT3;PRMIM=DAT4
42       DATA WXCS/1.0,2.1,2.2,2.3,2.4,3.1,3.2,3.3,3.4,4.0/
043  043 EMIT2=0.
044       RUM=100.0
045       EMIT1=0.0
050       DO 425 J=1,10
060       GAMSUM(1,J)=0.
070       GAMSUM(2,J)=0.
080       REFOUT(J)=10*J-95
090       AREFL=REFOUT(J)/57.29
100       DO 420 I=1,9
110       AOAZ=(I-1)/5.729
120       CSINC=COS(AINC)
130       CSREF=COS(AREFL)
140       CSOAZ=COS(AOAZ)
150       SNINC=SIN(AINC)
160       SNREF=SIN(AREFL)
170       SNOAZ=SIN(AOAZ)
180       A2=(CSINC*SNREF+SNINC*CSREF*CSOAZ)**2
190       A3=(SNINC*CSREF+CSINC*SNREF*CSOAZ)**2
200       A5=SNINC*SNREF*CSOAZ-CSINC*CSREF
210       CSLIN=(1.-A5)/2.
220       SNLIN=(1.+A5)/2.
230       CALL FRSNEL(SNLIN,CSLIN,PRMRE,PRMIM,RV,RH)
340       FSAM=A2*(A3+(SNREF*SNOAZ)**2)/((1+A5)**2)
350       FCRS=(SNINC*SNOAZ)**2*(A3+SNOAZ**2)/((1+A5)**2)
360       EXYSQ=SNINC**2+SNREF**2-2*SNINC*SNREF*CSOAZ
370       G=(6.28318*RGH*(CSINC+CSREF))**2
371       IF(G.LT.12.5) GO TO 377
372C ****VERY ROUGH EXPONENTIAL****
373       TEMP1=G**2+39.4748*SLP**2*EXYSQ
374       FEST=78.956*G*SLP**2/((CSINC+CSREF)**2*TEMP1*SQRT(TEMP1))
375       GO TO 400
376C ****SLIGHTLY ROUGH EXPONENTIAL****
377  377 SUMG=0.0
378       SMLST=0.
379       FACTM=1.
380       GTOM=1.
```

```
      DO 398 M=1,20
      GTOM=GTOM*G
      FACTM=FACTM*M
      TEMP1=1+39.4748*EXYSQ*(SLP/M)**2
      SUMG=SUMG+GTOM/(FACTM*M**2*TEMP1*SQRT(TEMP1))

      SUMDIF=ABS(SUMG-SMLST)
      IF(SUMDIF.LT..01*SUMG) GO TO 399
      IF(M.EQ.20)PRINT 396,REFOUT(J),SUMDIF
      SMLST=SUMG
  396 FORMAT("SERIES CONVERGENCE ERROR,ANGLE OF REF=",F5.2,"SUMDIF=",
     1      E11.4)
  398 CONTINUE
  399 REST=78.956*EXP(-G)*SUMG*(SLP/(CSINC+CSREF))**2
  400 CONTINUE
      SLOP=SLP/(1.414*RGH)
      IF(CSINC.GT.CSREF)GO TO 450
      TEMP1=ABS(SNREF/CSREF)
      SHADR=SHAD(SLOP,TEMP1)
      GO TO 800
  450 SHADR=1.0
  800 TEMP1=ABS(SNINC/CSINC)
      SHADI=SHAD(SLOP,TEMP1)
      REST=REST*SHADI*SHADR
      GAMSUM(1,J)=(ESAM*RV+ECRS*RH)*REST+GAMSUM(1,J)
      GAMSUM(2,J)=(ESAM*RH+ECRS*RV)*REST+GAMSUM(2,J)
  420 CONTINUE
      EMIT(1)=EMIT(1)+GAMSUM(1,J)
      EMIT(2)=EMIT(2)+GAMSUM(2,J)
  425 CONTINUE
      EMIT(1)=EMIT(1)*2.424E-3/CSINC
      EMIT(2)=EMIT(2)*2.424E-3/CSINC
      CALL FRSNEL(SNINC,CSINC,PRMRE,PRMIM,SPEC(1),SPEC(2))
      REST=EXP(-4*39.4748*(RGH*CSINC)**2)
      DO 668 L=1,2
      SPEC(L)=SPEC(L)*REST
      EMSV(L)=1.-EMIT(L)-SPEC(L)
      IF(EMSV(L).LT.0.)EMSV(L)=0.
      DO 668 K=1,10
      TD(K,L)=0.0
      DO 666 J=1,9
      GAMTOT=GAMSUM(L,9+J)+GAMSUM(L,10-J)
      TD(K,L)=TD(K,L)+GAMTOT*TSKY(J,K)
  666 CONTINUE
      TD(K,L)=TD(K,L)*2.424E-3/CSINC
      TEMIT(K,L)=GLTMP(K)*EMSV(L)
      TSPEC(K,L)=SPEC(L)*SPCSKY(KSPEC,K)
      TAPP(K,L)=TD(K,L)+TEMIT(K,L)+TSPEC(K,L)
  668 CONTINUE
      WRITE(21,754)RGH,SLP,PRMRE,PRMIM,QINC
  754 FORMAT(/"SURFACE PARAMETERS: ROUGHNESS=",F6.3,"  CORRELATION LENGTH="
     1  F5.2,"  PERMITIVITY=",F5.1,2H+J,F4.1,"  INCIDENCE ANGLE=",F4.1)
  755 FORMAT("PERMITIVITY=",F4.1,2H+J,F4.1,"  INCIDENCE ANGLE=",F4.1)
      WRITE(21,825)
      WRITE(21,826)
      WRITE(21,695)(WXCS(K),(TD(K,L),TSPEC(K,L),TEMIT(K,L),TAPP(K,L),
     1    L=1,2),K=1,10)
```

```
790 470 FORMAT("THETA2    VERTICAL    HORIZONTAL")
800 480 FORMAT(F5.1,4X,F11.4,1X,F11.4)
810 695 FORMAT(10(2X,F3.1,4(5X,F5.1),7X,4(5X,F5.1)/))
825 825 FORMAT(7HWEATHER,2X,8HDIFFUSE ,2X,8HSPECULAR,2X,8HEMITTED ,2X,
826&      8HAPPARENT,10X,8HDIFFUSE ,2X,8HSPECULAR,2X,8HEMITTED ,2X,8HAPPARENT)
827 826 FORMAT(" CASE",6X,3HSKY,7X,3HSKY,15X,"TEMPERATURE",10X,3HSKY,
828&      7X,3HSKY,15X,"TEMPERATURE"/10X,"VERTICAL POLARIZATION",20X,
829&      20X,"HORIZONTAL POLARIZATION")
830      READ 482,OINC
840 482 FORMAT(F10.4)
850      IF(OINC.NE.0.)GO TO 40
851      CALL DETACH(20,ISTAT,)
852      CALL DETACH(21,ISTAT,)
858      CALL DETACH(21,IS,)
860 STOP
870 END
880  FUNCTION SHAD(SLOP,TANA)
890      THET=SLOP/TANA
900      EREC=.5/((1+.278393*THET+.230389*THET**2+.000972*THET**3+.078108*
9106&           THET**4)**4)
920      SHAD=EXP(-.5*TANA*EREC)
930 870 RETURN
940 880 FORMAT("SHADOWING QUESTIONABLE)
950   END
1000 SUBROUTINE FRSNEL(SNLIN,CSLIN,PRMRE,PRMIM,RV,RH)
1010      B1=PRMRE-SNLIN
1020      A6SQ=SQRT(B1**2+PRMIM**2)
1030      B2=.5*ATAN2(PRMIM/B1)
1040      CSB=COS(B2)
1050      SNB=SIN(B2)
1060      PNORM=PRMRE**2+PRMIM**2
1070      RV=((PNORM*CSLIN)**2+4*A6SQ*(PRMRE*SNB)**2*CSLIN+A6SQ**2-2*
1080&          A6SQ*PNORM*CSLIN)/((PNORM*CSLIN+2*
1090 &         SQRT(A6SQ*CSLIN)*(PRMRE*CSB+PRMIM*SNB)+A6SQ)**2)
1100      CONTINUE
1110      RH=(CSLIN**2+A6SQ*4*SNB**2*CSLIN+A6SQ**2-2*A6SQ*CSLIN)/((CSLIN+
1120&          2*SQRT(
1130 &       A6SQ*CSLIN)*CSB+A6SQ)**2)
1140      RETURN
1150      END
```

SNUMB = 7379T, A = 01, REPORT CODE - 66, RECORD COUNT = 000150

SURFACE PARAMETERS: ROUGHNESS= 0.084 CORRELATION LENGTH= 0.20 PERMITIVITY= 5.5+J 0.5 INCIDENCE ANGLE=89.0

WEATHER CASE	DIFFUSE SKY	SPECULAR SKY	EMITTED	APPARENT TEMPERATURE	DIFFUSE SKY	SPECULAR SKY	EMITTED	APPARENT TEMPERATURE
	VERTICAL POLARIZATION					HORIZONTAL POLARIZATION		
1.0	0.0	108.2	186.8	295.0	0.0	246.6	48.4	295.0
2.1	0.0	94.2	179.0	273.2	0.0	214.7	46.4	261.0
2.2	0.0	94.5	179.0	273.5	0.0	215.4	46.4	261.8
2.3	0.0	97.8	179.0	276.8	0.0	223.0	46.4	269.3
2.4	0.0	102.1	179.0	281.2	0.0	232.8	46.4	279.2
3.1	0.0	102.5	179.0	281.5	0.0	233.6	46.4	279.9
3.2	0.0	102.7	179.0	281.7	0.0	234.1	46.4	280.4
3.3	0.0	103.5	179.0	282.6	0.0	236.0	46.4	282.4
3.4	0.0	103.7	179.0	282.7	0.0	236.3	46.4	282.7
4.0	0.0	86.4	169.7	256.2	0.0	197.0	44.0	241.0

SURFACE PARAMETERS: ROUGHNESS= 0.084 CORRELATION LENGTH= 0.20 PERMITIVITY= 5.5+J 0.5 INCIDENCE ANGLE=88.0

WEATHER CASE	DIFFUSE SKY	SPECULAR SKY	EMITTED	APPARENT TEMPERATURE	DIFFUSE SKY	SPECULAR SKY	EMITTED	APPARENT TEMPERATURE
	VERTICAL POLARIZATION					HORIZONTAL POLARIZATION		
1.0	0.2	76.3	218.5	295.0	0.2	228.7	66.1	294.9
2.1	0.0	52.3	209.3	261.6	0.0	156.5	63.3	219.9
2.2	0.0	52.6	209.3	262.0	0.0	157.6	63.3	221.0
2.3	0.0	56.7	209.3	266.1	0.0	170.0	63.3	233.3
2.4	0.0	64.8	209.3	274.2	0.0	194.1	63.3	257.4
3.1	0.1	71.6	209.3	281.1	0.1	214.6	63.3	278.0
3.2	0.1	71.8	209.3	281.2	0.1	215.2	63.3	278.6
3.3	0.1	72.8	209.3	282.3	0.1	218.2	63.3	281.6
3.4	0.1	73.1	209.3	282.6	0.1	219.0	63.3	282.5
4.0	0.0	46.0	198.5	244.5	0.0	137.9	60.0	197.9

SURFACE PARAMETERS: ROUGHNESS= 0.084 CORRELATION LENGTH= 0.20 PERMITIVITY= 5.5+J 0.5 INCIDENCE ANGLE=87.0

WEATHER CASE	DIFFUSE SKY	SPECULAR SKY	EMITTED	APPARENT TEMPERATURE	DIFFUSE SKY	SPECULAR SKY	EMITTED	APPARENT TEMPERATURE
	VERTICAL POLARIZATION					HORIZONTAL POLARIZATION		
1.0	1.5	61.3	232.2	294.9	1.3	215.6	77.9	294.8
2.1	0.1	33.5	222.5	256.1	0.1	117.9	74.7	192.7
2.2	0.2	33.8	222.5	256.4	0.1	118.9	74.7	193.7
2.3	0.2	37.2	222.5	259.9	0.2	131.1	74.7	205.9
2.4	0.2	45.0	222.5	267.8	0.2	158.5	74.7	233.4
3.1	0.6	56.7	222.5	279.8	0.5	199.5	74.7	274.7
3.2	0.6	56.9	222.5	280.0	0.5	200.2	74.7	275.4
3.3	0.7	58.1	222.5	281.3	0.6	204.6	74.7	279.8
3.4	0.9	59.7	222.5	282.1	0.8	206.5	74.7	282.0
4.0	0.1	28.9	210.9	239.9	0.1	101.6	70.8	172.5

C-2

SURFACE PARAMETERS: ROUGHNESS= 0.084 CORRELATION LENGTH= 0.20 PERMITIVITY= 5.5+J 0.5 INCIDENCE ANGLE=86.0

WEATHER CASE	DIFFUSE SKY	SPECULAR SKY	EMITTED	APPARENT TEMPERATURE	DIFFUSE SKY	SPECULAR SKY	EMITTED	APPARENT TEMPERATURE
	VERTICAL POLARIZATION				HORIZONTAL POLARIZATION			
1.0	3.8	53.0	238.1	294.8	3.3	205.0	86.3	294.7
2.1	0.4	23.9	228.2	252.5	0.3	92.6	82.7	175.7
2.2	0.4	24.2	228.2	252.7	0.3	93.5	82.7	176.6
2.3	0.4	27.0	228.2	255.6	0.4	104.4	82.7	187.5
2.4	0.6	33.8	228.2	262.6	0.6	130.8	82.7	214.1
3.1	1.5	47.8	228.2	277.4	1.3	185.0	82.7	269.0
3.2	1.5	48.0	228.2	277.6	1.3	185.8	82.7	269.8
3.3	1.8	49.7	228.2	279.6	1.6	192.2	82.7	276.5
3.4	2.3	50.7	228.2	281.2	2.1	196.2	82.7	281.0
4.0	0.3	20.4	216.3	237.0	0.3	78.8	78.4	157.5

SURFACE PARAMETERS: ROUGHNESS= 0.084 CORRELATION LENGTH= 0.20 PERMITIVITY= 5.5+J 0.5 INCIDENCE ANGLE=84.0

WEATHER CASE	DIFFUSE SKY	SPECULAR SKY	EMITTED	APPARENT TEMPERATURE	DIFFUSE SKY	SPECULAR SKY	EMITTED	APPARENT TEMPERATURE
	VERTICAL POLARIZATION				HORIZONTAL POLARIZATION			
1.0	9.3	45.2	240.1	294.7	8.2	188.0	98.2	294.4
2.1	0.9	15.1	230.1	246.1	0.8	62.7	94.1	157.6
2.2	0.9	15.2	230.1	246.3	0.8	63.4	94.1	158.3
2.3	1.1	17.3	230.1	248.4	0.9	71.8	94.1	166.9
2.4	1.5	22.5	230.1	254.1	1.3	93.7	94.1	189.1
3.1	3.5	37.8	230.1	271.4	3.1	157.2	94.1	254.4
3.2	3.6	38.1	230.1	271.7	3.2	158.3	94.1	255.6
3.3	4.2	40.6	230.1	274.9	3.8	168.7	94.1	266.6
3.4	5.7	43.0	230.1	279.7	5.0	178.5	94.1	277.7
4.0	0.7	12.7	218.1	231.6	0.7	52.6	89.2	142.6

SURFACE PARAMETERS: ROUGHNESS= 0.100 CORRELATION LENGTH= 1.00 PERMITIVITY= 3.2+J85.0 INCIDENCE ANGLE=89.0

WEATHER CASE	DIFFUSE SKY	SPECULAR SKY	EMITTED	APPARENT TEMPERATURE	DIFFUSE SKY	SPECULAR SKY	EMITTED	APPARENT TEMPERATURE
	VERTICAL POLARIZATION				HORIZONTAL POLARIZATION			
1.0	0.0	3.7	290.0	293.7	0.0	283.2	10.6	293.8
2.1	0.0	3.2	277.9	281.1	0.0	246.5	10.2	256.7
2.2	0.0	3.2	277.9	281.1	0.0	247.4	10.2	257.6
2.3	0.0	3.3	277.9	281.2	0.0	256.0	10.2	266.2
2.4	0.0	3.5	277.9	281.4	0.0	267.4	10.2	277.5
3.1	0.0	3.5	277.9	281.4	0.0	268.2	10.2	278.4
3.2	0.0	3.5	277.9	281.4	0.0	268.8	10.2	279.0
3.3	0.0	3.5	277.9	281.4	0.0	271.0	10.2	281.2
3.4	0.0	3.5	277.9	281.4	0.0	271.4	10.2	281.6
4.0	0.0	3.0	263.4	266.4	0.0	226.3	9.6	235.9

SURFACE PARAMETERS: ROUGHNESS= 0.100 CORRELATION LENGTH= 1.00 PERMITIVITY= 3.2+J85.0 INCIDENCE ANGLE=88.0

WEATHER CASE	DIFFUSE SKY	SPECULAR SKY	EMITTED	APPARENT TEMPERATURE	DIFFUSE SKY	SPECULAR SKY	EMITTED	APPARENT TEMPERATURE
	VERTICAL POLARIZATION				HORIZONTAL POLARIZATION			
1.0	1.3	26.9	266.7	294.9	1.3	278.0	15.5	294.8
2.1	0.1	18.4	255.6	274.1	0.1	190.3	14.9	205.3
2.2	0.1	18.6	255.6	274.3	0.1	191.6	14.9	206.6
2.3	0.1	20.0	255.6	275.7	0.1	206.6	14.9	221.6
2.4	0.2	22.8	255.6	278.6	0.2	235.9	14.9	251.0
3.1	0.5	25.3	255.6	281.3	0.5	260.9	14.9	276.3
3.2	0.5	25.3	255.6	281.4	0.5	261.6	14.9	276.9
3.3	0.6	25.7	255.6	281.8	0.6	265.3	14.9	280.7
3.4	0.8	25.8	255.6	282.1	0.8	266.3	14.9	282.0
4.0	0.1	16.2	242.3	258.6	0.1	167.6	14.1	181.8

SURFACE PARAMETERS: ROUGHNESS= 0.100 CORRELATION LENGTH= 1.00 PERMITIVITY= 3.2+J85.0 INCIDENCE ANGLE=87.0

WEATHER CASE	DIFFUSE SKY	SPECULAR SKY	EMITTED	APPARENT TEMPERATURE	DIFFUSE SKY	SPECULAR SKY	EMITTED	APPARENT TEMPERATURE
	VERTICAL POLARIZATION				HORIZONTAL POLARIZATION			
1.0	9.3	47.8	237.7	294.8	9.7	273.7	11.2	294.6
2.1	0.9	26.1	227.8	254.8	0.9	149.6	10.7	161.3
2.2	0.9	26.4	227.8	255.1	1.0	150.9	10.7	162.6
2.3	1.1	29.1	227.8	257.9	1.1	166.4	10.7	178.2
2.4	1.5	35.1	227.8	264.4	1.5	201.2	10.7	213.4
3.1	3.6	44.2	227.8	275.6	3.6	253.3	10.7	267.6
3.2	3.6	44.4	227.8	275.8	3.7	254.1	10.7	268.5
3.3	4.3	45.3	227.8	277.4	4.4	259.7	10.7	274.8
3.4	5.8	45.8	227.8	279.3	5.9	262.2	10.7	278.8
4.0	0.8	22.5	215.9	239.2	0.8	128.9	10.2	139.9

SURFACE PARAMETERS: ROUGHNESS= 0.100 CORRELATION LENGTH= 1.00 PERMITIVITY= 3.2+J85.0 INCIDENCE ANGLE=86.0

WEATHER CASE	DIFFUSE SKY	SPECULAR SKY	EMITTED	APPARENT TEMPERATURE	DIFFUSE SKY	SPECULAR SKY	EMITTED	APPARENT TEMPERATURE
	VERTICAL POLARIZATION				HORIZONTAL POLARIZATION			
1.0	22.5	64.4	207.3	294.2	23.7	269.7	0.6	294.0
2.1	2.3	29.1	198.7	230.0	2.3	121.8	0.6	124.7
2.2	2.3	29.4	198.7	230.3	2.3	123.0	0.6	125.9
2.3	2.6	32.8	198.7	234.1	2.7	137.3	0.6	140.5
2.4	3.7	41.1	198.7	243.4	3.7	172.1	0.6	176.3
3.1	8.7	58.1	198.7	265.5	8.9	243.4	0.6	252.8
3.2	8.8	58.4	198.7	265.9	9.0	244.4	0.6	253.9
3.3	10.4	60.4	198.7	269.5	10.7	252.9	0.6	264.1
3.4	13.9	61.7	198.7	274.3	14.4	258.1	0.6	273.1
4.0	1.9	24.8	188.3	215.0	1.9	103.7	0.5	106.1

SURFACE PARAMETERS: ROUGHNESS= 0.100 CORRELATION LENGTH= 1.00 PERMITIVITY= 3.2+J85.0 INCIDENCE ANGLE=84.0

WEATHER CASE	DIFFUSE SKY	SPECULAR SKY	EMITTED	APPARENT TEMPERATURE	DIFFUSE SKY	SPECULAR SKY	EMITTED	APPARENT TEMPERATURE
	VERTICAL POLARIZATION				HORIZONTAL POLARIZATION			
1.0	46.9	88.5	158.0	293.5	49.9	262.1	0.	312.0
2.1	4.6	29.5	151.4	185.6	4.7	87.4	0.	92.1
2.2	4.7	29.9	151.4	186.0	4.8	88.3	0.	93.1
2.3	5.4	33.8	151.4	190.7	5.5	100.1	0.	105.6
2.4	7.5	44.1	151.4	203.1	7.7	130.6	0.	138.3
3.1	17.8	74.0	151.4	243.3	18.4	219.1	0.	237.5
3.2	18.1	74.6	151.4	244.1	18.7	220.7	0.	239.4
3.3	21.5	79.5	151.4	252.4	22.2	235.2	0.	257.4
3.4	28.8	94.1	151.4	264.3	30.0	248.9	0.	278.9
4.0	3.8	24.8	143.6	172.2	3.9	73.4	0.	77.3

SNUMB = 6763T, ACTIVITY # = 01, REPORT CODE = 06, RECORD COUNT = 000075

SURFACE PARAMETERS: ROUGHNESS= 0.500 CORRELATION LENGTH= 3.20 PERMITIVITY= 10.0+J10.0 INCIDENCE ANGLE=89.0

WEATHER CASE	DIFFUSE SKY	SPECULAR SKY	EMITTED	APPARENT TEMPERATURE	DIFFUSE SKY	SPECULAR SKY	EMITTED	APPARENT TEMPERATURE
	VERTICAL POLARIZATION				HORIZONTAL POLARIZATION			
1.0	0.0	45.7	249.3	295.0	0.0	263.4	31.6	295.0
2.1	0.0	39.7	238.9	278.7	0.0	229.3	30.3	259.6
2.2	0.0	39.9	238.9	278.8	0.0	230.1	30.3	260.4
2.3	0.0	41.3	238.9	280.2	0.0	238.1	30.3	268.4
2.4	0.0	43.1	238.9	282.0	0.0	248.6	30.3	278.9
3.1	0.0	43.2	238.9	282.2	0.0	249.4	30.3	279.8
3.2	0.0	43.3	238.9	282.3	0.0	250.0	30.3	280.3
3.3	0.0	43.7	238.9	282.6	0.0	252.0	30.3	282.3
3.4	0.0	43.7	238.9	282.7	0.0	252.4	30.3	282.7
4.0	0.0	36.5	226.5	263.0	0.0	210.4	28.7	239.2

SURFACE PARAMETERS: ROUGHNESS= 0.500 CORRELATION LENGTH= 3.20 PERMITIVITY= 10.0+J10.0 INCIDENCE ANGLE=88.0

WEATHER CASE	DIFFUSE SKY	SPECULAR SKY	EMITTED	APPARENT TEMPERATURE	DIFFUSE SKY	SPECULAR SKY	EMITTED	APPARENT TEMPERATURE
	VERTICAL POLARIZATION				HORIZONTAL POLARIZATION			
1.0	2.5	24.1	268.4	294.9	2.7	243.5	48.7	294.9
2.1	0.2	16.5	257.2	273.9	0.2	166.7	46.7	213.6
2.2	0.2	16.6	257.2	274.0	0.2	167.8	46.7	214.8
2.3	0.3	17.9	257.2	275.4	0.3	181.0	46.7	227.9
2.4	0.4	20.5	257.2	278.0	0.4	206.7	46.7	253.7
3.1	0.9	22.6	257.2	280.7	0.9	228.5	46.7	276.1
3.2	0.9	22.7	257.2	280.8	0.9	229.1	46.7	276.7
3.3	1.1	23.0	257.2	281.3	1.1	232.3	46.7	280.1
3.4	1.5	23.1	257.2	281.7	1.5	233.2	46.7	281.5
4.0	0.2	14.5	243.8	258.5	0.2	146.8	44.3	191.3

SURFACE PARAMETERS: ROUGHNESS= 0.500 CORRELATION LENGTH= 3.20 PERMITIVITY= 10.0+J10.0 INCIDENCE ANGLE=87.0

WEATHER CASE	DIFFUSE SKY	SPECULAR SKY	EMITTED	APPARENT TEMPERATURE	DIFFUSE SKY	SPECULAR SKY	EMITTED	APPARENT TEMPERATURE
	VERTICAL POLARIZATION				HORIZONTAL POLARIZATION			
1.0	18.4	17.4	258.7	294.5	20.1	222.0	52.2	294.3
2.1	1.7	9.5	247.9	259.2	1.7	121.4	50.1	173.1
2.2	1.8	9.6	247.9	259.3	1.8	122.4	50.1	174.2
2.3	2.0	10.6	247.9	260.5	2.0	134.9	50.1	187.0
2.4	2.8	12.8	247.9	263.5	2.8	163.2	50.1	216.0
3.1	6.8	16.1	247.9	270.8	6.9	205.4	50.1	262.3
3.2	6.9	16.2	247.9	270.9	7.0	206.1	50.1	263.1
3.3	8.2	16.5	247.9	272.6	8.4	210.6	50.1	269.0
3.4	11.0	16.7	247.9	275.6	11.5	212.6	50.1	274.1
4.0	1.4	8.2	235.0	244.6	1.4	104.6	47.4	153.4

SURFACE PARAMETERS: ROUGHNESS= 0.500 CORRELATION LENGTH= 3.20 PERMITIVITY= 10.0+J10.0 INCIDENCE ANGLE=86.0

WEATHER CASE	DIFFUSE SKY	SPECULAR SKY	EMITTED	APPARENT TEMPERATURE	DIFFUSE SKY	SPECULAR SKY	EMITTED	APPARENT TEMPERATURE
	VERTICAL POLAPIZATION				HORIZONTAL POLARIZATION			
1.0	45.9	15.2	232.4	293.5	51.2	198.6	43.3	293.1
2.1	4.3	6.8	222.7	233.9	4.4	89.7	41.5	135.5
2.2	4.4	6.9	222.7	234.0	4.4	90.6	41.5	136.4
2.3	5.0	7.7	222.7	235.5	5.1	101.1	41.5	147.6
2.4	7.0	9.7	222.7	239.4	7.1	126.7	41.5	175.3
3.1	16.8	13.7	222.7	253.2	17.3	179.2	41.5	238.0
3.2	17.1	13.7	222.7	253.5	17.6	179.9	41.5	239.0
3.3	20.3	14.2	222.7	257.3	21.1	186.2	41.5	248.7
3.4	27.4	14.5	222.7	264.7	28.9	190.0	41.5	260.4
4.0	3.6	5.8	211.1	220.5	3.6	76.3	39.3	119.2

SURFACE PARAMETERS: ROUGHNESS= 0.500 CORRELATION LENGTH= 3.20 PERMITIVITY= 10.0+J10.0 INCIDENCE ANGLE=84.0

WEATHER CASE	DIFFUSE SKY	SPECULAR SKY	EMITTED	APPARENT TEMPERATURE	DIFFUSE SKY	SPECULAR SKY	EMITTED	APPARENT TEMPERATURE
	VERTICAL POLARIZATION				HORIZONTAL POLARIZATION			
1.0	105.9	13.9	172.1	291.9	122.1	149.3	19.5	290.9
2.1	9.6	4.6	164.9	179.1	9.9	49.8	18.7	78.4
2.2	9.7	4.7	164.9	179.3	10.1	50.3	18.7	79.1
2.3	11.2	5.3	164.9	181.5	11.6	57.0	18.7	87.3
2.4	15.6	6.9	164.9	187.5	16.2	74.4	18.7	109.3
3.1	37.7	11.6	164.9	214.2	39.9	124.8	18.7	183.4
3.2	38.3	11.7	164.9	214.9	40.6	125.7	18.7	185.0
3.3	45.7	12.5	164.9	223.0	48.7	134.0	18.7	201.3
3.4	61.9	13.2	164.9	240.1	67.2	141.8	18.7	227.7
4.0	7.9	3.9	156.3	168.1	8.2	41.8	17.7	67.7

SNUMB = 2559T, ACTIVITY # = 01, REPORT CODE = 06, RECORD COUNT = 000090

PATH ATTENUATIONS

RANGE= 2 KM

WEATHER CASE	GLIDE SLOPE=1 DEG.	2 DEG.	3 DEG.	4 DEG.	5 DEG.	6 DEG.	7 DEG.	8 DEG.	9 DEG.
1.0	-9.100	-9.100	-9.100	-9.103	-9.105	-9.107	-9.109	-9.111	-9.113
2.1	-0.184	-0.184	-0.181	-0.169	-0.162	-0.157	-0.153	-0.150	-0.148
2.2	-0.236	-0.236	-0.232	-0.207	-0.193	-0.182	-0.175	-0.169	-0.164
2.3	-0.911	-0.911	-0.877	-0.691	-0.580	-0.505	-0.452	-0.412	-0.380
2.4	-2.958	-2.958	-2.832	-2.158	-1.754	-1.484	-1.291	-1.147	-1.034
3.1	-0.215	-0.215	-0.215	-0.215	-0.214	-0.214	-0.213	-0.213	-0.213
3.2	-0.304	-0.304	-0.304	-0.304	-0.304	-0.304	-0.304	-0.304	-0.304
3.3	-1.442	-1.442	-1.444	-1.450	-1.455	-1.458	-1.464	-1.469	-1.479
3.4	-4.881	-4.881	-4.886	-4.913	-4.930	-4.946	-4.969	-4.987	-5.005
4.0	-0.093	-0.093	-0.092	-0.092	-0.091	-0.091	-0.091	-0.090	-0.090

RANGE= 6

WEATHER CASE	GLIDE SLOPE=1 DEG.	2 DEG.	3 DEG.	4 DEG.	5 DEG.	6 DEG.	7 DEG.	8 DEG.	9 DEG.
1.0	-27.301	-27.320	-27.341	-27.361	-27.451	-27.725	-27.923	-28.058	-28.151
2.1	-0.544	-0.472	-0.443	-0.424	-0.411	-0.399	-0.389	-0.380	-0.372
2.2	-0.695	-0.547	-0.493	-0.462	-0.441	-0.425	-0.411	-0.399	-0.389
2.3	-2.629	-1.514	-1.138	-0.946	-0.828	-0.747	-0.688	-0.642	-0.604
2.4	-8.492	-4.446	-3.093	-2.413	-2.002	-1.726	-1.527	-1.377	-1.258
3.1	-0.645	-0.641	-0.638	-0.634	-0.654	-0.737	-0.797	-0.844	-0.882
3.2	-0.913	-0.912	-0.912	-0.911	-0.922	-0.960	-0.989	-1.012	-1.031
3.3	-4.331	-4.376	-4.420	-4.465	-4.351	-3.819	-3.441	-3.159	-2.941
3.4	-14.658	-14.839	-15.019	-15.199	-14.709	-12.456	-10.849	-9.646	-8.713
4.0	-0.277	-0.273	-0.269	-0.266	-0.262	-0.258	-0.254	-0.251	-0.247

RANGE=16

WEATHER CASE	GLIDE SLOPE=1 DEG.	2 DEG.	3 DEG.	4 DEG.	5 DEG.	6 DEG.	7 DEG.	8 DEG.	9 DEG.
1.0	-72.891	-73.480	-74.829	-75.326	-75.463	-75.423	-75.295	-75.113	-74.963
2.1	-1.201	-1.084	-1.013	-0.956	-0.904	-0.856	-0.814	-0.777	-0.747
2.2	-1.352	-1.160	-1.064	-0.993	-0.934	-0.881	-0.836	-0.796	-0.764
2.3	-3.285	-2.127	-1.709	-1.477	-1.321	-1.204	-1.113	-1.039	-0.980
2.4	-9.148	-5.059	-3.664	-2.944	-2.495	-2.183	-1.952	-1.774	-1.634
3.1	-1.703	-1.827	-2.253	-2.485	-2.640	-2.757	-2.847	-2.918	-2.973
3.2	-2.431	-2.496	-2.699	-2.820	-2.908	-2.981	-3.039	-3.085	-3.122
3.3	-11.749	-11.060	-8.410	-7.104	-6.337	-5.840	-5.491	-5.233	-5.032
3.4	-39.899	-36.929	-25.660	-20.047	-16.695	-14.477	-12.899	-11.720	-10.803
4.0	-0.722	-0.695	-0.668	-0.642	-0.617	-0.593	-0.572	-0.554	-0.540

PATH TEMPERATURES

RANGE= 2 KM.

WEATHER CASE	GLIDE SLOPE=1 DEG.	2 DEG.	3 DEG.	4 DEG.	5 DEG.	6 DEG.	7 DEG.	8 DEG.	9 DEG.
1.0	102.725	195.691	256.728	249.288	252.112	257.123	254.932	256.017	257.161
2.1	11.260	11.601	11.560	10.795	10.349	10.038	9.777	9.595	9.422
2.2	14.251	14.806	14.689	13.152	12.240	11.618	11.133	10.774	10.481
2.3	44.588	51.238	51.665	41.563	35.307	31.036	27.906	25.538	23.670
2.4	84.661	122.958	135.410	110.676	93.903	81.819	72.691	65.583	59.883
3.1	13.062	13.526	13.649	13.576	13.568	13.557	13.512	13.491	13.465
3.2	17.941	18.840	19.095	19.026	19.054	19.074	19.048	19.051	19.049
3.3	60.574	74.714	79.513	78.811	79.623	80.314	80.266	80.664	80.973
3.4	94.740	157.891	189.072	184.270	187.385	190.862	189.727	191.069	192.161
4.0	5.540	5.624	5.640	5.596	5.576	5.555	5.521	5.497	5.471

RANGE= 8

WEATHER CASE	GLIDE SLOPE=1 DEG.	2 DEG.	3 DEG.	4 DEG.	5 DEG.	6 DEG.	7 DEG.	8 DEG.	9 DEG.
1.0	294.274	293.660	293.074	292.499	291.928	291.372	290.809	290.243	289.674
2.1	33.250	29.035	27.308	26.215	25.381	24.682	24.064	23.499	22.972
2.2	41.783	33.411	30.254	28.438	27.168	26.176	25.349	24.627	23.978
2.3	128.343	83.160	65.073	55.228	48.951	44.542	41.233	38.629	36.503
2.4	242.680	181.093	143.934	120.399	104.288	92.571	83.648	76.607	70.894
3.1	38.932	38.714	38.471	38.223	39.255	43.767	46.983	49.407	51.311
3.2	53.374	53.377	53.327	53.264	53.732	55.669	57.088	58.184	59.069
3.3	176.709	178.256	179.358	180.313	177.893	164.402	153.723	145.105	138.029
3.4	271.883	272.104	272.186	272.185	271.224	264.792	257.640	250.234	242.874
4.0	16.554	16.315	16.073	15.834	15.599	15.367	15.137	14.909	14.685

RANGE=16

WEATHER CASE	GLIDE SLOPE=1 DEG.	2 DEG.	3 DEG.	4 DEG.	5 DEG.	6 DEG.	7 DEG.	8 DEG.	9 DEG.
1.0	293.836	292.050	290.272	288.514	286.783	285.067	283.496	283.043	282.785
2.1	68.005	62.079	58.316	55.178	52.340	49.702	47.360	45.234	43.549
2.2	75.343	65.879	60.899	57.145	53.935	51.047	48.525	46.264	44.472
2.3	149.794	109.086	91.430	80.851	73.380	67.579	62.929	59.046	55.962
2.4	248.136	194.143	160.576	138.519	122.777	110.813	101.392	93.715	87.511
3.1	91.203	96.161	113.083	121.289	126.271	129.717	132.240	132.768	133.977
3.2	120.352	122.562	129.436	133.064	135.433	137.192	138.543	138.269	138.829
3.3	261.107	258.745	239.881	225.165	214.014	205.476	198.824	192.740	188.216
3.4	281.513	280.240	279.265	276.821	273.082	268.521	263.645	258.622	253.793
4.0	40.876	39.380	37.900	36.457	35.063	33.729	32.563	31.530	30.740

PAGE INTENTIONALLY BLANK

APPENDIX F

MLS CONFIGURATION K AIRBORNE EQUIPMENT

PHYSICAL DESCRIPTION OF FAA-K AIRBORNE EQUIPMENT

The H-80 Airborne Equipment Set offers operational and installation flexibility through compact, modular equipment packaging.

The H-80 airborne system will meet all FAA-K equipment requirements. Figure F-1 shows two airborne sets in a typical redundant aircraft installation. Features include a standardized package design and simplified interconnections that will permit straightforward installation of the equipment in the DC-6 or CV-880 aircraft. When the airborne equipment is used in the dual configuration illustrated, provisions are made for interconnection of the two HN-700 Angle Receiver/Processors to implement built-in cross monitoring capability.

The physical characteristics of each H-80 subsystem are summarized below and discussed in detail in the following paragraphs.

Physical Characteristics of H-80 Equipment Set

	Angle Rec/Proc (HN-700)	DME Interr. (HN-800)	Control Unit (HC-400)	Antennas	
				(HL-181)	(HL-362) (HL-363)
Size	3/4 ATR Long	1/2 ATR Short	5.75"W, 4.125"H, 2.5"D	4"H, 5"W, 6"D	Not Defined " "
Weight	20 lbs	10 lbs	3 lbs	1 lb	Not Defined
Power	145 w	40 w	15 w	--	--

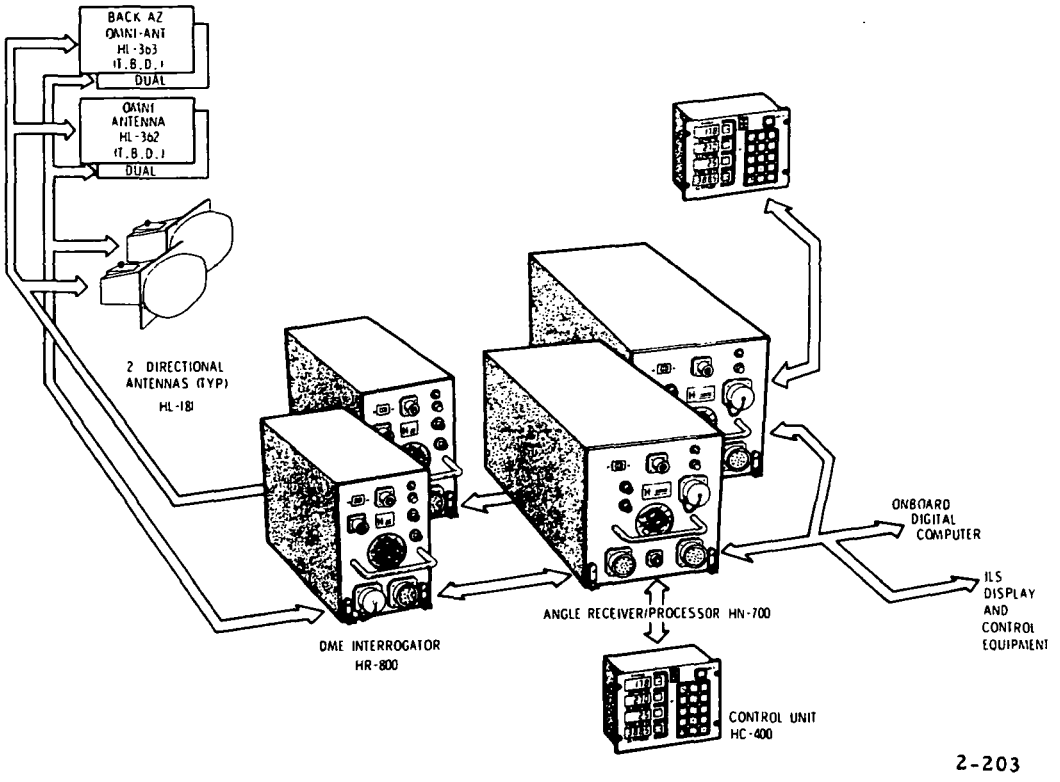

Figure F-1 - - Redundant Installation

Although the HR-800 DME Interrogator is considered an integral subsystem, the HN-700 Angle Receiver/Processor can operate independently.

The H-80 airborne set is designed to use about 200 watts of 400 Hz, single phase, 115v aircraft power. The HN-700 connects to the aircraft power source and supplies the required dc power to the other units as required.

The airborne units have been designed for hard-mounting in the aircraft, and will operate and withstand expected prototype aircraft environmental conditions:

Temperatures -40 degrees to +65 degrees C

Vibration +2 g's per MIL-STD-810B (Curve B, Figure 514-1)

The HN-700 is packaged in a standard 3/4 ATR long case and has been dimensioned for hard mounting to the test aircraft equipment rack for ease of installation. Mechanical holddown clamps allow quick installationand removal of equipment. Plug-in circuit boards allow fast replacement of defective circuits for ease of maintenance.

System interconnections have been simplified and provide ready access to connectors and test points for in-flight equipment monitoring during the test program. These connectors, as well as the test point access, are located on the front panel. The HN-700 interconnects to the HC-500 control unit for channel select and azimuth and elevation path selection. Additionally, The HN-700 provides basic low dc voltages, RF signal down conversion, and a frequency synthesizer signal for the HR-800. The HN-700 angle deviation outputs are scaled to standard ILS course width sensitivities and are therefore compatible with the existing set of avionics in the test aircraft.

The HR-800 has similar packaging, mounting, and interconnect features and is housed in a 1/2 ATR short case. Case size (and cost) has been substantially reduced by a sharing of the HN-700 RF components.

The Control Unit (HC-400 provides a system on-off switch, a system go/no-go status light, azimuth and elevation tracking status lights, channel select and MLS path select. The HC-400 unit is of modern keyboard type entry with gas discharge display characters formed against a black background for optimum readability. Polarized non-reflective filters combined with proper contrast ratio and brightness make the display readable in any ambient light conditions including direct sunlight. The control unit is sized to fit standard instrument panel mounting slots and is held in place with Dzus fasteners.

Three antennas are used for both equipments. In a dual installation both H-80 sets may share the same three antennas.

The HL-181 directional antenna is a conventional horn intended for mounting externally on the nose, or inside the aircraft radome. It is about 4 x 5 inches with a depth of 6 inches, including the fiberglas cover.

The HL-362 and HL-363 omnidirectional antennas are not defined and must be customized to the aircraft considering available locations, aircraft geometry and MLS equipment location. Typically it is expected that "thimble-sized" linear stub type antennas will find wide application.

PERFORMANCE CHARACTERISTICS OF FAA-K AIRBORNE EQUIPMENT

The performance characteristics of the configuration K-FAA Airborne Doppler MLS Equipment Set, designated H-80, will meet the FAA requirements for high-capability guidance equipment for aircraft engaged in autoland operations at primary hub airports.

The H-80 airborne equipment has been designed to provide precise takeoff and landing terminal area guidance information, under Category III weather conditions, for fixed-wing civil aircraft operating with autoland avionics at suitably equipped major runways. The airborne set will provide the accuracies and functional characteristics in Tables F-1 and F-2.

The HN-700 provides the 200 channel frequency synthesizer, down conversion of both the angle guidance and DME, as well as the signal processing for the angle data. The accuracy of the angle guidance information is preserved even under heavy multipath conditions by the use of a digitally implemented, matched tracking filter that acquires and tracks the direct signal. In acquiring the angle data, the processor employs a search algorithm that prevents lock-on to bright flashes or other spurious signals. Once in track, the receiver verification circuitry continuously checks the video spectrum to assure that the tracked signal is the correct one. In case of failure to verify, the receiver is forced to re-acquire the signal.

Table F-1. Functional Characteristics of the FAA-K Airborne Equipment

Item	Description				
Guidance Functions	Azimuth, Elevation 1, Elevation 2, Back Azimuth, DME, Aux Data				
Coverage	AZ, EL, DME		BAZ		EL2
Horizontal	±60 deg		±40 deg		±45 deg
Vertical	1 to 20 deg				1 to 8 deg
Range	30 nmi		5 nmi		5 nmi
MGA	50 feet or TD				
Accuracies (2σ)	MGA				Wide Angle or Max Range
Noise: Azimuth	0.026 deg				0.10 deg
Elevation 1	0.06 deg				0.08 deg
Elevation 2	0.03 deg				-
Back AZ	0.052 deg				0.052 deg
DME (1σ)	±20 ft				±20 ft ±0.1%R
Bias: Azimuth	0.03 deg				0.06 deg
Elevation 1	0.045 deg				0.06 deg
Elevation 2	0.025 deg				-
Back AZ	0.06 deg				0.12 deg
DME (1σ)	±20 ft				±20 ft ±0.1%R
Airborne Antenna Coverage					
Horizontal	360 deg				
Vertical	+5, -40 deg				
	AZ	EL1	EL2	BAZ	DME
Acquisition Time (sec)	1.6	1.4	1.4	1.6	.25
Verification Interval	continuous (1 sec delay)				N/A

Table F-2. Specific Performance Features of Configuration K, FAA Airborne Equipment

Item	Description
Lateral Path	
Azimuth Select	Pilot select of ±30 deg in 5-degree increments
Sensitivity	ILS compatible deviation with course softening option within desired range.
Wide Angle	±60 degree suitable for display.
Missed Approach	Automatic front-to-back AZ switching with DME.
Vertical Path	
Glidepath Select	2 to 12 degrees in 0.5-degree increments
Sensitivity	ILS compatible, with course softening option within desired range.
Coordinates	Conical, with option of EL1 planar equivalent through DME algorithm.
Flare Altitude and Rate	Suitable for Collins 860F-1 display and 11SA435 A flare coupler.
Range and Range Rate	Suitable for Collins 860-3 digital DME indicator.
Monitoring	On-line monitoring, self-monitoring push-to-test confidence test. Comparison test.
Altitude/Range Discretes	Marker beacon, flare, and decrab options.

The integrity of the angle receiver is enhanced by a combination of on-line monitoring, self-monitoring, and a press-to-test confidence check. The on-line monitoring is achieved by requiring the correct function identity (FI) to be decoded each data frame, and by the requirement that a minimum signal level be present before decoding of FI can start. The self-monitoring design makes extensive use of the microprocessor to monitor and test the status of the unit in a time share mode to ensure that the MLS is operational. The press-to-test confidence check circuitry injects a video signal to produce a cross-pointer deviation of predetermined magnitude and direction which provides a check, not only of the angle processor, but also of the interface circuits and pilot display.

The HR-800 DME interrogator shares the channel selection local oscillator and RF front end with the angle data receiver. The channel selection also provides the pulse pair coding of the DME transmitter and decoding of the DME transponder signals. The DME range information may be used in automatic course softening of angle deviation signals, as well as in the computation of altitude to provide selectable Decision Height (DH) annunciation.

The HN-400 control unit panel provides keyboard entry selection of any of 200 MLS angle channels and the paired DME channel. The panel also allows keyboard selection of azimuth elevation paths for deviation output reference. The selected paths, as well as the selected channel, are full-time displayed by gas-discharge type characters. The panel also has the confidence test

pushbutton and MLS subsystem status lights which are activated by the self-monitoring circuitry in the MLS equipment. The HN-400 control panel further provides access to the HN-700 microprocessor programming, wherein certain operational options may be implemented. For example, although normal Elevation 1 output is conical, both deviation and total angle may be converted to a planar equivalent through keyboard entry of proper coding to implement an appropriate DME conversion algorithm.

The HL-362 and HL-363 omnidirectional antennas are provided to assure full MLS airborne antenna coverage during the diverse aircraft maneuvers associated with curved approach paths, missed approach, and departures. The HL-181 sector horn antenna provides effective gain enhancement of the guidance signals, as well as assuring adequate coverage for the critical final approach phase of the terminal area mission.